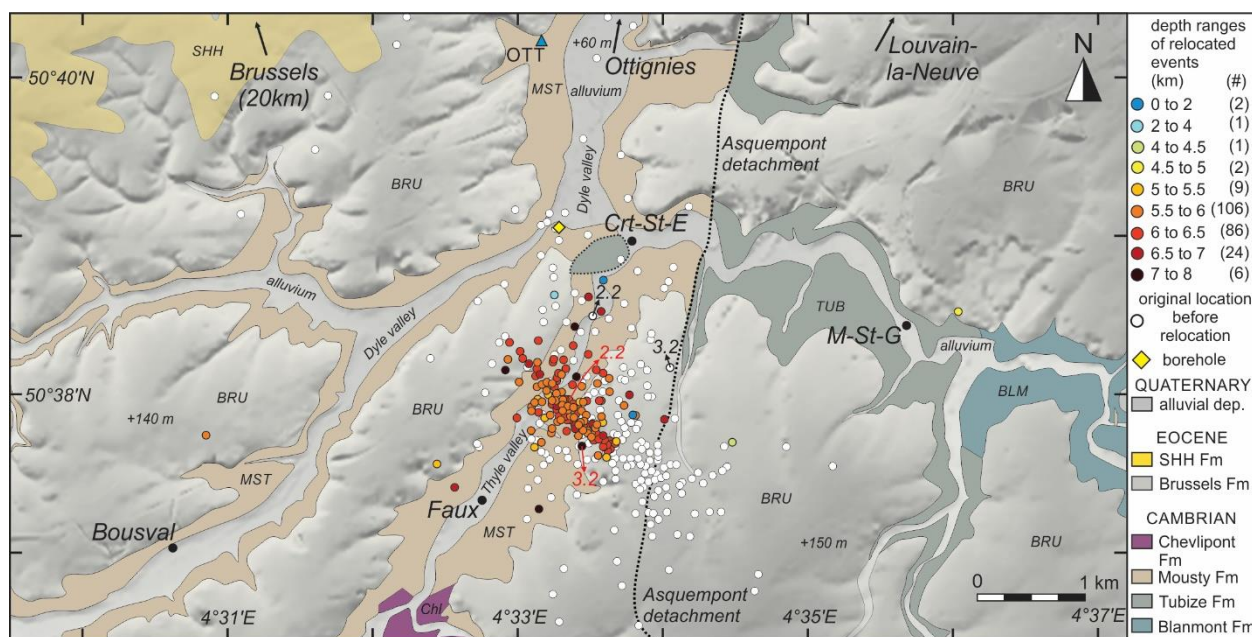




**ROYAL OBSERVATORY OF BELGIUM**  
**DEPARTMENT 1: REFERENCE SYSTEMS AND GEODYNAMICS**  
**SECTION 2: SEISMOLOGY-GRAVIMETRY**  
Ringlaan 3, 1180 Brussels



*The seismic activity in the Walloon Brabant and its relationship with the local and regional geological structure*

**Contract MO/33/028 - Action 1**  
**Final Report**

Authors:  
**Dr. Koen Van Noten**  
**Dr. Thomas Lecocq**  
**Dr. Thierry Camelbeek**

### ***Reference***

***Van Noten, K., Lecocq, T. & Camelbeeck, T. 2015. The seismic activity in the Walloon Brabant and its relationship with the local and regional geological structure. Final BELSPO report contract MO/33/028. Royal Observatory of Belgium. 79 p.***

### ***Contact information:***

Royal Observatory of Belgium, Seismology-Gravimetry, Ringlaan 3, 1180 Brussels

Koen Van Noten: [koen.vannoten@seismology.be](mailto:koen.vannoten@seismology.be); +32 2 790 39 18

Thomas Lecocq: [thomas.lecocq@seismology.be](mailto:thomas.lecocq@seismology.be); +32 2 373 02 52

Thierry Camelbeeck: [thierry.camelbeeck@oma.be](mailto:thierry.camelbeeck@oma.be); +32 2 373 03 16

### ***Cover illustration***

*Relocated earthquake epicentres of the 2008-2010 seismic sequence  
illustrated on the local geological map of Walloon Brabant*

## Acknowledgements

Many aspects in this BELSPO project benefited from the work of other scientists, technical staff and engineers working at the Seismology-Gravimetry Section who have a temporary or permanent position at the Royal Observatory of Belgium. Consequently, as the participation of these scientists was necessary, this project also benefited from the financial support of several other scientific projects.

G. Rapagnani, F. Colin, C. Caudron and B. Bukasa are thanked for station installation and maintenance during the seismic swarm. H. Martin is thanked for the focal mechanism calculation in the DP console available at the Royal Observatory of Belgium. K. Vanneste and B. Vleminckx frequently helped with python script development and seismic catalogue analyses. K. Verbeeck is acknowledged for fieldwork and discussions on the geology of the Brabant Massif. J. Molron (ULB), L. Meyer (ULB), D. Kusters, D. Natamangala and many ULB students helped during geophysical field work.

For the geological interpretation of the aeromagnetic maps, we cooperated with Dr. Anjana K. Shah of the U.S. Geological Survey, Denver, Colorado, USA.

The authors would like to acknowledge B. Lamarche (OTT), G. Wyseur (OT1), M. Gosuin (OT2), M. Piaser (OT3), K. de Wit (OT4), J.-P. Deckens (OT5) and P. Paquet (GRZ) for their hospitality when housing the temporary seismic stations in Court-Saint-Etienne, Ottignies and Grand-Leez.

We are grateful to M. Deceukelaire (Geological Survey of Belgium) for her help with the borehole information available at the archives of the Geological Survey and the online Gisel application. Borehole data in this report are used with agreement of the Geological Survey of Belgium (Archief Geodoc, 2012).

F. Waldhauser and L. Krischer (Uni. Munchen) are thanked for their help with, respectively, the HypoDD2+ beta version and HypoDDpy. We very much appreciate the fruitful discussions with T.N. Debacker (FrogTech), A. Herbosch (ULB), M. Sintubin (KULeuven), and J. Phillips (USGS) on the geology and aeromagnetism of the Brabant Massif.

Constructive remarks of V.E. Langenheim (USGS), N. Woodcock (University of Cambridge), M. Van Camp and *Tectonophysics* editor K. Wang greatly helped to improve chapter A published in *Tectonophysics*.

K. Van Noten was fully funded by this BELSPO project MO-33-028 from March 2012 until February 2014 but also benefited from the Fonds de la Recherche Scientifique (FNRS) under grant PDR T.0116.14 when writing this final report. K. Van Noten additionally benefited from travel funding K1F7913N of the Fonds voor Wetenschappelijk Onderzoek Vlaanderen (FWO) to attend AGU2013. Relocation tools were developed during the FRIA scholarship FC76908 of T. Lecocq.

The DEM model in Figure 1 and Figure 5 is published with authorisation A3134 of the Nationaal Geografisch Instituut.

Last but not least we would like to thank all the people that responded to the online “*Did You Feel It?*” inquiry available on the *seismology.be* website. More than two thousand people reported to have felt one or several of the earthquakes during the 2008-2010 Court-Saint-Etienne seismic swarm. Without their contributions we could not have performed this study!

Koen Van Noten  
Thomas Lecocq  
Thierry Camelbeeck





# Table of Contents

<b>Introduction</b> .....	<b>1</b>
<b>Research objectives</b> .....	<b>2</b>
<b>A. Seismotectonic significance of the 2008-2010 seismic swarm</b> .....	<b>4</b>
TASK 1 – Spatiotemporal analysis of seismicity .....	4
1.1. Introduction: seismic swarms.....	4
1.2. Temporary network and time history of seismicity .....	5
1.3. Magnitude-frequency distribution.....	7
1.4. Earthquake location, waveform cross-correlation and event relocation .....	9
TASK 2 – Calculation of focal mechanisms and tectonic stress inversion.....	13
2.1. Fault plane solutions .....	13
2.2. Fault plane solutions .....	14
TASK 3 – Seismotectonic setting of the Brabant Massif and integration of results.....	17
3.1. Regional geological setting.....	17
3.2. Structural grain of the Brabant Massif.....	18
3.3. Historical seismicity in the Brabant Massif .....	20
3.4. The 1953 – 1957 seismic sequence near Court-Saint-Etienne.....	20
3.5. Seismotectonic significance of the seismic swarm by magnetic matched bandpass filtering.....	23
3.5.1. Aeromagnetic interpretation of the Brabant Massif.....	23
3.5.2. Methodology of matched bandpass filtering.....	25
3.5.3. Interpretation of aeromagnetic bandpass filtered maps .....	26
TASK 4 – Discussion of results obtained in Tasks 1, 2 and 3 .....	29
4.1. Stress release within a limited-sized fault zone .....	29
4.2. Seismotectonic interpretation.....	30
4.3. General implications for intraplate earthquake activity .....	31
Conclusions.....	32
<b>B. Identification of the fault in the field – Relationship between seismicity and (sub)surface geology?</b> .....	<b>33</b>
TASK 5 – Data collection.....	33
5.1. Topography .....	33
5.2. Geomorphological data.....	33
5.3. Geology.....	33
5.4. Hydro(geo)logical data .....	34

5.5. Geophysical data.....	35
5.6. Low-risk nuclear data.....	35
TASK 6 – Geomorphological study on field and on the DEM to evaluate the relationship between geomorphology and the underlying geological structure.....	37
TASK 7 – Geophysical survey by Electrical Resistivity Tomography.....	38
7.1. Methodology.....	38
7.2. Conducted ERT profiles.....	38
TASK 8 – Interpretation of data in Tasks 4, 5 & 6: the relationship between faults and the shallow geological structure.....	40
<b>C. Site effects and S-wave attenuation in the Brabant Massif .....</b>	<b>41</b>
TASK 9 – Resonance frequency maps determined by H/V ambient noise recording .....	41
9.1. Methodology .....	41
9.2. Results.....	43
9.2.1. Establishing the resonance frequency – sediment thickness powerlaw relationship .....	43
9.2.2. Additional H/V measurements & applying the powerlaw equation.....	45
TASK 10 – Macroseismic investigation of internet earthquake inquiries .....	48
10.1. The transferability of the Brabant Massif .....	48
10.2. Macroseismic internet inquiries related to the Walloon Brabant seismic swarm .....	48
10.3. Developing a proper research methodology .....	53
10.4. Research results.....	55
10.4.1. Geocoding addresses for individual macroseismic intensity maps.....	55
10.4.2. Macroseismic intensity analysis of the seismic swarm.....	56
10.4.3. Thickness map of the cover sediments.....	59
10.4.4. Link between macroseismic intensity and sediment thickness? .....	62
<b>General Conclusions .....</b>	<b>63</b>
<b>D. Scientific publications and attendance to (inter)national conferences.....</b>	<b>65</b>
Peer reviewed publications .....	65
Presentations at international conferences and national meetings .....	65
<b>References.....</b>	<b>67</b>
<b>Appendix A: Catalogue of events of the 2008-2010 seismic swarm.....</b>	<b>73</b>
<b>Appendix B: AGU2013 poster presentation .....</b>	<b>78</b>
<b>Appendix C: TSG2015 poster presentation.....</b>	<b>79</b>

## Introduction

The region of Court-Saint-Etienne, a community at about 20 km SE of Brussels in Walloon Brabant, has experienced a seismic sequence from 12 July 2008 to 18 January 2010. This seismic sequence is characterised by several periods of swarm activity, of which the largest swarm activity took place in the summer of 2008 and spring 2009, alternating with periods of seismic quiescence. In total, 239 earthquake events have been recorded by the dense modern permanent seismic network in Belgium, among which 7 temporary stations that were installed in the vicinity of the epicentres soon after the first earthquake took place. The largest event of the sequence had a local magnitude  $M_L$  3.2, struck on 13 July 2008 and was felt in the whole Walloon Brabant, even to the NE of Brussels more than 30 km from the epicentre. In general the local earthquake magnitudes of the whole swarm ranges between  $-0.7 \leq M_L \leq 3.2$ .

Remarkably 60 events have been felt or heard only sometimes by the local population in spite of the often very small magnitudes of the earthquakes (e.g. 12 responses for a  $M_L = 0.7$  event). This was detected by the “*Did You Feel It?*” macroseismic internet inquiries (after Wald et al., 1999) on the *seismology.be* website. The macroseismic maps drawn for each of these events show the spatial variability in the way the earthquakes were felt. Thanks to the high responsiveness of the people we are quite confident that these very low earthquakes were really felt/heard because several DYFI?-webforms were submitted even before any information was published on the seismology website or in the media.

During the Court-Saint-Etienne seismic sequence, the local and the provincial authorities were concerned about the seismic risk in the Walloon Brabant. In the past, a detailed local study on the seismic risk assessment of the Walloon Brabant has, however, never been performed, mainly due to a lack of seismic info after the installation of modern seismic equipment in 1985. This study supported by BELSPO therefore aims to perform a full investigation of the seismic swarm and the local site effects of the earthquake area in order to provide some answers to the authorities on the seismic source of the earthquakes, their impact at the surface and the seismic risk.

Thanks to the important quantity of (macro)seismic data, this seismic sequence is the first event in the Brabant Massif (an ancient Palaeozoic massif underlying Brabant and Flanders) that can be studied by modern quantitative seismology methods. Moreover, the analysis of seismicity allows us to investigate the possible link between seismicity and the reactivation of ancient geological structures in the Brabant Massif. Additionally, this case also offers us an unique scientific opportunity to better understand the origin of continental intraplate earthquakes in low seismicity regions, one of the major tasks of the Seismology-Gravimetry section at the Royal Observatory of Belgium.

## Research objectives

This project aims to answer several questions related to the seismic activity and its impact on the southern part of the Brabant Massif in order to evaluate earthquake development in continental intraplate tectonic settings.

### **A. First objective: The seismotectonic significance of the seismic sequence in the Walloon Brabant**

The first objective of this project is to perform a comprehensive analysis of the seismic sequence in the Walloon Brabant to deduce information on the seismotectonic framework of the Brabant Massif. In order to localise the active structure in the subsurface that was responsible for the seismic sequence, it is necessary to relocate all the routinely determined seismic events with a greater precision. This will be done by the method of seismic waveform cross-correlation (**Task 1**). In this method, the waveforms of co-located earthquakes (i.e. very close at each other) recorded at a single station are compared to each other, which allows improving the spatial distribution of the original hypocentres. Based on these relocations, an analysis of seismicity will be performed in order to visualise and understand the evolution of rupturing in time and space, i.e. the spatiotemporal analysis.

The fault geometry, fault mechanism and the associated current stress orientation will be derived from calculating focal mechanisms for the largest individual events (**Task 2**). This will be determined by using the full body wave signals and studying the first arrivals of P-waves observed at stations located in various directions. Subsequently, a tectonic stress inversion will be done by using specialised stress analysis programs. The results of stress inversion allows estimating the current stress field acting on this part of the Brabant Massif.

In order to link the seismic sequence and the fault geometry to the local geology, a full synthesis of the seismotectonic setting of the Brabant Massif will be realised (**Task 3**). This synthesis will include (i) an overview of the historical seismicity in the Brabant Massif, (ii) a literature review on the tectonic grain of the Brabant Massif based on structural analyses of field data and potential data (Bouguer gravity anomaly and the magnetic field) and (iii) an integration of the seismological research results into the seismotectonic framework of the Brabant Massif by a technique called *matched bandpass filtering* of the magnetic field.

In Task 4, the obtained results of Tasks 1, 2 and 3 are discussed.

### **B. Second objective: Identification of the fault in the field**

The second objective focuses on a possible surface identification of the geological fault structure that is exemplified by the spatial distribution of the relocated hypocentres. It will be investigated if it is possible to identify a structure at the surface or in the shallow subsurface that corresponds to the geometry of the fault. The first important task (**Task 5**) is to gather all (cartographic) information on the local and regional geology, geomorphology, hydro(geo)logy and soil characteristics in order to have a full overview of the geology and the already performed studies in the area.

An possible identification of the fault structure at the surface can only be confirmed by performing a geomorphological study of the earthquake area (**Task 6**). Fault-related structures will be searched on a Digital Elevation Model (DEM) and on the field by analysing river traces, hill morphology and differences in lithology. In this part of the work it is also intended to select some potential field sites to perform a geophysical prospection by which the fault can be visualised (**Task 7**). Geophysical methods such as ambient noise measurements (HVSR) and 2D electrical resistivity tomography (ERT) will be used to image the subsurface (max 40 m) in search of a possible offset of layers along a fault. 7

In **Task 8**, the results of Tasks 4, 5 and 6 will be interpreted and discussed in order to provide a synthesis on the geometry of the possible fault structure at the surface.

### **C. Third objective: Site effects and S-wave attenuation in the Brabant Massif**

Depending on the site conditions and the local geological structure, ground motions produced by earthquakes can be amplified or attenuated. The third objective therefore aims to investigate these ground motions by studying the local site effects and attenuation of S-waves inside the Brabant Massif. Taking into account the pronounced hilly topography of the research area, each site can be described by the resonance frequency of the soil that varies according to the thickness of the soil above the bedrock. These are important aspects to quantify the impact of the earthquakes and to evaluate the seismic risk in the region of Court-Saint-Etienne.

The site resonance frequency will be evaluated by a field campaign of H/V measurements (**Task 9**). The empirical H/V method consists in recording the ambient vibrations of the ground during a limited time and the calculation of the spectral ratio of the horizontal component over the vertical component (H/V). The resulting curve allows to analyse the soil natural period of resonance which can be illustrated by drawing detailed maps of the site effects. The detailed maps of the site effects can later be used in other projects at the ROB that focus on seismic hazard (earthquake ground motion probability) and seismic risk (social and environmental consequences of the seismic hazard) assessment in Belgium (not an objective of this study).

The final task will focus on the analysis of the “Did you feel it?” internet inquiries (**Task 10**). We need to develop a proper methodology on how the macroseismic results can be analysed. 60 events have been reported to be felt/heard, so all these formularies need to be evaluated and mapped properly. The results of this task will allow evaluating the local/regional seismic impact of earthquakes with respect to the local geology and site effects.

### **D. Scientific output**

In order to improve our methodology and to discuss the obtained results of the different tasks, several presentations were given at national and international scientific meetings during the project (**Task 11**).

The results obtained in chapter A are published in the *Tectonophysics* journal in Van Noten et al. (2015). This BELSPO project will further lead to two other additional papers focusing on the methodology of analysing macroseismic inquiries and the mapping of the bedrock below a sedimentary cover by geophysical tools.

## **A. Seismotectonic significance of the 2008-2010 seismic swarm**

### **TASK 1 – Spatiotemporal analysis of seismicity**

#### **1.1. Introduction: seismic swarms**

Earthquake swarms or seismic swarms are defined as episodic sequences of a large number of seismic events that are clustered in space and time (Mogi, 1963). In contrast to a classical foreshock-mainshock-aftershock sequence, in which aftershock sequences may consist of numerous lower-magnitude earthquakes, seismic swarms are not marked by one single dominant event. The time history of a swarm is rather characterised by a gradual increase, or sometimes by a burst, of microseismic activity alternating with periods of low seismic rate or seismic quiescence. Sometimes dominant earthquakes may reach larger magnitudes during the course of a seismic swarm. The many small events in a seismic swarm are often not linked to an identifiable mainshock. This is explained as a consequence of a rather heterogeneous stress field in a weakened crust that lacks a single well-defined fault structure. If such a fault structure was present, it might be capable releasing higher strain resulting in a higher magnitude earthquake (Fischer et al., 2014; Mogi, 1963). To precisely localise and relocate the numerous events within a seismic sequence, it is necessary to analyse waveform data that is recorded by a dense local seismic network close to the epicentre of an earthquake swarm, allowing the detection of a large number of small events.

In an intraplate continental tectonic setting, seismic swarms are commonly associated with stress perturbations caused by magmatic intrusions, volcanic activity and with gradual fluid transport in the seismogenic part of the crust (Hainzl, 2004; Hiemer et al., 2012; Schenk et al., 2012; Špičák, 2000). In volcanic areas, continental rift and subduction zones, large fluid- and gas movements such as CO<sub>2</sub> release along prominent faults or fault intersections can generate earthquakes swarms (e.g. Ibs-von Seht et al., 2008; Lindenfeld et al., 2012). Within the Eurasian tectonic plate, far away from any plate boundary, intense geothermal seismic swarms occur for example in the western French Alps (e.g. Daniel et al., 2011; Leclère et al., 2012) or in the West Bohemia/Vogtland area in the Eger rift zone (e.g. Fischer et al., 2014; Parotidis et al., 2003; Schenk et al., 2012). In these cases, the presence of suprahydrostatic overpressured fluids rising along a fault zone is often considered to trigger fault activity due to pore pressure changes, even when the fault is unfavourably oriented for reactivation (Leclère et al., 2012; Sibson, 1985) and especially if the crust is in a critical state (Parotidis et al., 2003).

Between 2008 and 2010, a seismic swarm occurred in the central part of Belgium, more specifically in the basement rocks of the Lower Palaeozoic Anglo-Brabant Massif, here further referred to as the Brabant Massif. Although the studied 2008-2010 Walloon Brabant seismic sequence resembles other seismic swarms in terms of its temporal evolution, the lack of a main shock and the narrow spatial distribution, the Brabant Massif is not associated with any of the volcanic, geothermal or tectonic settings described above. Although the seismicity within the seismotectonic zone of the Brabant Massif is considered as to be rather moderate, still few of the largest (historical) earthquakes in Western Europe have occurred within this slate belt (Camelbeeck et al., 2007). Linking these historical large earthquakes to potential individual fault structures has been difficult in the past, because of a lack of aftershocks and due to the limited seismic network that was unable to record small seismic events. The rapid installation of a local network in the epicentral area of the 2008-2010 seismic swarm, however, allows us to visualize and to study for the first time an extremely well documented seismic event in the old geological structure of the Brabant Massif. This study aims at investigating to what specific part of a geological structure the swarm may correspond. First, the hypocentre location is improved by the cross-correlation of waveforms of co-located events. Waveforms of the largest earthquakes are compared to analogue waveforms of a seismic swarm that occurred between 1953 and 1957 at Court-Saint-Etienne in the same epicentral area as the 2008-2010 swarm. A 3D analysis of the relocated hypocentre distribution allows understanding the dimension of the structure and framing the seismic sequence within the tectonic structure of the Brabant

Massif. Using the orientation of the seismic swarm, we attempt to link the fault structure to a relevant tectonic structure via magnetic data. These data are matched-filtered to highlight anomalies that are likely to be due to sources at depths of interest. Such structures are of interest as they can play an important role accommodating deformation in a current stress field. Finally, stress inversion of the focal mechanisms of the largest-magnitude events is performed, allowing derivation of a best-fitting stress tensor and discussion of its correspondence to the regional stress field in northwestern Europe.

## 1.2. Temporary network and time history of seismicity

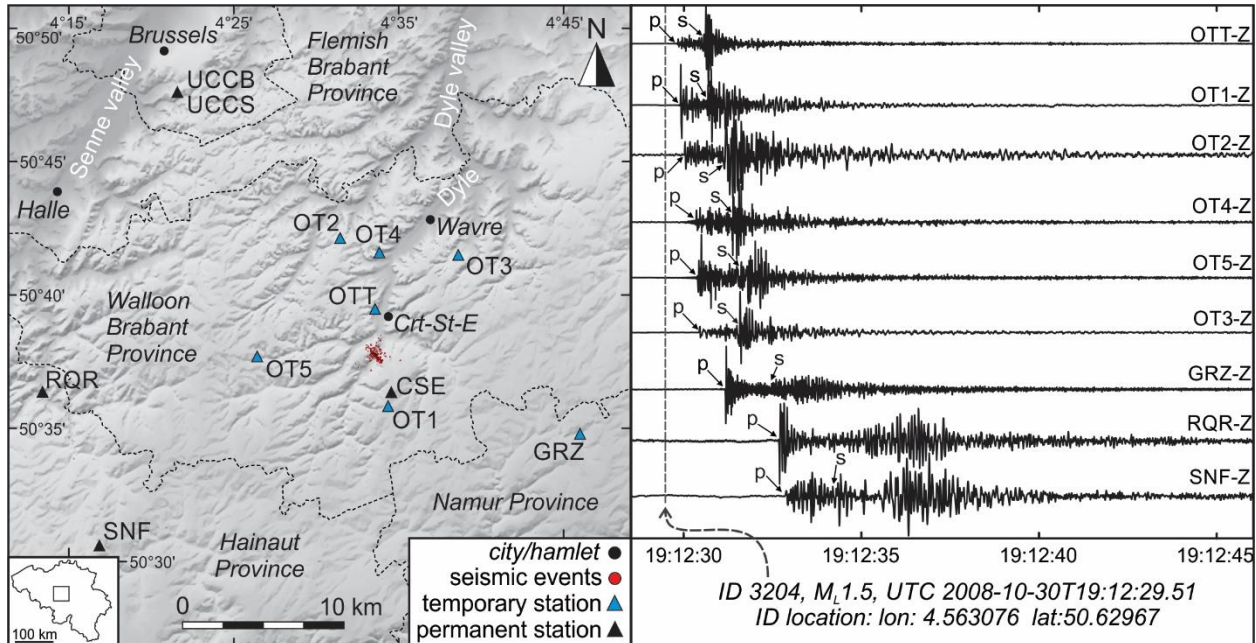


**Figure 1: a)** Localisation map of the temporary seismic network (blue triangles) and the nearby permanent stations (black triangles) in the Walloon Brabant Province. Abbreviations of stations can be found in the text. The red circles show the relocated seismic events of the 2008-2010 seismic swarm. Background DEM map © Nationaal Geografisch Instituut. **b)** Waveforms of a  $M_L$  1.5 earthquake recorded by the temporary and permanent seismic network, sorted by increasing distance to the epicentre.

The Brabant Walloon seismic swarm started on 12 July 2008 with a  $M_L$  2.2 earthquake at a depth of 6.3 km. It was followed the day after by a  $M_L$  3.2 earthquake at 5.9 km depth, the largest earthquake in the seismic sequence. As soon as seismologists of the Royal Observatory of Belgium started to realise that the seismic activity potentially could last for a very long time, a dense temporary seismic network was deployed in the Court-Saint-Etienne – Ottignies area in a 10 km radius around the epicentres (Figure 1). Installing a temporary network is important as detailed seismic records allow recording very small events that cannot be detected by distant stations, and allow relocating all seismic events properly. Immediately after the occurrence of the first events, two stations were installed on 14 July 2008. Afterwards, another 5 seismic stations were installed. The temporary network with 7 local stations was fully operational between 12 August 2008 and 20 July 2010 and consisted of 4 short period LE-3D/5s seismometers and 3 CMG-3ESPC broadband seismometers that were installed in the hamlets of Grand Leez (GRZ), Mellery (OT1), Rixensart (OT2), Dion-le-Mont (OT3), Limal (OT4), Genappe (OT5) and Ottignies (OTT). After the removal of the temporary network, a permanent station was installed on 13 July 2010 in Court-Saint-Etienne (CSE) to monitor the area continuously. The closest active permanent stations are the Senefte (SNF), Ronquières (RNQ), Uccle (UCCS, UCCB) and Steenkerque (SKQ) stations (Figure 1).

Station	Name	Longitude	Latitude	d_epi (km)	Altitude (m)	Seismometer	Installation	End time
OTT	Ottignies	4.5600	50.6590	3.27	77	CMG-3ESPC	7/14/2008	8/6/2010
OT1	Mellery	4.5729	50.5971	3.69	156	LE-3D	8/11/2008	8/6/2010
OT2	Rixensart	4.5251	50.7041	8.70	102	LE-3D	8/12/2008	8/6/2010
OT3	Dion-le-Mont	4.6440	50.6934	9.09	102	LE-3D	8/12/2008	8/6/2010
OT4	Limal	4.5644	50.6948	7.24	84	LE-3D	8/11/2008	1/19/2009
OT5	Genappe	4.4409	50.6284	8.62	130	LE-3D	8/11/2008	7/20/2010
GRZ	Grand-Leez	4.7670	50.5790	15.45	152	CMG-3ESPC	7/14/2008	8/6/2010
CSE	Court-Saint-Etienne	4.5767	50.6061	2.79	157	CMG-3ESPC	Permanent since 2010-07-13	
UCCB <sup>a</sup>	Uccle	4.3605	50.7973	23.47	-10	CMG-3T	Permanent	
UCCS <sup>b</sup>	Uccle	4.3605	50.7973	23.47	104	CMG-3ESPC	Permanent	
SNF	Seneffe	4.2820	50.5077	24.05	108	L4-C	Permanent	
RQR	Ronquières	4.2246	50.6062	24.02	40	L4-C	Permanent	
SKQ	Steenkerque	4.0796	50.6487	34.16	63	LE-3D	Permanent	

<sup>a</sup> UCCB: seismometer installed in the basement rocks of the Brabant Massif in a 114 m deep borehole.

<sup>b</sup> UCCS: surface seismometer above UCCB.

**Table 1:** Location of temporary and permanent stations and their installed equipment. *d\_epi*: Epicentral distance of each station to the relocated epicentre of the  $M_L$  1.5 event (see Appendix A) shown in Fig. 3.

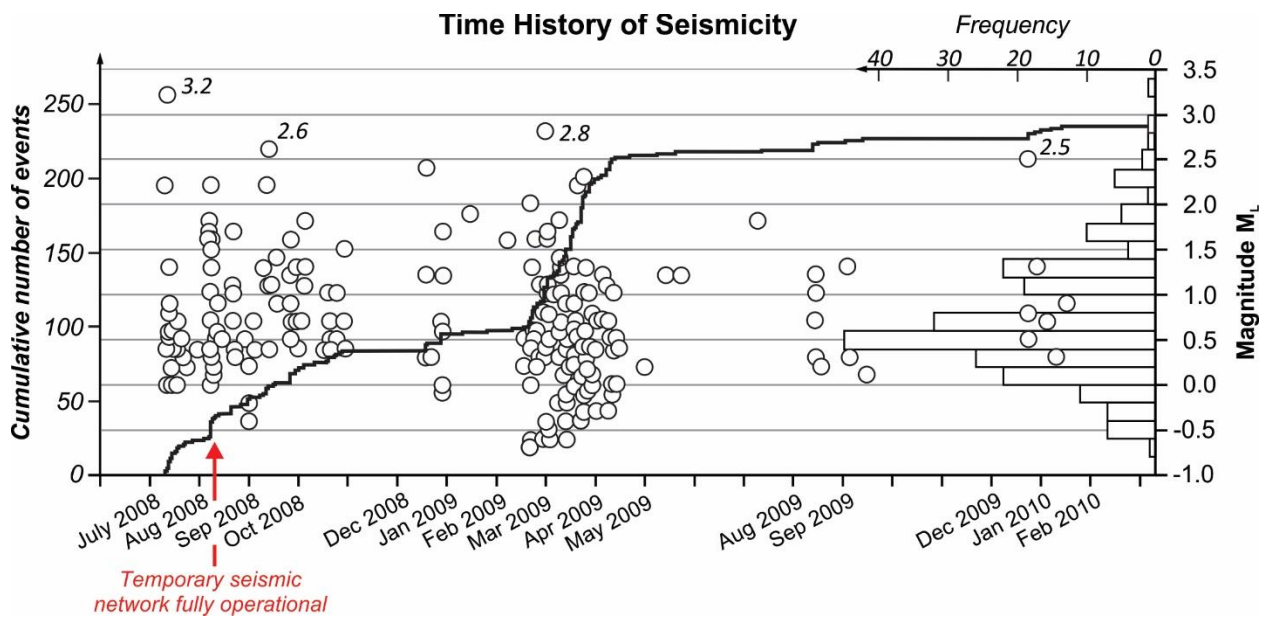


**Figure 2:** Time history of seismicity of the 2008-2010 seismic swarm in function of the cumulative amount of events and the local magnitude of earthquakes. The histogram displays the distribution of events in function of magnitude steps of  $M_L$  0.2. Five periods of increased seismicity are detected: summer 2008, winter 2008, spring 2009, autumn 2009 and winter 2010. There is no relationship between time history of earthquake occurrence and earthquake magnitude.

P- and S-wave arrival times were manually picked on a daily basis. Based on the time difference between P- and S-wave arrivals, amplitude and period measurements, a local magnitude  $M_L$  was estimated for each individual event. Earthquake magnitudes of the Walloon Brabant seismic swarm range randomly from  $M_L$  -0.7 to  $M_L$  3.2 without any clear relationship between earthquake magnitude and the time history of seismicity. Such absence of correlation between earthquake magnitude and time history of events is typical for seismic swarms (Mogi, 1963) although higher magnitude earthquakes are often detected at the onset of a seismic swarm (e.g. in West-bohemia, Fischer et al., 2014).

The time history of seismicity of the 239 recorded events shows that the seismic sequence can be subdivided in several periods of seismic activity alternating by periods of seismic quiescence (Figure 2). A first large swarm activity (109 events) took place in the summer and autumn of 2008. After inactivity during 51 days the swarm shortly revived between 20 and 29 December 2008 (11 events). A second large



activity took place in the spring of 2009 (119 events) during which the seismic rate increased to sometimes ten events per day. Subsequently, some sole events occurred in the summer of 2009. A minor amount of activity was detected in December 2009 (5 events) and January 2010 (3 events). Finally, 1.5 years after it started, the seismic sequence ended with two seismic events on 30 January 2011. Recently, however, a single  $M_L$  1.0 event occurred on 10 January 2014. A full catalogue of all events with their timing, magnitude and location can be found in the Appendix A.

The individual seismic moment  $M_0$ , i.e. the amount of energy released by each earthquake, has been calculated. The cumulative energy release of  $M_0$  is totally dominated by the  $M_L$  3.2 event, noting that more than half of the total energy was released during this event. Apart from the  $M_L$  3.2 event,  $M_L > 2$  events characterise most of the remaining energy release through time. The total cumulative seismic moment, i.e.  $M_0 = 2.58 \times 10^{14}$  N.m would correspond to an individual earthquake with magnitude  $M_L$  3.9 using the local empirical relationship between  $M_0$  and  $M_L$  of Reamer and Hinzen (2004) applicable for Northern Rhine region. Given the time interval of 2 years, the Walloon Brabant swarm did release its seismic energy rather slowly over a small scale.

The online “*Did You Feel It?*” macroseismic data acquisition system of the Royal Observatory of Belgium (Lecocq et al., 2009) showed that 60 events, with magnitudes between  $M_L$  0.4 and  $M_L$  3.2, of 239 events of the 2008-2010 seismic sequence were felt by the local population. The macroseismic spatial distribution of the  $M_L$  3.2 event evidences that this earthquake was felt at distances larger than 75 km, from Charleroi to the north of Brussels, and from the west of Brussels to Liège. Remarkably, sometimes also very small events with a magnitude as low as  $M_L$  0.7 were perceived by the respondents. Most of these small events were actually more often heard than felt. Given these small magnitudes this sound perception is indicative of a local high-frequency earthquake source.

### 1.3. Magnitude-frequency distribution

The recurrence of earthquakes with various magnitudes that are generated by a faults can be visualised in a cumulative magnitude-frequency distribution (MFD) and is commonly described by the Gutenberg-Richter relationship (Gutenberg and Richter, 1956):

$$\text{Log}_{10} N = a - b.M \quad (\text{Equation 1})$$

where  $N$  is the number of earthquake,  $M$  is the magnitude of those events, and  $a$  and  $b$  are the intercept and slope of a least squares best fit to the MFD. The Gutenberg-Richter relationship is effectively a measure of the relative occurrence of small to large earthquakes. The range of  $b$ -values can vary widely and depends on the nature and spatiotemporal evolution of earthquake swarms. Volcanic swarms produce  $b$ -values up to 2.5, indicating a large proportion of small earthquakes relatively to large ones, whereas  $b$ -values of non-volcanic, intraplate tectonic swarms range 0.8-1.1 (Hainzl and Fischer, 2002; Ibs-von Seht et al., 2008).

The minimum magnitude of complete recording ( $M_c$ ) is an important parameter that indicates the magnitude below which no proper  $b$ -value can be calculated due to incompleteness of the dataset. This is usually expressed by a change of the slope of the MFD fit towards lower magnitudes. The MFD for the 2008-2010 seismic swarm shows that small-magnitude events between  $M_L$  0.0 and  $M_L$  0.8 are highly represented (Fig. 4a). Below magnitude  $M_L$  0.4, the slope of the cumulative MFD changes considerably. This is partly because small events were not recorded before the local network was fully operational and also because human and industrial activity during daytime hours results in low signal-to-noise levels. This is particularly apparent in the magnitude versus time plot (Fig. 4b). Consequently, seismic events with magnitude below  $M_L$  0.4 in the swarm catalogue could only be detected during evening- and nightly hours (18h00 – 06h00). This suggests that the catalogue is incomplete and underrepresented for events below  $M_L$  0.4. Based on the 89 events below  $M_L$  0.4 that were picked during the night (18h00 - 06h00), one may add a same amount of 89 events below  $M_L$  0.4 to the 239 detected events in the catalogue to

account for those events that were missed during the working hours. Such a modified catalogue of 328 events would, however, only slightly affect the  $b$ -value as only low magnitudes would be added.

For  $M_c = M_L$  0.4,  $a$ - and  $b$ -values of 2.017 and 0.662, respectively. The  $b$ -value of the whole 2008-2010 catalogue is only a little lower than the 0.87  $b$ -value calculated for the entire ROB catalogue representative for all earthquakes that occurred in Belgium and the surrounding areas (Leynaud et al., 2000). This  $b$ -value is in agreement with a  $b$ -value range between 0.8 and 1.1 calculated from other intraplate seismic swarms (Hainzl and Fischer, 2002; Ibs-von Seht et al., 2008). Additionally, it has to be noted that global  $b$ -values for seismic swarms in literature are sometimes calculated from moment magnitudes ( $M_w$ ), whereas the  $b$ -value of the Walloon Brabant seismic sequence is calculated from local magnitudes. Based on local conversions between  $M_L$  and  $M_w$ , the  $b$ -value estimated from  $M_L$ , however, will slightly underestimate a  $b$ -value estimated from  $M_w$ . Nevertheless, our results are interesting because they indicate that individual structures or an individual fault visualised by earthquake swarms can produce a robust Gutenberg-Richter relationship, something that has been questioned and discussed (e.g. Hofmann, 1996).

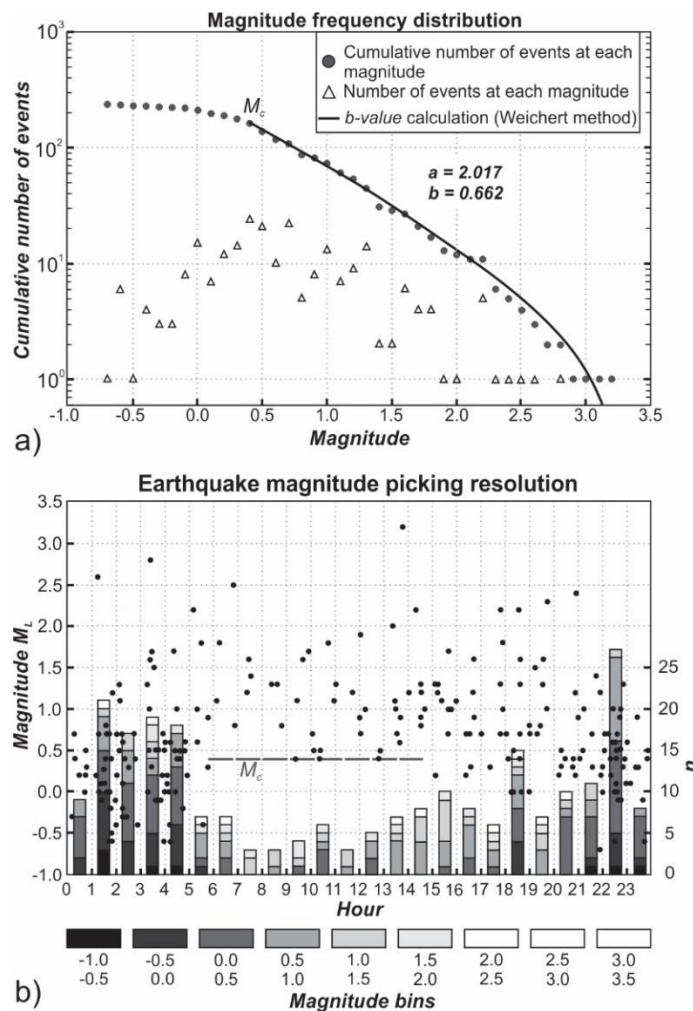


**Figure 3:** **a)** Individual and cumulative magnitude frequency distribution (MFD) for the entire 2008-2014 earthquake catalogue (239 events). The  $a$ - and  $b$ -values of the Gutenberg-Richter relationship have been calculated in the range of  $M_c = 0.4 < M_L < 2.5$  and are 2.017 and 0.662, respectively. **b)** Resolution of the picked events after installation of the local seismic network. Due to the high signal-to-noise ratio during the daytime (6h-21h), minimum magnitude of detection was  $M_L$  0.4. During the night-time, events down to  $M_L$  -0.7 could be picked. Magnitude completeness ( $M_c$ ) of the seismic catalogue is therefore set at  $M_L$  0.4.

### 1.4. Earthquake location, waveform cross-correlation and event relocation

To localise the structure that was responsible for the seismic sequence, it was necessary to first locate all seismic events of the swarm spatially and then relocate all the determined locations with a greater precision. For each seismic event, the P- and S-phases have been eye-picked when feasible. The epicentre location of each event is computed using Hypo2000, i.e. a ROB-modified version of Hypo71 (Lee and Lahr, 1972). This modified algorithm computes 500 locations (instead of one in Hypo71) for each earthquake event by adding or subtracting random noise to P- and S-wave measurements, with a maximum error of 0.05 s and 0.10 s, respectively. The centroid of the 500 location "cloud" is then taken as final solution and the location error is determined by evaluating the size of the cloud.

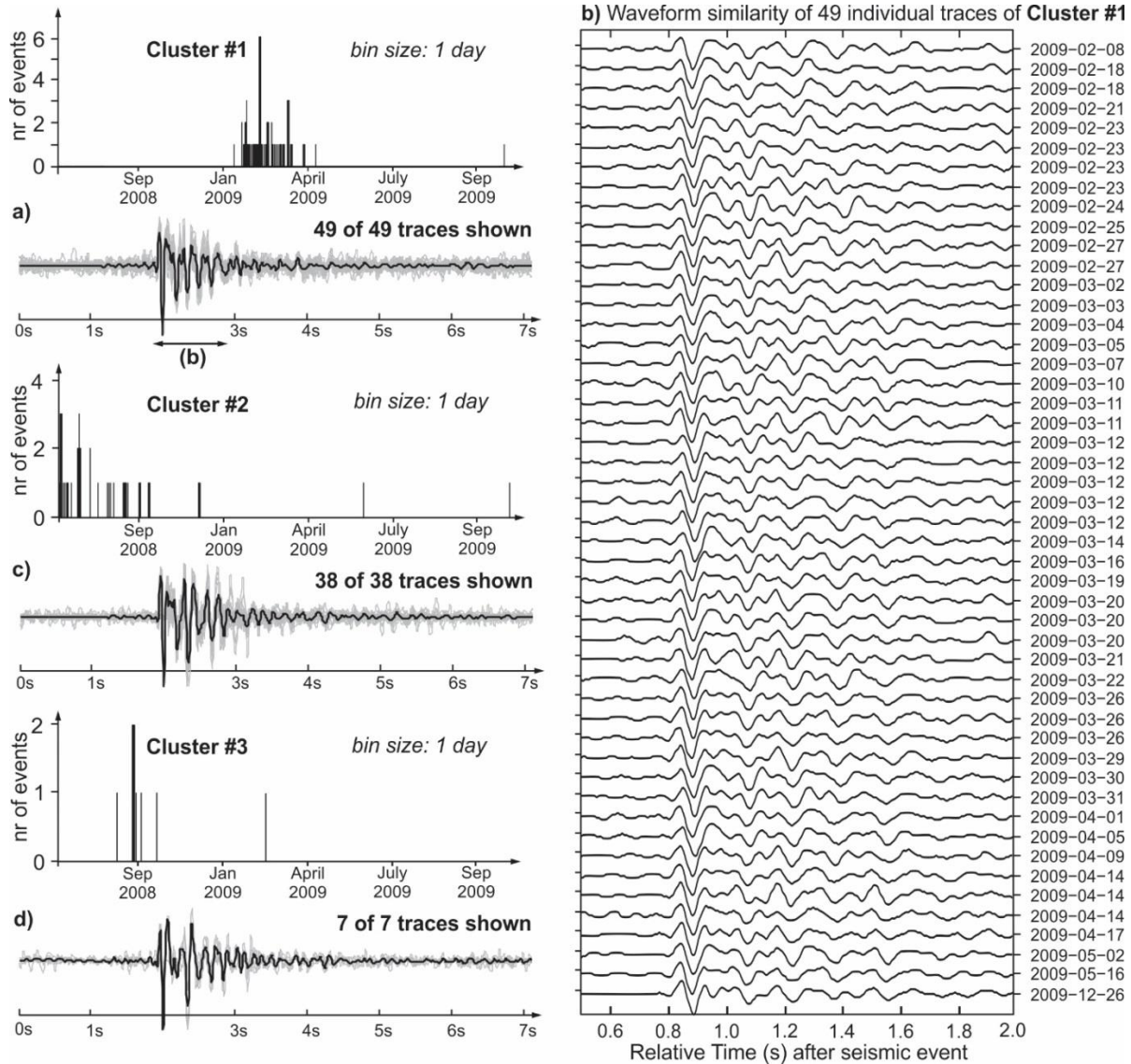


**Figure 4:** Example of waveform comparison, event clustering and overlay of events recorded at the Ottignies (OTT) temporary seismic station. All first P-wave arrivals of different events are placed simultaneously to correlate and compare the difference waveforms. This allows improving the arrival time and the hypocentre location. Three different clusters can be deduced. **a)** Cross-correlation of waveforms of the spring 2009 activity shows a high similarity. **b)** Cross-correlation of 49 individual traces. Note that the similarity of the first 0.6s after the first P-wave arrival is strikingly similar. **c)** Cross-correlation shows that 34 events of the autumn 2008 activity are comparable to 4 other events of the swarm. **d)** Cross-correlation and timing of additional 7 events.

Many P- and S-events have very similar waveforms (Lecocq, 2011). As the seismic sequence seems to occur in a very small rock body, relocation tools are applied in order to improve the relative location between nearby events by calculating travel time corrections between events and stations. To execute this task the double-difference algorithm HypoDD (Waldhauser and Ellsworth, 2000) is used. In this software method, the waveforms of co-located earthquakes, i.e. very closely located events, recorded at a single station are compared to each other, allowing further improvement of the hypocentre locations (Schaff and Waldhauser, 2005).

Cross-correlation differential times for HypoDD are obtained by using hypoDDpy (Krischer, 2015) and ObsPy (Beyreuther et al., 2010). Clustering has been done using the Correlation Toolbox from the GISMO suite, a Matlab toolbox for seismology (University of Alaska Fairbanks). In the relocation method, the first P- and S-wave arrivals of each event, recorded either at a permanent or at a temporary single station, are mutually compared in a time frame window to the P-wave and S-wave arrivals of all other events recorded at the same station (Fig. 5).

Waveform similarity of co-located earthquakes indicates that the source of these events is nearly equivalent and that the ray trajectories from source to receiver are at about the same and travelled through an almost identical medium. Differences between travel times are then solely attributed to the corresponding distance between hypocentres. Identification of repeated events or multiplets can be performed either by comparing all traces visually or by calculating the cross-correlation coefficient of an event that is cross-correlated with all other events in a similarity cross-correlation matrix, indicating the degree of waveform similarity between events. The correlation function only measures the normalised similarity of the waveform shape but not the amplitude of the events. For events with a higher correlation the travel path will be identical but the strength of the source might differ.

Many of the events of different swarm activity periods show similar waveforms. For the spring 2009 activity, for example, cross-correlation shows that 49 events of all events recorded at the Ottignies station (OTT, station deployed directly on the bedrock) show a waveform similarity of more than 75% (Figure 4a, b). Events of the autumn 2008 period also show a high similarity similar (Figure 4c,d). Cross-correlation thus demonstrates the tight spatial grouping of the events.

The original locations of the seismic swarm (see white dots in Figure 5 for original location before cross-correlation) show a dense patch of events that are separated from the first two  $M_L$  2.2 and  $M_L$  3.2 earthquakes by a northward offset of 900 m. This offset is attributed to the absence of local network during the two first events. In order to calculate the precise focal mechanisms of these two large events (see section 3.5), these two event needed to be relocated properly. Based on the strongly comparable waveforms and on the large cross-correlation in the similarity matrix of the Steenkerque seismic station (SKQ), the July 12 2008  $M_L$  2.2 and July 13 2008  $M_L$  3.2 events cross-correlate to the waveform of the September 13 2008  $M_L$  2.6 event and to some other minor events in the September cluster. The waveforms of the September 2008 cluster on their turn cross-correlate to many of the events of the 2009 spring cluster. Consequently, given the large similarity of these different events, the  $M_L$  2.2 and  $M_L$  3.2 events can be relocated relatively close to the other clusters (Figure 5). Cross-correlation thus allows applying a location correction to account for the northwards shift of the epicentre location of the first two large earthquakes in the final earthquake catalogue (Appendix A). This northwards error is not present anymore for all subsequent events as, due to the installation of the temporary network, the closest station being at 1.5 km from the epicentre. All events that took place after the local network was removed, e.g. such as the 14 January 2014 event (see Appendix A), are still cross-correlated with the 2008-2010 events to relocate these new events.

By cross-correlation, the manually picked P- and S-wave arrival times could be refined to subsample spacing of a few milliseconds (below 0.008s for 125Hz sampling rate, Deichmann and Garcia-Fernandez, 1992). Afterwards, these new picks are used as an input to HypoDD to improve the quality of the original hypocentre locations.



Ultimately, by considering the difference in travel times between the different events, the original location of the Walloon Brabant seismic swarm was considerably improved (Figure 5). The relocated hypocentres form a dense cluster both in horizontal and vertical direction. The orientation of the epicentres suggest that the swarm occurred along a narrow, 1.5 km-long NW-SE oriented fault zone in the Faux area, a small hamlet 3 kilometre south of Court-Saint-Etienne (see depth plots in Figure 5).

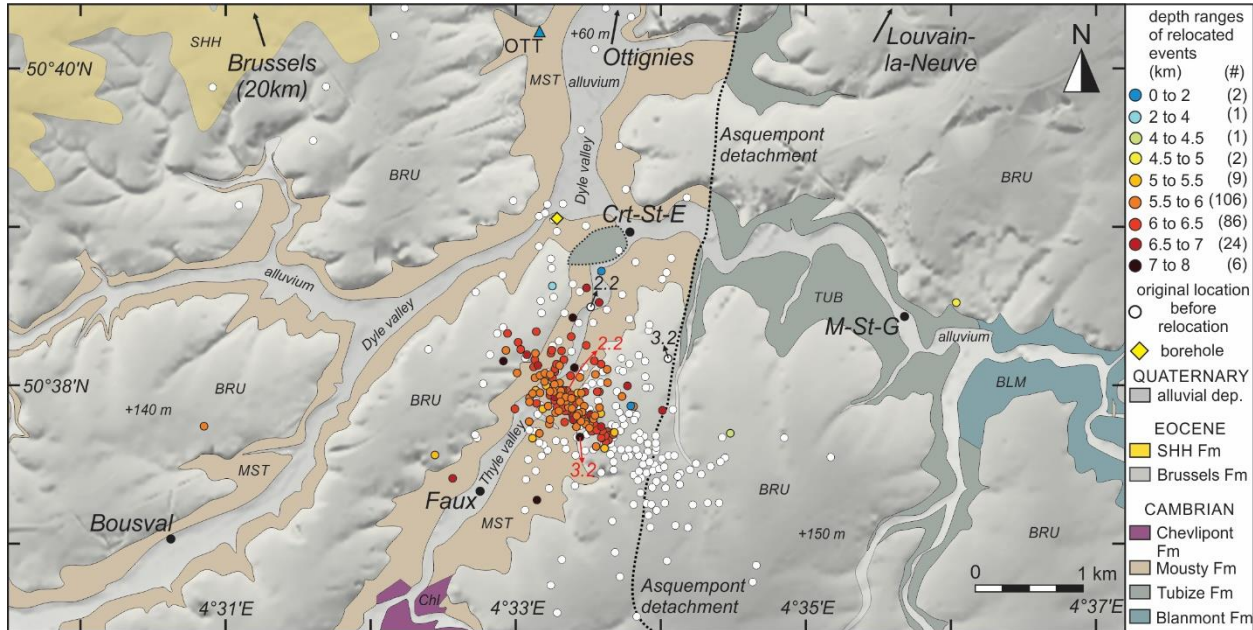


**Figure 5:** Simplified geological map of epicentral area. The Thyle and Dyle river valleys incised in the Cambrian basement rocks of the Brabant Massif. The basement rocks on the hill tops are only covered by the sandy Eocene Brussels Formation. Comparison of the epicentral distribution of the seismic swarm before (white dots) and after (dots coloured by depth) relocation by cross-correlation. The relocated epicentres delimit a narrow NW-SE oriented fault zone dipping steeply to the NE. The contact between the Tubize (TUB) and Mousty (MST) Formation indicates the position of the Asquempont detachment fault (dotted grey line). Basemap is the digital elevation model (©Nationaal Geografisch Instituut) of the epicentral area. Crt-St-E: Court-Saint-Etienne; M-St-G: Mont-Saint-Guibert; SHH= Sint-Huibrechts Hern.

Relocating all hypocentres allows performing a 3D analysis on the hypocentre distribution in function of depth versus time of occurrence (Figure 6a). From this hypocentre distribution it is clear that the swarm activity is restricted to a rather narrow volume situated between 5 km and 7 km depth. To estimate the true dip of the fault structure, we use the method of Camelbeeck (1993), which describes an ellipsoid defined by 95% of the hypocentres. Applying this method to the hypocentre cloud of relocated events shows that the NW-SE fault zone dips steeply to the NE at an angle of  $\sim 87^\circ$  (Figure 6a). The swarm is thus clearly limited both in vertical and horizontal dimension.

Only in very short time slots a spatial distribution and depth correlation can be found. For example, 6 events of the spring 2009 cluster occurred within three hours (i.e. between 2009-03-26-22:31:19 and 2009-03-27-01:57:12). Spatially, these events were only separated from each other by a distance of 100 m (between 5.846 km and 5.947 km depth; see event numbers 180-185 in the catalogue in the supplementary data). Similarly, other depth correlations can be found in other very short time windows. However, if the whole swarm is considered, hardly any correlation between depth and rupture propagation through time can be found. This absence of correlation conflicts with fluid- or gas-driven seismic swarms that are characterised by an upwards migration of events.

All events that took place after the local network has been removed, e.g. the event that took place on 14 January 2014, (Appendix A), are still cross-correlated with the 2008-2010 events to relocate these events.

The locally installed network can currently thus be applied as a *phantom network* to validate and cross-correlate new events that would occur on the same location.

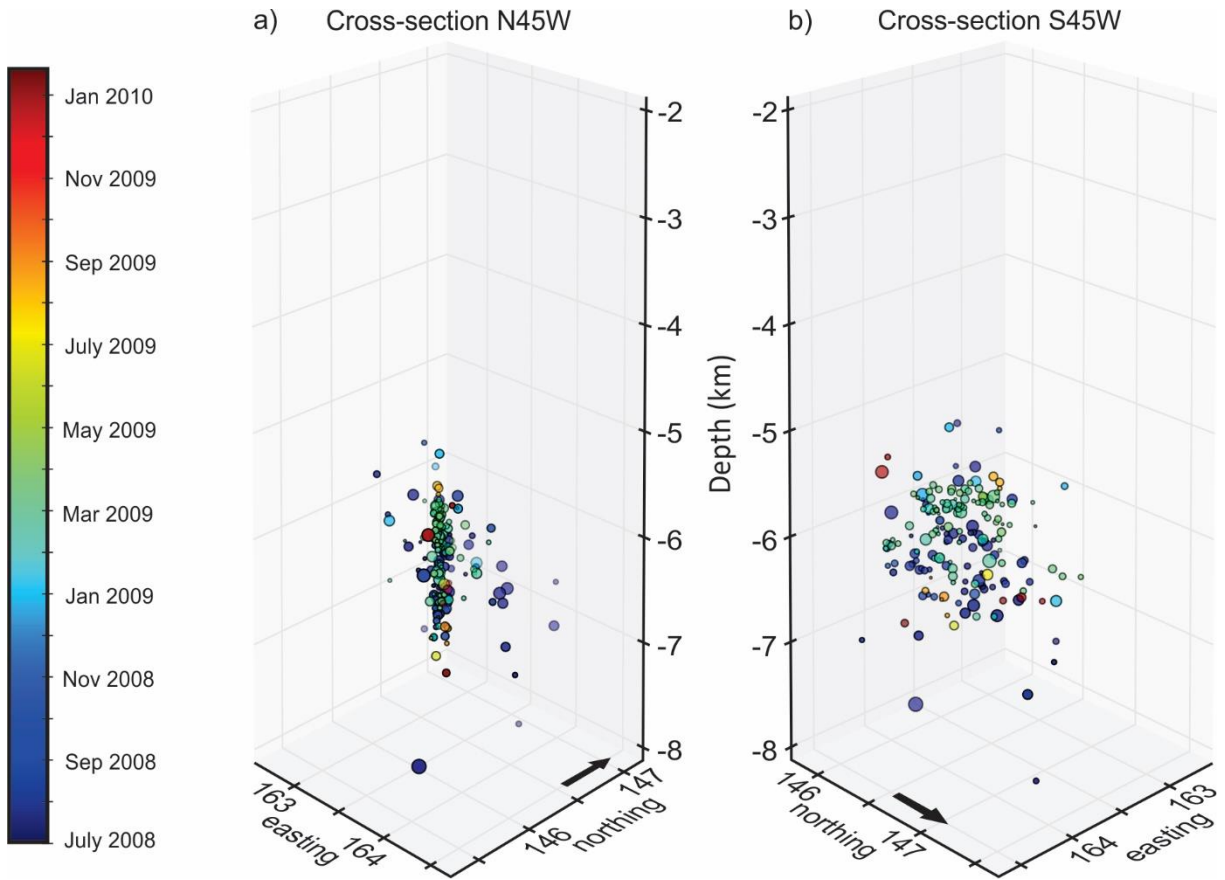


**Figure 6:** Three-dimensional hypocentral distribution of the 2008-2010 seismic swarm in function of depth and the time past after the first event. The colours display the temporal evolution of the earthquake swarm from the first event (12-07-2008) onwards. Note the linearity of the events and the limited horizontal distribution of the swarm. Size of the events corresponds to the magnitude variation within the swarm. **a)** N45W cross-section parallel to the fault structure. **b)** S45E in plane section perpendicular to the fault. The horizontal axis is in local Belgium Lambert 1972 coordinates (kilometre scale); vertical and horizontal dimensions are to scale. Black arrow = North.

## TASK 2 – Calculation of focal mechanisms and tectonic stress inversion

### 2.1. Fault plane solutions

The focal mechanism is the geometric description of the brittle deformation produced by earthquakes. These were calculated from the P-wave first motion polarities of the individual earthquakes that arrive at different seismic stations using *fpsol*, an algorithm that computes the nodal planes by minimising the misfit between theoretical and observed P-wave first motions projected on the focal sphere (Camelbeeck, 1993). The calculation of focal mechanisms allows determining the orientation (strike, dip) and slip vector on each plane of the fault zone. These can then be used to derive the associated tectonic stress responsible of the fault and thus of the earthquake activity. The Belgian network geometry and station spacing allowed for the determination of 10 fault plane solutions with a probability of 95% for events  $> M_L$  1.6. For each of these fault plane solutions, the focal sphere was centred on the relocated hypocentre, assuming that the relocations provide a better homogeneity of the dataset (Figure 7).

The comparison between the spatial distribution of relocated earthquakes and their focal mechanisms show a clear match between one of the two nodal planes and the distribution (Figure 8). Based on the spatial distribution of the different events, the distinct, steeply dipping, NW-SE to NNW-SSE fault zone automatically distinguishes the NW-SE nodal planes as the actual fault plane and the NE-SW-oriented planes as the auxiliary planes (Table 2, Figure 8). Each of the 10 focal mechanisms defines a left-lateral oblique to purely left-lateral strike-slip movement of the nearly vertical fault zone.

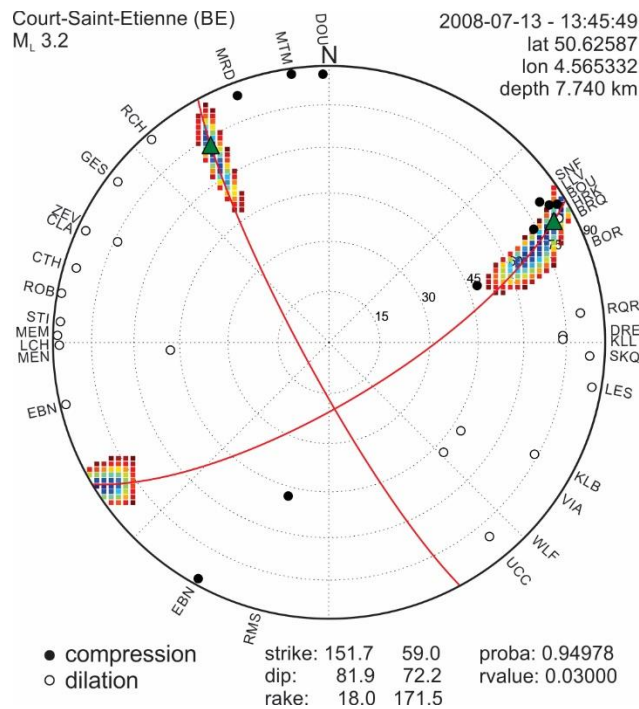


**Figure 7:** Focal mechanism computation of the  $M_L$  3.2 event (at a depth of 5.7 km) on the focal sphere. Degrees in the focal sphere correspond to the angle of the position of the seismic station relative to the event. The coloured contours represent a 95% probability or higher. Explication of the station abbreviations of the Belgian network can be found on [www.seismology.be](http://www.seismology.be).

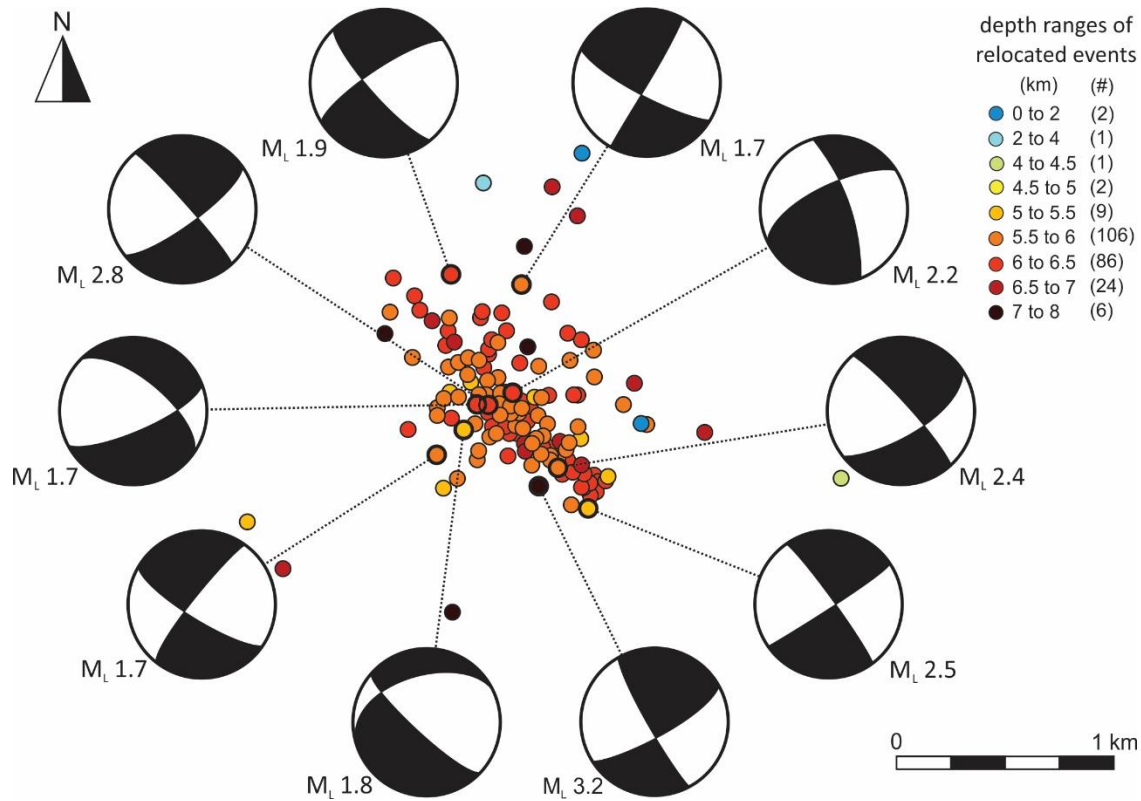


**Figure 8:** Focal mechanisms of all events for which a reliable mechanism could be calculated. The seismic swarm is dominated by left-lateral strike-slip motion. The orientation of the swarm indicates that the NW-SE nodal plane can be interpreted as the true fault plane.

Event		Location			Magn.	Fault Plane			Nodal Plane			SH		Stress Regime
Id	Time	Lon	Lat	Depth	$M_L$	Strike	Dip	Rake	Strike	Dip	Rake	Max	Min	Regime
3069	20080713-13:45:49	50.62587	4.565332	7.740	3.2	151.7	81.9	18.0	59.0	72.2	171.5	105	15	SS
3090	20080808-09:54:39	50.63412	4.564285	6.336	1.7	119.2	74.0	0.9	28.9	89.1	164.0	74	164	SS
3094	20080808-17:52:02	50.62817	4.560497	5.474	1.8	133.0	73.7	-62.0	250.8	32.1	-148.1	102	12	NF
3165	20080912-05:08:55	50.62995	4.562925	6.406	2.2	341.8	72.0	32.0	240.8	59.7	159.0	111	21	SS
3225	20081220-20:53:08	50.62695	4.566024	5.652	2.4	318.8	80.1	-30.0	54.4	60.5	-168.6	97	7	SS
3232	20081229-03:27:55	50.62709	4.558643	5.715	1.7	123.0	70.4	-12.5	217.2	78.3	-160.0	80	170	SS
3239	20090115-12:02:24	50.63454	4.559644	6.458	1.9	139.5	72.0	-20.0	235.9	71.0	-160.9	98	8	SS
3273	20090303-03:23:32	50.62994	4.561393	6.264	2.8	319.8	82.2	-20.0	52.6	70.2	-171.7	96	6	SS
3276	20090305-04:21:42	50.62936	4.561387	6.088	1.7	310.7	49.7	-35.0	65.1	64.0	-134.0	98	8	NS
3552	20091226-06:50:13	50.62489	4.568443	5.469	2.5	324.7	82.8	-6.0	55.5	84.0	-172.7	101	11	SS

**Table 2:** Database of the 10 reliable earthquake focal mechanisms of the 2008-2010 seismic swarm used for stress inversion. Location gives the orientation after relocation.  $M_L$  = Local earthquake magnitude. Strike, dip and rake of the nodal plane interpreted as the fault plane and the auxiliary nodal plane are given. SH: Horizontal Shortening. Stress regime: SS = strike-slip; NF = normal faulting; NS = combined normal and strike-slip faulting.

## 2.2. Fault plane solutions

Principal stress orientations active during faulting can be derived from fault slip data along representative faults. Stress inversion assumes the Wallace-Bott hypothesis (Bott, 1959; Wallace, 1951), which states that slip occurs parallel to the resolved shear stress on a pre-existing or along a newly formed fault plane. The inversion technique involves the concept of (i) deriving the best-fitting stress tensor capable of explaining the direction of slip along the fault and (ii) deriving the magnitude of the principle stress



directions. In this method, the data are first processed interactively using the Right Dihedral Method (Angelier and Mechler, 1977) optimised in the Win-Tensor programme (version 4.0.4), a software tool specifically developed for the derivation of the orientation of the principal stress axes of the regional stress tensor (Delvaux and Sperner, 2003). The Right Dihedral Method is independent of the choice of nodal planes and gives a range of possible orientations of  $\sigma_1$ ,  $\sigma_2$  and  $\sigma_3$ . The iterative grid search “Rotational Optimisation” method is applied to the results of the inversion by using a misfit (F5 in the Win-Tensor programme, see Delvaux and Sperner, 2003 for details).

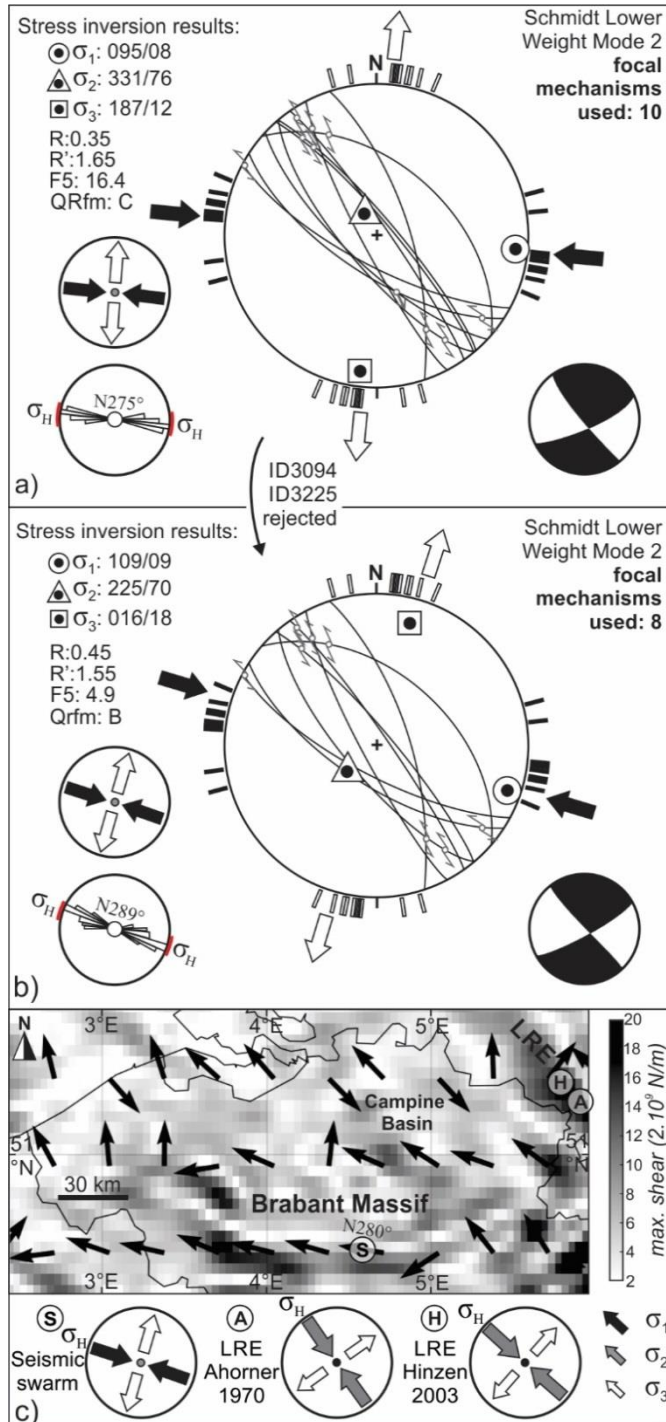


**Figure 9:** Lower-hemisphere equal-area stereoplots of the true nodal planes showing stress inversion results (Win-Tensor programme). Results are represented by (i) the orientation (in plunge/trend convention) of three principal stress axes and (ii) the direction of  $S_{Hmax}$  (black arrows) and  $S_{Hmin}$  (white arrows). The bars outside the stereograms show the stress inversion result of each individual focal mechanism ( $\sigma_H$  = black and  $\sigma_h$  = white). The lower right inset shows the corresponding focal mechanism of all weighted fault plane solutions. The two lower left insets show the maximum principal component ( $\sigma_H$ ). The uncertainty of  $\sigma_H$  is expressed by the red bars outside the lower left stereoplots and is within the range of the individual stress inversion bars.

**a)** Inversion of 10 selected events representative for the seismic swarm.  $\sigma_H$  has a N275° (WNW–ESE) orientation but a high misfit of 16.4%.

**b)** Rejection of a normal and oblique event results in a lower misfit (4.9%) and a more reliable stress tensor with a  $\sigma_H$  oriented N289° (WNW–ESE). R = stress ratio; QRfm = quality factor of stress tensor following World Stress Map criteria (C = medium, B = good); F5 = misfit function of results (Delvaux and Sperner, 2003); R' = stress regime index (R' = 2-R for a strike-slip regime).

**c)** Map showing local stress tensor variation in central and north Belgium estimated from differences in the gravitational potential energy after the method of Camelbeeck et al. (2013). Black arrows indicate local stress orientations. LRE: Lower Rhine Embayment. S = location of the seismic swarm. Note the similarity between local stresses and the stress orientation derived in b). See Task 4 for a discussion of this figure.

By using the Win-Tensor programme, first both nodal planes of each calculated focal mechanisms, with their accompanying slip lines, are inverted to a stress tensor. As the alignment of epicentres identifies the NW-SE oriented nodal plane in the focal mechanism as the actual ruptured fault plane and the NE-SW oriented planes as the auxiliary plane, the final inversion includes only those focal planes that are best fit to the local stress field. The graphical output of the inversion into an equal-area stereographic projection then allows evaluation of the overall quality of the stress inversion. During the inversion process, an exponential weighting factor that is a function of the magnitude of the earthquakes is used. This factor effectively emphasizes higher magnitude events. For example, stress inversion of the  $M_L$  3.2 event is weighted as much more important on the overall result as stress inversion of the  $M_L$  2.2 event.

Stress inversion of the 10 different focal mechanisms shows a local WNW-ESE oriented  $\sigma_H$  ( $\sigma_1 \sim 08/095$ ), NNE-SSW  $\sigma_h$  ( $\sigma_3 \sim 12/187$ ) and a nearly vertical  $\sigma_v$  ( $\sigma_2 \sim 76/331$ ) which corresponds to a left-lateral and nearly pure strike-slip stress regime (*Figure 9*). The orientation of individual stress axes are indicated in a plunge/trend convention. The relative magnitude of the three principle stresses, i.e. the stress ratio  $R = (\sigma_1 - \sigma_2) / (\sigma_1 - \sigma_3)$ , has a value of 0.46 and defines three different and well-defined stress magnitudes indicative of the pure strike-slip nature of the seismicity (Table 3). The relative magnitude of the three principal stresses, i.e. the stress ratio  $R = (\sigma_1 - \sigma_2) / (\sigma_1 - \sigma_3)$ , has a value of 0.46 and defines three different stress magnitudes indicative of the pure strike-slip nature of the seismicity (Table 3).

It has to be noted that there is an uncertainty in the stress tensor as only 10 focal mechanisms of the swarm are analysed. The uncertainty (express as the misfit function F5 in Fig. 11; Table 3) is improved considerably after removal of a normal (ID 3094) and an oblique (ID 3225) event, resulting in a slightly different stress tensor with an orientation of  $N289^\circ$  for  $\sigma_H$ . Based on these results we can thus attribute a left-lateral fault mechanism to the seismic swarm as the current driving force of deformation.

$\sigma_1$	$\sigma_2$	$\sigma_3$	R	F5	R'
095/08	331/76	187/12	0.35	15.2	1.54

**Table 3:** Stress tensor parameters derived from inversion of the focal mechanisms.

## TASK 3 – Seismotectonic setting of the Brabant Massif and integration of results

### 3.1. Regional geological setting

The study area is located in Belgium in NW Europe, more than thousand kilometre away from the boundaries of the Eurasian plate. The 2008-2010 Walloon Brabant seismic sequence occurred within the borders of the Lower Palaeozoic Brabant Massif, a slate belt situated in the subsurface of the central and northern part of Belgium. Outcrops of the Brabant Massif are sparse and are only present in some incised river valleys along the southern rim of the Brabant Massif. The top of the Brabant Massif dips towards the north and is mostly covered by Cretaceous chalc, Cenozoic sand and clays, and Quaternary loess sediments. Towards the north, the thickness of the cover rapidly increases to 1000 m at the Belgium – Dutch border (Legrand, 1968). Not much is known about the current seismicity in the Brabant Massif, but incised river outcrops suggest uplift of the southern part and gradual deepening of its northern part. The only exposed outcrops of the Brabant Massif are situated in the incised river valleys of the Dendre, Senne, Sennette, Dyle, Thyle, Orneau, Gete and Méhaigne in the Brabant, Limbourg and Hainaut Provinces.

To the West, the Brabant Massif laterally extends towards the UK forming part of the larger tectonic unit of the Anglo-Brabant Deformation Belt (Verniers et al., 2002). To the east, its prolongation has been traced using borehole data and geophysical data below the Devonian of the Campine Basin, as far as to the seismically active Lower Rhine Embayment (Mansy et al., 1999). At its southern border, it is unconformably overlain by undeformed Middle Devonian deposits of the Brabant parautochton (white area between Brabant Massif and Ardenne allochton in *Figure 10*). Further to the south, the Brabant parautochton is tectonically overthrust by the Variscan Ardenne allochton along the Midi-Aachen thrust, i.e. the Variscan front of the Rhenohercynian Zone (*Figure 10*), during the late stage of the Variscan Orogeny in the Late Carboniferous. Because of its crystalline rigidity, the Brabant Massif acted as a backstop during the Variscan deformation resulting in oroclinal bending of the Palaeozoic deposits of the Ardenne allochton (Van Noten et al., 2012).

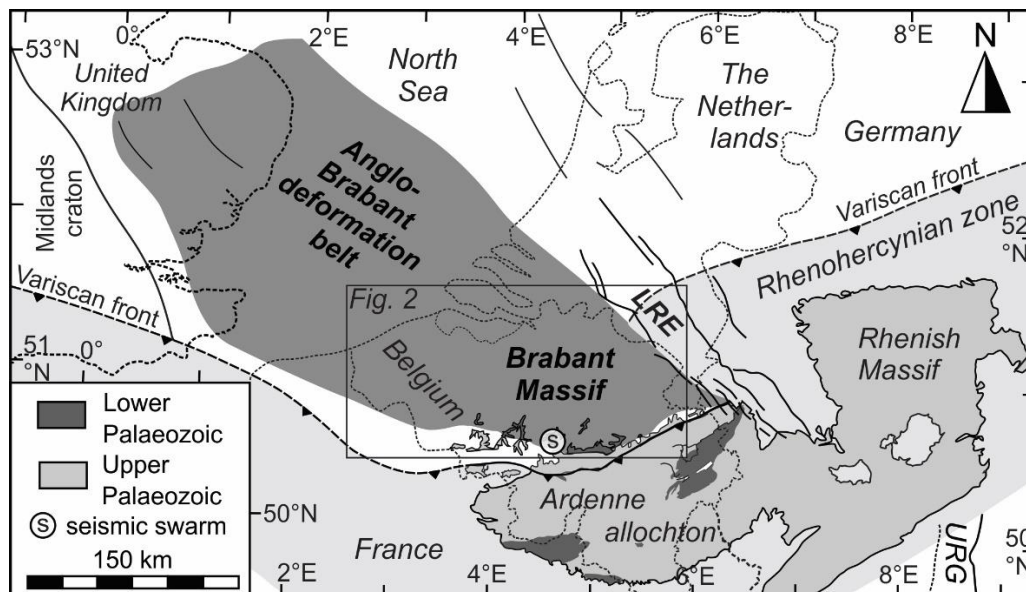


**Figure 10:** Intraplate tectonic setting of the Brabant Massif. The Brabant Massif forms part of the Anglo-Brabant deformation belt that extends from central and north Belgium to the southeastern part of the UK. The seismic swarm is situated at the southern border of the Brabant Massif. The Brabant Massif is partly overthrust in the south by the Ardenne allochton along the Midi–Aachen thrust, i.e. the Variscan front of the Rhenohercynian zone. Deposits of the Rhenohercynian zone are exposed in the Ardenne allochton and Rhenish Massif. Tectonic terrains after Verniers et al. (2002) and Sintubin et al. (2009). LRE: Lower Rhine Embayment; URG: Upper Rhine Graben.

### 3.2. Structural grain of the Brabant Massif

The structure of the Brabant Massif resulted from the ~30 Ma long-lasting – Acadian – Brabantian Deformation event that took place between the late Llandovery (c. 430 Ma) and Emsian (c. 400 Ma) (Debacker et al., 2005; Sintubin et al., 2009). As indicated on lithostratigraphic subcrop maps (Figure 11a), the Brabant Massif has an apparent symmetrical disposition with a central Cambrian core flanked at both sides by Ordovician and Silurian metasediments (De Vos et al., 1993b; Legrand, 1968; Piesens et al., 2005). Structural field work, gravimetric (Figure 11b) and aeromagnetic anomaly maps (Figure 11c) show that the Brabant Massif has a NE-SW trending structural grain that curves into a ENE-WSW orientation towards the east. Owing to the high magnetic susceptibility of the rock formations (slate, siltstone, metasandstone, metagreywacke) of the Lower Cambrian Tubize Group, the Cambrian backbone is clearly visible on the aeromagnetic anomaly map (Chacksfield et al., 1993). In contrast, the Bouguer gravity anomaly (Figure 11b) shows the opposite pattern, with high density anomalies related to the Ordovician-Silurian rim and low densities associated with the Cambrian core or other deep-seated bodies (Everaerts and De Vos, 2012; Piesens et al., 2005). The arcuate geometry of fold-and-cleavage patterns deduced from potential-field data throughout the slate belt is apparent and illustrates the change in orientation of the structural grain from west to east (Sintubin, 1999; Sintubin et al., 2009). Tectonic inversion of the Brabant Basin resulted in the formation of a steep compressional wedge in which the Cambrian core is strongly deformed and is covered by a less deformed Ordovician-Silurian at its peripheral domains. The decrease in deformation from the core to the peripheral domain is characterised by a decrease in metamorphic grade towards the Silurian flanks of the Brabant Massif and by a change of a steep fold belt in the central part to rather wide and open fold belt in the peripheral part. The SW boundary of the Brabant Massif corresponds with a sharp east-west oriented gravity gradient on the Bouguer anomaly map and the highest relief and strongest density on the aeromagnetic anomaly map. *La Bordière fault* (Figure 11b) borders the southern limit of the Brabant Massif and coincides with a sharp gravimetric anomaly gradient (Legrand, 1968) juxtaposing the dense rocks of the Brabant Massif from less dense Upper Palaeozoic rocks of southern Belgium (Chacksfield et al., 1993).

In the SW part of the Brabant Massif, a NW-SE trending Bouguer anomaly low was interpreted as low-density crystalline basement (Chacksfield et al., 1993; De Vos et al., 1993a; Everaerts et al., 1996; Lee et al., 1993) (Figure 11c). The NNE-SS shortening and arcuate shape of the Brabant Massif is believed to be caused by the compression of the Cambrian core of the slate belt against this low-density body. This compression led to the lateral tectonic escape of the Cambrian core along dextral transpressional shear zones. Northeast of the low-density body, these shear zones coincide with several NW-SE trending aeromagnetic gradient lineaments (Sintubin, 1999; Sintubin and Everaerts, 2002). These NW-SE trending structures are also seen as gradient anomalies on the Bouguer anomaly map (Figure 11b) and are interpreted as Palaeozoic NW-SE strike-slip fault zones (Everaerts and De Vos, 2012; Sintubin and Everaerts, 2002). Detailed stratigraphic and structural work, however, revealed that these shear zones are blind structures that not reach the present-day erosion surface of the Brabant basement. The only structural indicators of these shear zones at the surface are short and local fold transitions of steeply- and gently plunging folds (Debacker, 2012; Debacker et al., 2004a; Debacker et al., 2003; Debacker et al., 2004b).



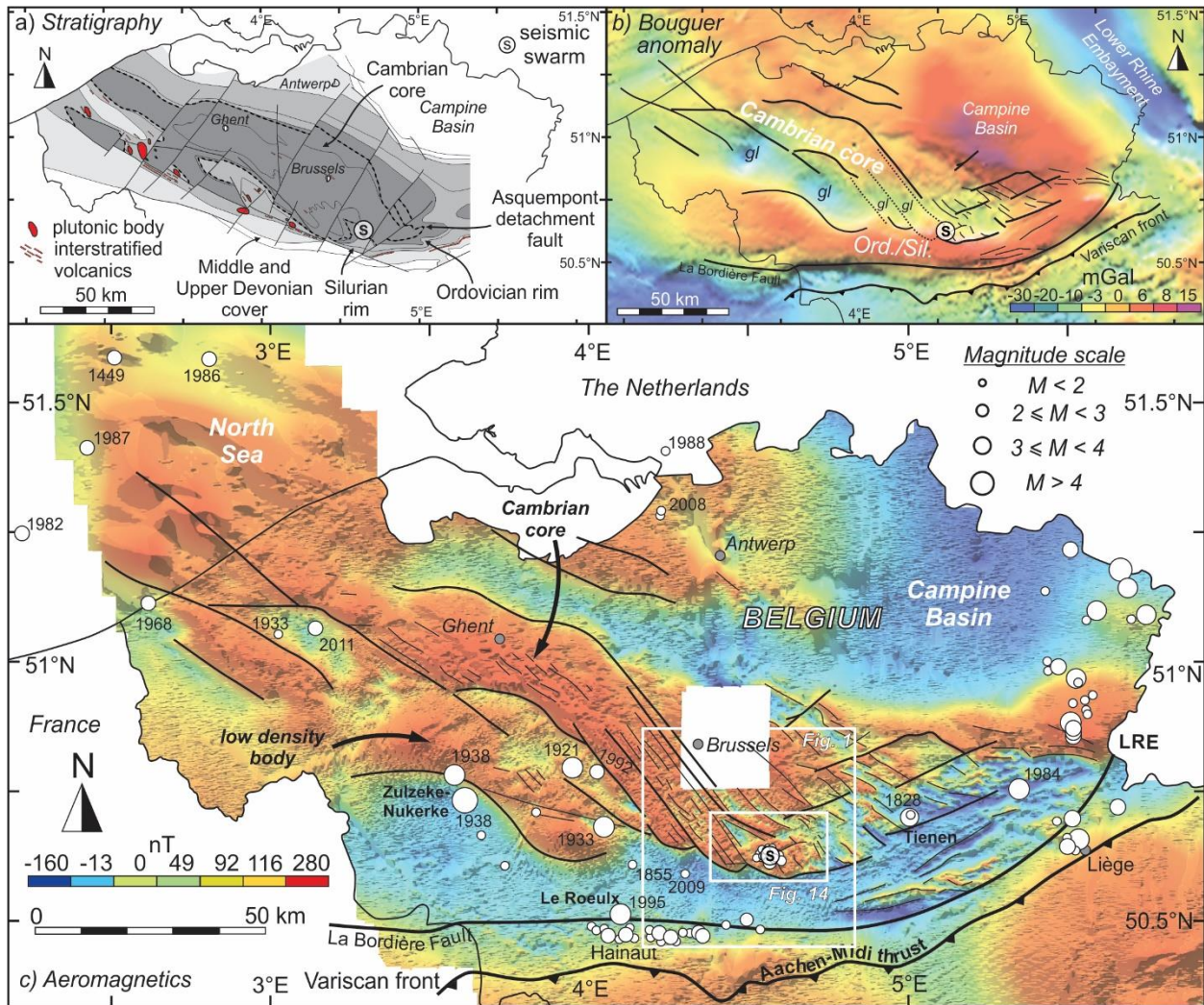


**Figure 11:**

**a)** Geological subcrop map and general stratigraphic structure of the Lower Palaeozoic Brabant Massif after De Vos et al. (1993b) and Debacker (2012). Location of the 2008–2010 Walloon Brabant seismic swarm at Court-Saint-Etienne is indicated. The dashed line shows the trace of the Asquempont detachment fault around the Brabant Massif.

**b)** Bouguer gravity anomaly with a low density Cambrian core and a high density Ordovician and Silurian rim. The 2008-2010 seismic swarm is situated at the NW-SE oriented, gently, NE-dipping gravity gradient marking the transition of the core and the rim of the Brabant Massif. Aeromagnetic lineaments (black lines) of Fig. 2c) are indicated. gl: gravity low. Data from De Vos et al. (1993a).

**c)** The aeromagnetic map shows prominent NW-SE-oriented crustal lineaments in the Cambrian core of the Brabant Massif highlighting an arcuate shape of the slate belt. Historical seismicity (white circles) and structural grain of the Brabant Massif illustrated (black lines) on the aeromagnetic reduced-to-the-pole anomaly in the central and northern part of Belgium. The 2008-2010 Walloon Brabant seismic swarm is situated in the SE part of the slate belt. The white boxes show the locations of Figure 1 and Figure 14. Aeromagnetic anomaly data from Belgian Geological Survey (1994). LRE: Lower Rhine Embayment.

### 3.3. Historical seismicity in the Brabant Massif

In the past, researchers of the Royal Observatory of Belgium (ROB) have performed a regional study on the delimitation of seismotectonic zones in Belgium in order to evaluate the seismic impact and evaluate the maximum earthquake magnitude that can occur within a certain zone. These seismotectonic zones are areas with a certain geological, geophysical and seismological homogeneity within which a uniform occurrence of earthquakes can be supposed. It can be viewed as the crustal blocks within the present day stress field. A first attempt to seismotectonic zoning around Belgium has been performed by Leynaud et al. (2000) and was recently improved by Verbeeck et al. (2009).

The seismic swarm is situated in the seismotectonic zone of the Anglo-Brabant Massif. This zone encloses a tectonic block that consists of the Caledonian Brabant Massif which extends to the west below the North Sea until the Anglia Basin in England and is bordered in the east by the Campine Basin. In the south, the Bordière Fault separates the Brabant Massif from the Upper Palaeozoic Massifs, such as the Variscan Ardenne allochthon, the Namur Basin and the Mons Basin. The northern border of the Anglo-Brabant seismotectonic zone more or less corresponds to outline of the BM in the Dutch province Noord-Brabant. Seismicity within the seismotectonic zone of the Brabant Massif is considered low to moderate (Camelbeeck et al., 2007; Leynaud et al., 2000). The largest onshore historical event on the Belgian territory was the 11 June 1938 earthquake ( $M_s = 5.0$ ) that occurred in the Brabant Massif at Zulzeke-Nukerke, near Oudenaarde (Figure 11b). Reported damage (Somville, 1939) was primarily in an E-W oriented area surrounding that earthquake. The damage distribution was attributed to the site effects associated with soft-sediments overlying the Brabant Massif (Camelbeeck et al., 2014; Nguyen et al., 2004). Another significant event was the 20 June 1995 earthquake near Le Roeulx ( $M_L = 4.5$ ,  $M_S = 4.3$ ) at a depth of 24 km. Other historical earthquakes that occurred before the installation of the current Belgian permanent network and which caused considerable damage in the Brabant Massif are the 23 February 1828 ( $4.5 < M_L < 5.0$ ;  $M_s \sim 4.6$ ) near Jauche and the 21 May 1382 ( $M_s 6.0$ ) and 23 April 1449 ( $M_s 5.5$ ) events in the North Sea (Figure 11b).

### 3.4. The 1953 – 1957 seismic sequence near Court-Saint-Etienne

Importantly, between 1953 and 1957 a seismic sequence took place a few kilometres south of Court-Saint-Etienne. Only the largest events of this sequence were recorded by the Uccle seismic station, which was in 1953 the only operational seismic station in Belgium. At that time one vertical (1300 kg) and two horizontal (1000 kg) Wiechert seismographs were installed in the Uccle seismological lab and recorded all vertical and E-W and N-S horizontal ground motions by printing earthquake waveform data on smoked paper (Charlier and Van Gils, 1953).

ID	$M_L$	Date			Time	P-wave arrival	Time between P- and S-wave	Zero-to-peak S-wave amplitude (nm)	P-wave polarity	Longitude	Latitude	Depth	
Nr	ROB-ID	Year	Month	Day	(h:min:s)	(h:min:s)				(°N)	(°E)	(km)	
3	3069	3.2	2008	7	13	13:45:49.96	13:45:54.40	2.38 s	14,781	Dilatation	50.6259	4.5653	7.740
56	3167	2.6	2008	9	13	01:14:17.28	01:14:20.71	2.82 s	4897	Dilatation	50.6251	4.5674	5.874
87	3225	2.4	2008	12	20	20:53:08.52	20:53:11.90	2.48 s	2140	Compression	50.6269	4.5660	5.652
118	3273	2.8	2009	3	3	03:23:32.64	03:23:36.98	2.54 s	6056	Compression	50.6299	4.5614	6.264
229	3552	2.5	2009	12	26	06:50:13.47	06:50:17.88	2.71 s	3700	Compression	50.6249	4.5684	5.469
Wie-V <sup>a</sup>	4	1953	1	6	23:58:44	–	2.4–2.6 <sup>b</sup>	55,000 <sup>b</sup>	Dilatation	50.617	4.600	–	
Wie-V <sup>a</sup>	3.6	1953	8	28	0:05:21								
Wie-V <sup>a</sup>	3.4	1953	8	28	0:06:16								
Wie-V <sup>a</sup>	<3	1956	4	51	22:47:07								

<sup>a</sup> Wie-V: vertical Wiechert seismogram.

<sup>b</sup> Graphically estimated.

**Table 4:** Phase arrival time measurements at the Uccle seismic station (UCCS) of the largest events of the 2008-2010 Walloon Brabant seismic swarm and phase arrival time of the  $M_L 4.0$  1953 seismic event estimated from the scanned 1953 waveform. The timing of three other events of the 1953–1957 seismic sequence is given.

The 1953-1957 seismic sequence started on 5 January 1953 with a  $M_L$  4.0 earthquake and was followed by two  $M_L$  3.6 and 3.4  $M_L$  events on 28 August 1953 (data from the ROB catalogue, [www.seismology.be](http://www.seismology.be)). Three years later, on 21 April 1956, a  $M_L < 3.0$  occurred. However, historical records from testimonies of people living in the epicentral area at Court-Saint-Etienne report that during the first earthquake event on 5 January 1953, four different events were felt, although only one event was recorded at Uccle. It is thus possible that the 1953-1957 sequence might also have been a seismic swarm of which the spatiotemporal evolution is unfortunately unknown due to absence of testimonies and of recordings of small-magnitude events.

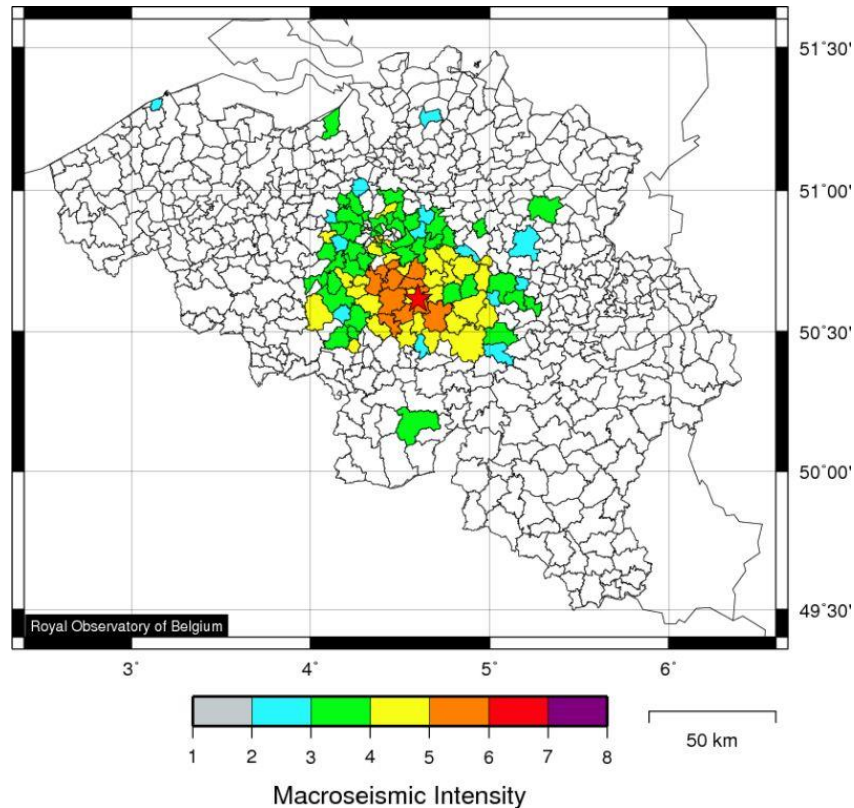


**Figure 12:** *Macroseismic map of the  $M_L$  4.0 earthquake of 6 January 1953 near Court-Saint-Etienne*

A comparison between the Z-component waveforms of the 5 January 1953 event recorded using the historical Wiechert seismograph and those of the largest events of the 2008-2010 swarms recorded by the Güralp broadband seismometer (CMG-ESPCD) located next to the Wiechert seismograph at Uccle shows notable similarity (Figure 13). The Güralp recordings were digitally processed and filtered to provide displacements. The time period range between the P- and S-wave arrivals of the five largest earthquakes of the 2008-2010 sequences is between 2.38 s and 2.82 s (Table 5). The time period for the 5 January 1953 event is between 2.3 and 2.8 s, indicating that travel distance from the source of the different earthquake events to the seismometer at Uccle was almost similar for the 1953 event and the largest of the 2008-2010 events. It is worth noting the S-wave asymmetry for both sequences: it shows first a minor negative amplitude ( $\sim -33.5 \mu\text{m}$  and  $-8.1 \mu\text{m}$  for  $M_L$  4.0 1953 and  $M_L$  3.2 2008, respectively) and then a large positive amplitude ( $\sim 55 \mu\text{m}$  and  $14.7 \mu\text{m}$  for  $M_L$  4.0 1953 and  $M_L$  3.2 2008, respectively; Table 5; Figure 13). Also the peaks following the first S-wave arrivals all have a similar waveform pattern. This indicates an identical travel path of earthquake waves from the source to Uccle. The maximum S-wave amplitude of the 1953  $M_L$  4.0 earthquake is at least four times as large as the maximum S-wave amplitude of the 2008  $M_L$  3.2 earthquake. Considering these similar amplitude changes, the source and focal mechanisms of the 2008-2010 and 1953 earthquakes are likely similar.



ID	$M_L$	Date	Time	P-wave arrival	Time between P- and S-wave	Zero-to-peak S-wave Amplitude (nm)	P-wave Polarity	Longitude	Latitude	Depth
Nr	ROB-ID	Year Month Day	(h:min:s)	(h:min:s)				(°N)	(°E)	(km)
3	3069	3.2 2008 7 13	13:45:49.96	13:45:54.40	2.38s	14781	Dilatation	50.625867	4.565332	7.740
56	3167	2.6 2008 9 13	01:14:17.28	01:14:20.71	2.82s	4897	Dilatation	50.625073	4.567440	5.874
87	3225	2.4 2008 12 20	20:53:08.52	20:53:11.90	2.48s	2140	Compression	50.626949	4.566024	5.652
118	3273	2.8 2009 3 3	03:23:32.64	03:23:36.98	2.54s	6056	Compression	50.629940	4.561393	6.264
229	3552	2.5 2009 12 26	06:50:13.47	06:50:17.88	2.71s	3700	Compression	50.624890	4.568443	5.469
Wie-V*	~4.0	1953 1 6	23:58:44	-	2.4-2.6s**	55000**	Dilatation	50.617	4.600	-

**Table 5:** Phase arrival time measurements at the Uccle seismic station (UCCS) of the largest events of the 2008-2010 Walloon Brabant seismic swarm and phase arrival time of the  $M_L$  4.0 1953 seismic event estimated from the scanned 1953 waveform. \*Wie-V: vertical Wiechert seismogram; \*\*Graphically estimated.

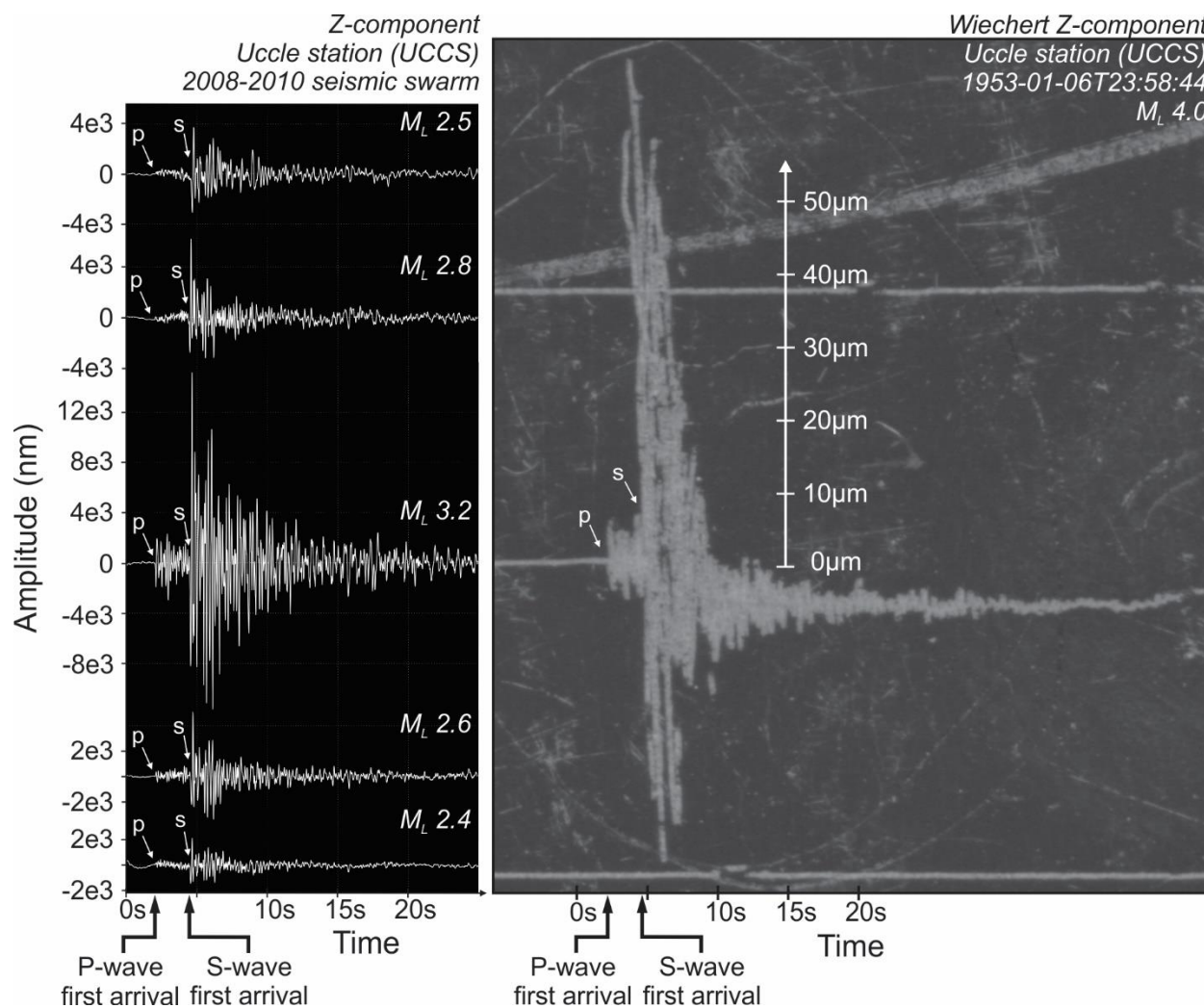


**Figure 13:** Comparison of waveforms of the two 2008-2010 and 1953-1957 seismic swarms. Note the waveform similarity between the Z-component of the five largest events of the 2008-2010 seismic swarm (left) and the Z-component of the 5 January 1953  $M_L$  4.0 earthquake (right). 2008-2010 waveforms are displacement restitution and highpass (0.3Hz, 2 corners) filtered. Scan of the smoked paper of the 1953 earthquake is printed by the vertical Weichert seismograph at the Royal Observatory of Belgium at Uccle. Note the permanent displacement of the vertical Weichert seismograph because of the 1953 earthquake.



Due to a lack of recorded data and the absence of a dense seismometer network in the 1950's, the different events of the 1953-1957 earthquake sequence cannot be relocated properly. The sequence epicentre is estimated to lie in the vicinity of the Héவில்lers hamlet, 4 km SE of the epicentral area of the 2008-2010 swarm. However, given the large error in earthquake location and on the similarity in the waveforms, the 1953-1957 epicentral area might be as well be easily located in the epicentral area of the 2008-2010 swarm, suggesting that both seismic sequences may indeed have a similar source.

### 3.5. Seismotectonic significance of the seismic swarm by magnetic matched bandpass filtering

#### 3.5.1. Aeromagnetic interpretation of the Brabant Massif

The tectonic grain of the buried Brabant Massif has been previously interpreted using Bouguer gravity and aeromagnetic anomaly maps and their derivatives (Debacker, 2012; Everaerts et al., 1996; Sintubin, 1997; Sintubin and Everaerts, 2002). The airborne magnetic data over the Cambrian core of the Brabant Massif were collected in 1994 with a flight line spacing of 0.5 km at a nominal height of 120 m above the ground (Belgian Geological Survey, 1994). Tie lines were 10 km apart. This flight line spacing should provide the resolution necessary for a detailed study of the seismic swarm. The raw flight lines are available in the online supplementary data (Appendix B) for an evaluation of the analysis presented in this work. Other parts of the Brabant Massif and Belgium were covered with flight line spacing of 1.0 km.

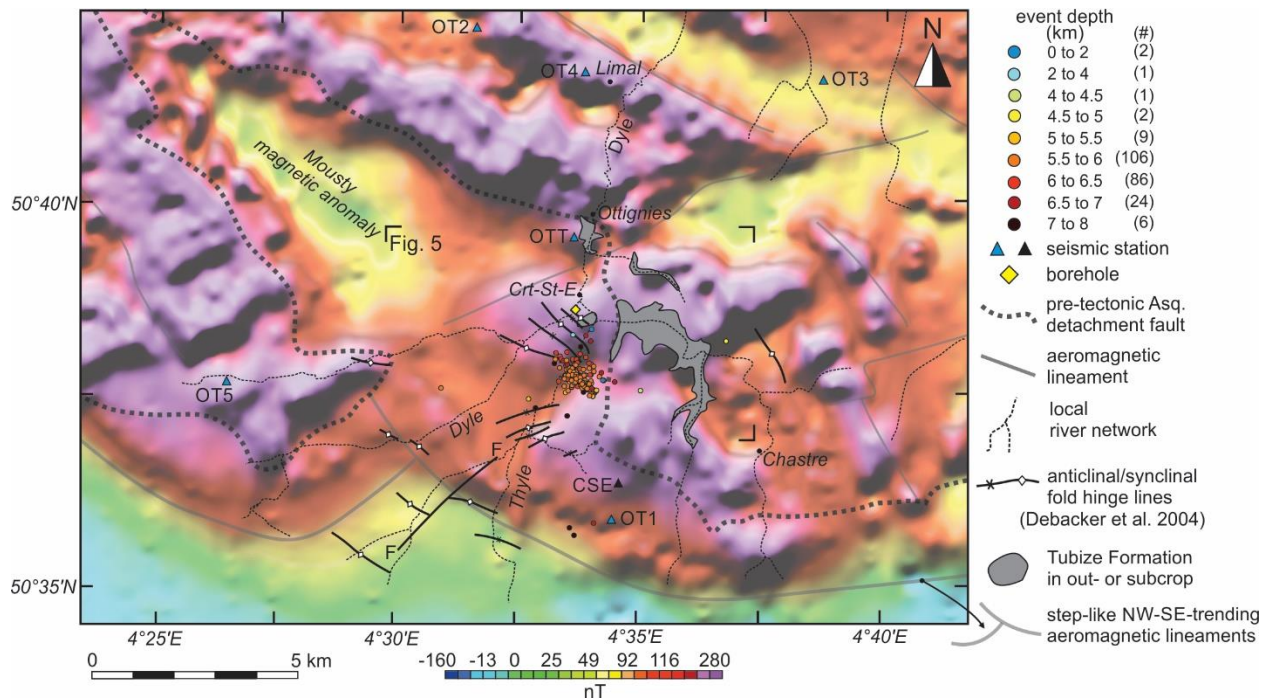


**Figure 14:** Total magnetic field reduced-to-the-pole representing the integrated effect of deep-seated and shallow sources. Aeromagnetic positive anomalies correspond to the (shallow) presence of the high-magnetic Tubize Formation. East of the seismic swarm, a low magnetic through coincides with a thick sequence of the low-magnetic pelitic Mousty Formation. The through is bordered by a steep magnetic lineament in the north. The pre-cleavage, pre-folding Asquempont Detachment System (cf. Debacker et al. 2004a, see Fig. 1a) is determined by the edges of magnetic highs. The 2008-2010 seismic swarm is situated between an ENE-WSW and a NW-SE-trending magnetic ridge. Raw total field aeromagnetic data from BGS (1994). Crt-St-E: Court-Saint-Etienne.

In particular, we consider the reduced-to-pole (RTP) magnetic field. Reduction to the pole is a transformation that works to align magnetic anomalies with the sources that generate them by showing how the magnetic field might appear if the ambient field and remanent magnetisation sources were

vertical. We note that the RTP field is similar to that of the total-field anomaly, not surprisingly given the relatively steep inclination of the magnetic field ( $66^\circ$ ) in our study area. Within the core of the Brabant Massif, the amplitude of the magnetic anomaly is primarily lithology-dependant. The slaty metasediments within the Tubize Formation (Figure 14) of the lower Cambrian Tubize Group (Herbosch and Verniers, 2013) are considered highly magnetised and appear as magnetic ridges. Other studies in the Tubize Formation have confirmed the bedding-parallel nature of magnetic highs and bedding (e.g. de Magnée and Raynaud, 1944; De Vos et al., 1992; Debacker et al., 2004a; Vander Auwera and André, 1985).

In order to find any relevant tectonic structure that could correspond to the 2008-2010 seismic swarm, the epicentral distribution of events is plotted on the total magnetic RTP map (Figure 14). The two NW-SE magnetic ridges north of the epicentral area, i.e. at Ottignies and north of Limal, correspond to subsurface shallowing of the highly magnetised part of the Lower Cambrian Tubize Formation. The lower-magnetic body between the ridges might represent the more poorly magnetised sedimentary layers within the Tubize Formation and poorly magnetised overlying formations (Debacker, 2012). Various lineaments are associated with changes of large-scale fold limbs and to high-strain deformation zones at depth that modify this Formation (Debacker, 2012; Everaerts et al., 1996; Sintubin and Everaerts, 2002). The most prominent of aeromagnetic lineaments is situated along the SW boundary of the Brabant Massif, where step-like NW-SE-trending lineaments are interpreted as dextral transpressional shear zones (Figure 11 and Figure 14).

Locally at Court-Saint-Etienne, a positive anomaly corresponds to shallowing and surface expression of the Tubize Formation (see grey isolated lens of the Tubize Formation below the city of Court-Saint-Etienne in Figure 14). In this area, the low-magnetic Upper Cambrian slaty metasediments of the Mousty Formation are mapped near the surface in the Dyle and Thyle valleys (see Figure 14) (Delcambre and Pingot, 2002; Herbosch and Verniers, 2013). The presence of 5-km long ENE-WSW magnetic ridges below Court-Saint-Etienne suggests that the Tubize Formation is still present at shallow depth below the mapped Mousty Formation at the surface (Debacker et al., 2004a). A shallow  $45^\circ$ S-plunging cored borehole (161 m; Herbosch, Pingot and Delcambre, unpublished data; see yellow diamond in Figure 14) only demonstrated the presence of Mousty slates but, more importantly, showed that bedding is steeply dipping ( $70^\circ$ - $85^\circ$ ) to the NE near the isolated lens of the Tubize Formation.

Northwest of Court-Saint-Etienne, a NW-SE oriented, triangular-shaped aeromagnetic low coincides with the Mousty Formation on the geological subcrop map (Figure 14). This aeromagnetic low reflects a thick sequence of Mousty slates that is positioned in a synclinal structure, strongly reducing the aeromagnetic signal of the underlying Tubize Formation (Debacker et al., 2004a; Sintubin, 1997; Van Tassel, 1986). The northern part of this triangular aeromagnetic low is bounded by a steep, N60W-trending aeromagnetic gradient separating the Mousty Formation from the Tubize Formation. Throughout the eastern part of the Brabant Massif, the contact between the Upper Cambrian Mousty and the Lower Cambrian Tubize Formation is characterised by a pre-folding, pre-cleavage low-angle extensional detachment reflecting a  $\sim 25$  Ma hiatus, referred to as the Asquempont detachment (Debacker et al., 2003; Debacker et al., 2004b). This detachment is folded and can be traced following the curvature of the core of the massif. In the area around the seismic swarm, the Asquempont detachment, and thus the separation of Mousty and Tubize, follows the steep aeromagnetic gradients north and south of the Mousty aeromagnetic low (Figure 14). This lineament suggests that the bedding at depth is steeply dipping in this area presumably situated within a high-strain shear zone (Debacker, 2012; Debacker et al., 2004a; Sintubin, 1997). These shear zones have never been observed at the surface, but the rapid transition between gently plunging and steeply plunging higher-order folds which coincide with a pronounced magnetic anomaly gradient is interpreted to be the surface expression of these inferred shear zones.

The observed magnetic field anomaly is composed of signals that reflect the integrated effects of geological features of different sizes at different depths. The precise depth of a given magnetic anomaly cannot be uniquely determined. However, it is possible through filtering approaches to estimate magnetic anomalies that are likely to be associated with a given depth. Everaerts *et al.* (1996) and Sintubin and

Everaerts (2002) briefly compared the differences between the ‘residual’ high-frequency and the ‘regional’ low-frequency aeromagnetic signal for the whole Brabant Massif by arbitrarily choosing a limit of a wavelength of 5 km to filter for shallow and deep structures. In both cases, the strong superposition of lineaments exists, inferring the predominantly vertical architecture of the slate belt. However, their arbitrarily chosen filter cannot definitively account for the anomalies associated specifically with depths of the seismic swarm.

### 3.5.2. Methodology of matched bandpass filtering

Aeromagnetic and Bouguer gravity data have been proven to be very useful in providing information that links seismicity and deep-seated tectonic structures (e.g. Blakely et al., 2002; Shah et al., 2015). In order to separate short-wavelength anomalies that originate from shallow depths from long-wavelength anomalies that typically originate at greater depths (Phillips, 1997, 2001), matched bandpass filtering may be used. The methodology of the matched filtering approach works as follows: first the amplitude power spectra of the observed anomalies are calculated in the Fourier domain. Characteristically, the log power spectrum may have natural breaks between ranges of frequencies that correspond to different depth ranges representing geological layers (Phillips, 2001). Matched bandpass filters using sections of the power spectra separated at these natural breaks (Figure 15a) can then be applied to decompose the observed magnetic anomaly (Figure 15b). The resulting magnetic anomalies then highlight the sources at corresponding “equivalent” depths that are indicated by the natural breaks. For the area of investigation, the frequency-amplitude function was fitted with straight-line segments across the aeromagnetic RTP map until natural breaks that represent a source depth range corresponding to the depth of interest, i.e. in this study the hypocentre depths of the seismic swarm, were found.

We note that whilst this method can effectively separate magnetic layers, it cannot uniquely filter anomalies due to sources at specific depths. Whereas deep sources cannot generate short wavelengths, wide shallow sources with uniform magnetic properties can sometimes generate longer wavelengths that not necessarily represent deeper sources. However, shallow, gently-dipping structures are unlikely to occur in the study area; after all, outcrop studies and boreholes clearly indicate a steep lithological contact between the Mousty and Tubize Formations near Court-Saint-Etienne and the abundant presence of steeply dipping fold hinges (Figure 5). Moreover, throughout the Cambrian core of the Brabant Massif, Legrand (1968) described many shallow boreholes and indicated that bedding in the Lower Cambrian formations is predominantly vertical.

Two sets of bandpass filters were considered, one which corresponds to layers centred at depths of approximately 45 m, 90 m, 0.47 km, 1.1 km, and 4.5 km (Filter 1, Table 6), and a second corresponding to depths of 47 m, 0.2 km, 0.55 km, 2.1 km, and 7.2 km (Filter 2, Table 6). For both sets, the deepest “layers” represent a halfspace and result from lowpass filtering. Magnetic anomaly maps corresponding to depths shallower than 1 km generally represent survey noise, aliasing artefacts (noting north-south survey flight line spacing of 0.5 km), and ringing from deeper sources. These maps were not used for interpretation and thus are not presented in Figure 16. For the interpretation of depths deeper than 1 km, the flight height of 120 m needs to be included in the filtered depth resulting in depths corresponding to approximately 1.1 km, 2.0 km, 4.4 km and 7.1 km (Table 6). The effect of filtering is highlighted in cross-section A-A’ and B-B’ through the different generated maps (Figure 15 and Figure 16).

Filter 1			Filter 2		
Layer	Depth (m)	Amplitude	Layer	Depth (m)	Amplitude
P4	45.15	1.40E-02	P4	45.58	1.63E-02
P3	190.02	2.015	P3	202.63	2.867
P2	468.31	74.67	P2	553.34	153.7
P1	1180.73	886.8	P1	2144.92	4967
P0	4550.52	23.09	P0	7267.36	37.68

**Table 6:** Bandpass filter parameters and matched-filter depths.

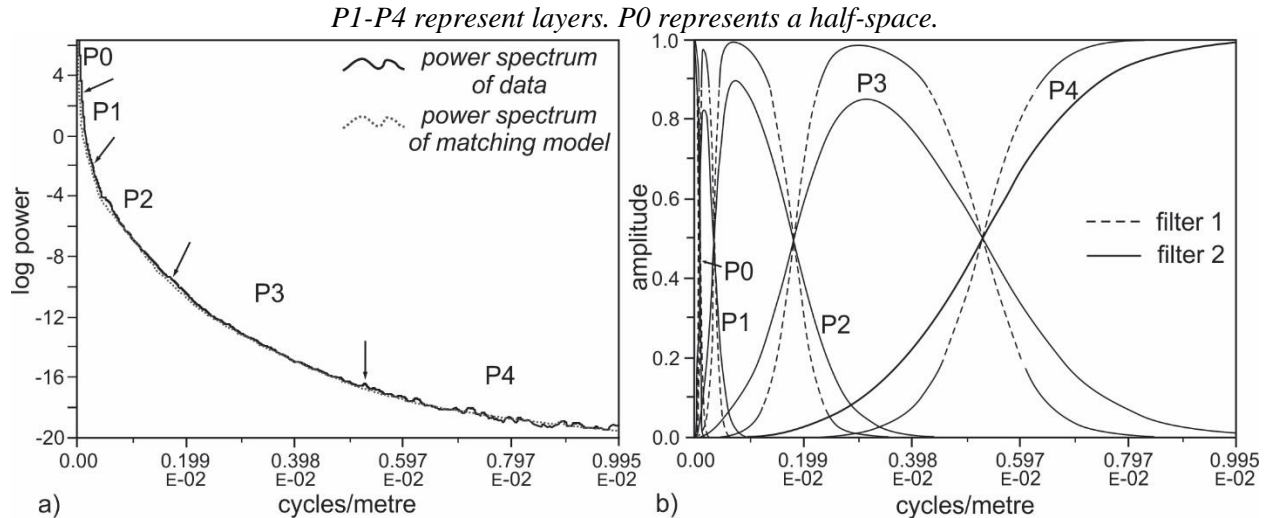


**Figure 15:** Matched filtering decomposition of total-field aeromagnetic data from selected segments. Equivalent depths are determined by fitting straight lines to the power spectrum adjusted by the least-squares technique (Phillips, 1997, 2001). **a)** Power spectrum of the chosen line segments (black line) and of the matching five-layer equivalent model in **b)**. **b)** Magnetic field is decomposed into five components (P0 to P4). P1-P4 result represent short- to medium-wavelength layers. P0 represents half-space long-wavelengths and results after lowpass filtering. Filter 1 filters to 4.4 km. Filter 2 filters to 7.1 km.

### 3.5.3. Interpretation of aeromagnetic bandpass filtered maps

#### 3.5.3.1. Observations made on the 1.1 km and 2.0 km maps

Many of the aeromagnetic lineaments deduced from the RTP map (Figure 14) persist to equivalent depths of 1.1 km (Figure 16a) and 2.0 km (Figure 16b). There is a clear persistence of the Mousty magnetic anomaly, the NW-SE trending ridges, the Asquemont detachment fault and the southern dextral shear zones from the surface to a depth of 2.0 km. This persistence clearly suggests a pronounced vertical attitude of these features. Furthermore, the similarity between the ENE-WSW and NW-SE orientation of the surface folds mapped by Debacker et al. (2004a) and the ENE-WSW and NW-SE orientation of the magnetic ridges at equivalent depths of 1.1 km and 2.0 km clearly shows that the structural style and the variation of first-order folds persist to this depth.

The anomalies filtered for equivalent depths of 1.1 km and 2.0 km show magnetic sources associated with the geological structure above the seismic swarm. On these maps, the seismic swarm is situated below an area with a negative magnetic anomaly and is in line with the structural style marked by the mapped NW-SE trending folds. The negative anomaly east of the swarm corresponds to the presence of the low-magnetic quartzites of the Blanmont Formation (see Figure 5 for the distribution of the Blanmont Formation).

#### 3.5.3.2. Observations made on the 4.4 km and 7.1 km maps

The anomaly maps filtered for equivalent depths of 4.4 km and 7.1 km, roughly represent the geology of the roof and the base of the 2008-2010 seismicity, respectively. Detailed observations at the size of the seismic swarm (1.5 km length) cannot be made due to the large filtered wavelengths (see wavelength versus size of the swarm in Figure 16). Nonetheless, some interesting observations can be made. The Mousty anomaly and Asquemont detachment remain persistent up to 4.4 km but appear to be lost at a depth of 7.1 km. With the exception of the dominant NW-SE oriented magnetic lineaments, other aeromagnetic lineaments deduced from the RTP anomaly map do not seem to persist to a depth of 7.2 km or might not be resolvable given their size and the strong attenuation with depth in the magnetic data.



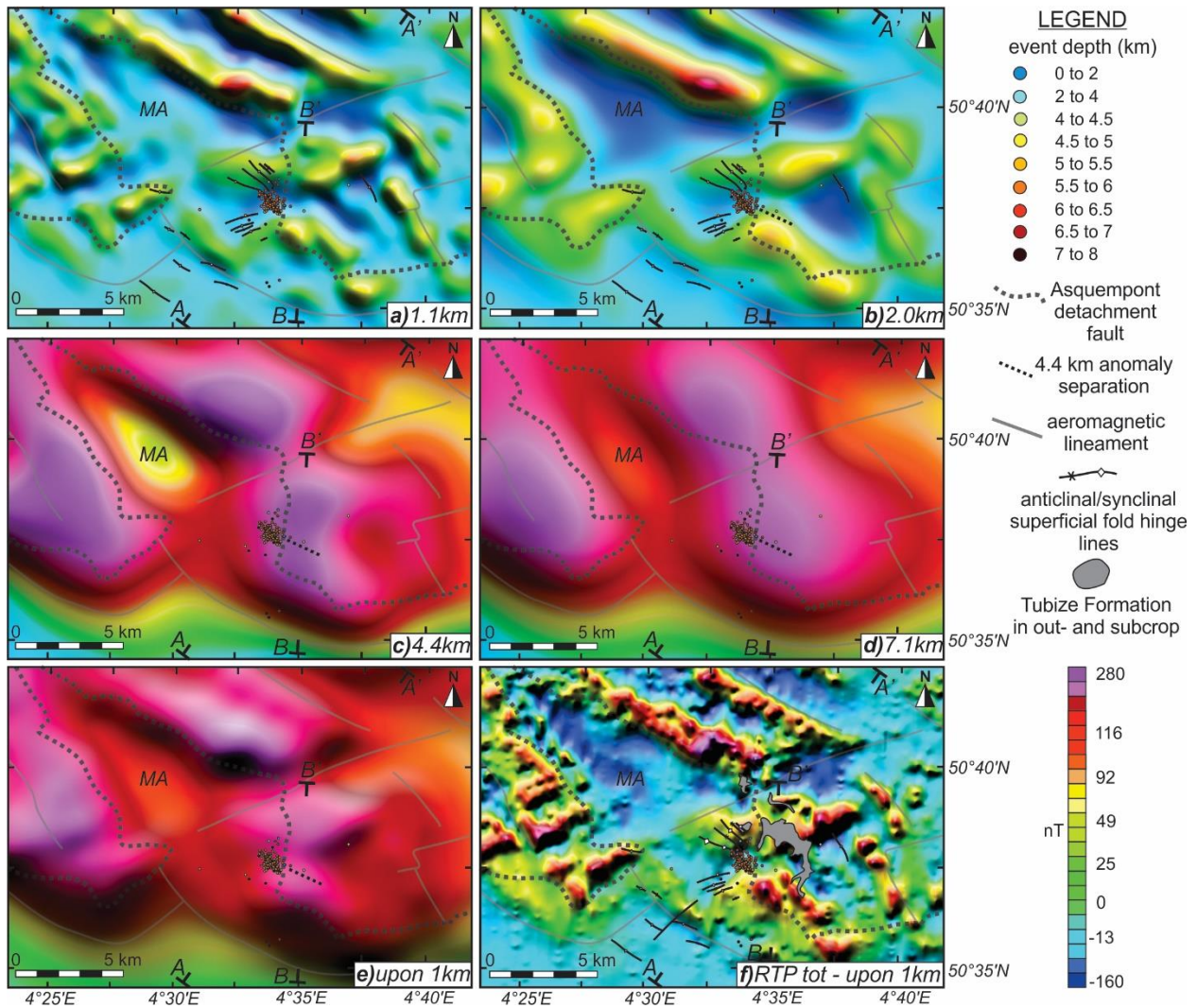


**Figure 16:** Results of total magnetic intensity (RTP) matched filtering. MA: Mousty anomaly

**a–b)** Bandpass filtering for equivalent depths of 1.1 and 2.0 km. Note the pronounced similarity between the WNW–ESE and ENE–WSW oriented folds, respectively NW and SE of the seismic swarm, and the orientation of the magnetic anomaly in the subsurface. The swarm is situated between an E–W oriented magnetic ridge and the northwestern end of a NW–SE oriented ridge. The trace of the detachment fault remains persistent at depth.

**c–d)** Bandpass filtering for equivalent depths of 4.4 and 7.1 km. The trace of the detachment fault persists to 4.4 km and 7.1 km. The swarm is situated east of a positive magnetic anomaly that is present as a single anomaly at 7.1 km but as two anomalies at 4.4 km. Note the dashed line as the separation of the positive magnetic anomaly at 4.4 km (Fig. 16 B–B'). The 2008–2010 hypocentres are situated approximately aligned with this separation.

**e)** Total magnetic field RTP, lowpass filtered using an upward continuation distance of 1 km, highlighting deeper sources.

**f)** Subtraction of the 1 km upward anomaly in e) from the total magnetic field RTP emphasises shallower sources.

The southeastern end of seismic swarm is coincident with a NNW-SSE oriented western edge of a positive magnetic anomaly. On the 7.1 km map, this magnetic anomaly has only one apparent source because of its large wavelength. However, from the 4.4 km and the 1 km-upward maps it is clear that the anomaly observed at 7.1 km can be separated into two individual sources with a NW-SE and WSW-ENE oriented attitude for the northern and southern anomalies, respectively. This orientation has been detected by evaluating several N-S cross-sections through these magnetic highs. These anomalies also coincide with the orientation of anomalies observed at the 2.0 km map. The anomaly gradient that separates these two anomalies has a NW-SE orientation (indicated as a dashed black line in Figure 15b-e) and is situated slightly north of the southeastern tip of the seismic swarm. On the 2.0 km map, this anomaly coincides with the northern edge of the NW-SE oriented anomaly that is situated southeast of the swarm.

3.5.3.3. Shallow magnetic sources

Magnetic anomaly maps corresponding to depths shallower than 1 km generally represent survey noise, aliasing artefacts (noting north-south survey flight line spacing of 0.5 km to 1 km), and ringing from deeper sources. These maps were not used for interpretation and are not illustrated in Figure 16. To enhance anomalies due to shallow sources, an upward continuation strategy was chosen. The upward continued field shows what the magnetic anomaly would look like if the sensor had flown 1 km higher during survey effectively filtering shorter wavelengths. The resulting anomaly reflects deeper sources as can be seen by the congruency between the 4.4 km map (Figure 16c) and the 1 km-upward continued map (Figure 16e). An anomaly associated with shallow sources can then be generated by subtracting the RTP upward continued anomaly from the total magnetic intensity aeromagnetic field. The resulting map is much better suited towards interpretation of shallow geological structures. Local magnetic variations are apparent after applying the upwards strategy and strongly correspond to higher-order fold styles mapped at the surface (Figure 16f) than do the matched-filtered maps in Figure 16a and b.

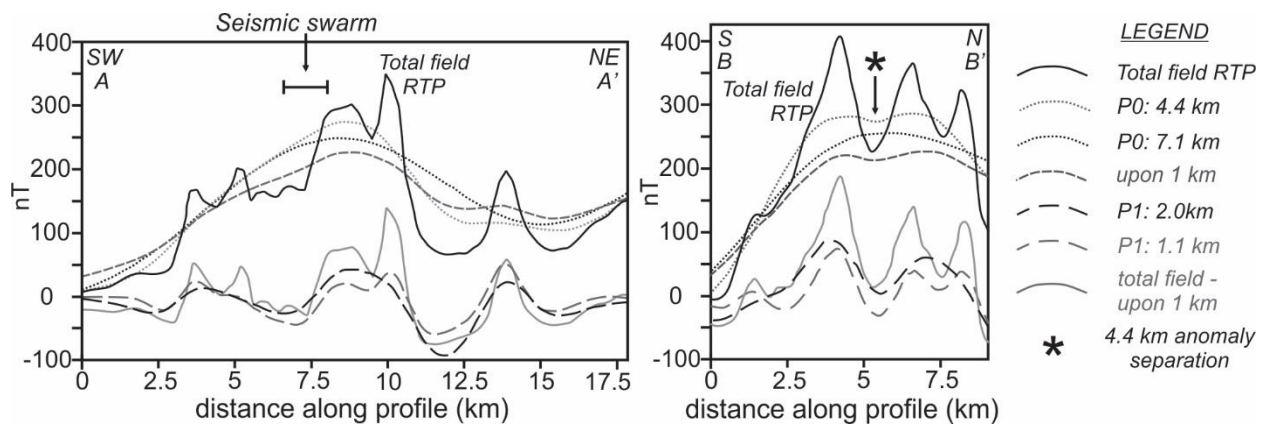


Figure 17: Magnetic anomaly variation along profiles A-A' and B-B' for all filtered depths in Figure 16. The RTP field is separated into different components. The seismic swarm is located at the southwest edge of a positive magnetic anomaly. The separation of the positive magnetic anomaly at 4.4 km in profile B--B' corresponds to the dashed line in Figure 16.

## **TASK 4 – Discussion of results obtained in Tasks 1, 2 and 3**

In literature seismic swarm occurrences are commonly related to fluid- or gas migration in the crust. This association relies both on the direct observation of hot springs and fluid- or gas outflow at the surface accompanying the swarm and on the observation of well-defined depth-related migration of seismicity (Daniel et al., 2011; Fischer et al., 2014; Lindenfeld et al., 2012; Schenk et al., 2012). According to the study of seismic swarms, triggering of seismicity by fluid overpressure at depth is often explained to be a likely cause (Fischer et al., 2014). In this section, however, we discuss that the 2008–2010 seismic swarm in the Brabant Massif is likely not affected by any fluid migration, nor that any overpressure needed to be present to have caused the two year activity along the causative fault. Reactivation of the causative fault by local stress conditions is a more likely hypothesis.

### **4.1. Stress release within a limited-sized fault zone**

Unlike seismic swarms related to fluid migration in the crust (e.g. Lindenfeld et al., 2012; Schenk et al., 2012), the 3D hypocentre distribution of the Walloon Brabant swarm does not show depth-related migration with time, supporting an alternative cause. The seismic activity was restricted to a fault length of 1.5 km in a narrow ~200 m wide rock volume, and repetitively covered the entire zone. The spring 2009 events, for example, all took place in the same area as the initiation of the swarm in August - September 2008. Consequently, within the hypocentral distribution, no relationship between the time history of events and a direction in rupture propagation is present. As

- (i) the seismic swarm is restricted to a rather small volume,
- (ii) seismic energy is released over large time span of 2 years in the same volume,
- (iii) no significant rupture propagation direction is deduced,

earthquake stress release is likely related to a heterogeneous stress field in a weakened crust. This indicates that the earthquakes in the seismic swarm do not correspond to the opening of a new structure but to the minor reactivation of a weakened and pre-existing, well-developed blind single fault structure that slowly released its energy in response to the current stress field. The incapability to build up high stress accumulations is reflected in the low *b*-value of the 2008–2010 catalogue. Given their small magnitudes and the consistent focal mechanisms, the earthquakes thus reflect millimetre to centimetre displacements along the fault plane.

Due to the small size of the swarm relative to its depth, a specific fault structure cannot be easily visualised by matched filtering of the magnetic anomaly. However, as matched filtering is consistent with superficial structures deduced from field mapping and confirms that the steep bedding attitude of Lower Cambrian deposits encountered in boreholes and at the surface persist to large depths (cf. Sintubin and Everaerts, 2002), the significance of the causative structure responsible for the near-vertical 2008–2010 Walloon Brabant seismic can be deduced by interpreting the different filtered maps. Given this verticality, the tectonic structure observed from the 2.0 km map (Figure 16b) can be used to explain the seismic swarm. At both ends, the fault structure associated with the 2008–2010 earthquake seismicity in Walloon Brabant seems to be confined by magnetic sources that have a different orientation than the orientation of the seismic swarm (Figure 16). The northwestern tip of the swarm does not extend into the ENE–WSW magnetic anomaly high (Figure 16b), whereas its southeastern tip terminates near a NW–SE oriented positive anomaly that is visible in the 2.0 km (Figure 16b), 4.1 km (Figure 16c) and 7.1 km maps (Figure 16e). The fact that the locally N–S-trending Asquemont detachment fault is consistently present near the southeastern end of the swarm at the discussed depths strongly suggests that the southeastern part of the causative fault structure is confined by a density and rheological contrast that exists between the slates of the Mousty Formation and the metasandstones of the Tubize Formation. Consequently, assuming that the structures are indeed nearly vertical, the steeply-dipping Asquemont detachment fault, illuminated by a magnetic gradient at 2.0 km, 4.4 km and 7.1 km depth, demonstrates a geological contrast in rock formations that can be considered to have limited the seismic swarm activity

(Figure 18). These findings indicate a NW—SE trending causative fault structure that is only situated in the Mousty slates and which is limited in length as it probably does not exist in the footwall of the detachment fault in the Tubize Formation. Matched filtering thus strongly suggests that the limited spatial extent of the seismic swarm is due to limited length of the corresponding fault.

We also speculate that the 1953–1957 seismicity, which included events with slightly larger magnitudes, resulted from the activity along the same fault although at that time it was capable of releasing more seismic energy than the 2008–2010 seismicity. If all the cumulative energy of the 2008–2010 swarm would have been released at the same time, it would have generated a  $M_L$  3.9 event, i.e. comparable to the total moment release of the  $M_L$  4.0 event in 1953. However, considering all the events of the 1953–1957 swarm (Table 4), the total moment release of the 1953–1957 swarm is larger than the total 2008–2010 swarm. It remains an open question whether or not the 51-year time gap between the 1953–1957 and 2008–2010 seismic swarms can be interpreted as a seismic cycle.

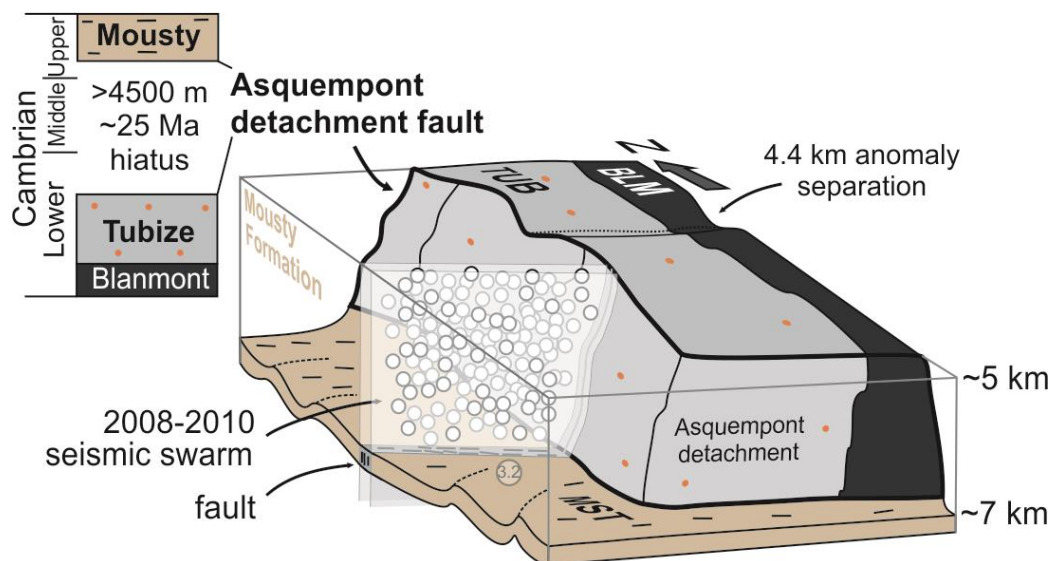


**Figure 18:** Schematic 3D representation summarising the geology in the hypocentre area of the 2008–2010 seismic swarm in the Brabant Massif. Seismicity took place between 5 and 7 km within the slaty Mousty Formation along a limited-sized, NW—SE oriented fault that is bordered at its southeastern end by the early-orogenic, steeply-dipping and folded Asquemont detachment fault. In the hypocentre area, this detachment fault separates the highly magnetised Tubize Formation from the younger, poorly magnetised slaty Mousty Formation. Local fold variations in the Mousty Formation are projected from surface geological maps (Debacker et al., 2004a). Figure not to scale.

#### 4.2. Seismotectonic interpretation

Earthquake analysis of events that occurred at the many normal faults bordering the Lower Rhine Embayment (LRE; Fig. 2c, Fig. 11c), i.e. the closest active regional structure that forms the northwestern relay of the Rhine Graben, indicates a current extensional regional stress regime (Camelbeeck and van Eck, 1994; Camelbeeck et al., 2007; Hinzen, 2003; Hinzen and Reamer, 2007; Reamer and Hinzen, 2004; Vanneste et al., 2013). The NW-SE-directed maximum horizontal stress ( $\sigma_H$ ; Figure 9c) defined from the inversion of focal mechanisms of these earthquakes agrees well with the seismotectonic model of NW Europe (Ahorner, 1975, 1983) and the World Stress Map (Zoback, 1992) showing that the regional stress of the LRE is controlled by plate driving forces acting on plate boundaries.

The stress field inferred from inversion of focal mechanisms of the Walloon Brabant seismic swarm, however, resulted in a local stress field with a WNW-ESE maximum horizontal stress ( $\sigma_H = N289^\circ$ ; Figure 9b) which differs and deviates from the regional trend ( $\sigma_H = N312^\circ$ ; Hinzen, 2003). To evaluate our obtained stress inversion and to derive a local stress field orientation for the studied part of the



Brabant Massif, we need to compare the focal mechanisms of the 2008-2010 seismic swarm with the focal mechanisms of other seismic events. Unfortunately, apart from the seismic swarm, the studied region has limited historical seismic activity. Only one focal mechanism, the 1995  $M_L$  4.5 Le Roeulx earthquake (35 km WSW of the seismic swarm, Figure 11c), can be compared with that of the seismic swarm. This earthquake occurred at a depth of 24 km, considerably deeper than the 2008-2010 swarm, and is interpreted to have occurred along the southern border of the Brabant Massif. Its mechanism is reverse along a steeply dipping NNE-SSW trending fault (Camelbeeck, 1993; Camelbeeck et al., 2007). Aftershocks are unfortunately lacking and a reliable stress field cannot be calculated from this one event.

Another significant earthquake in the Brabant Massif is the damaging  $M_s$  5.0 1938 earthquake (75 km WNW of the swarm, Figure 11c) and its two  $M_L > 4.0$  aftershocks. No reliable fault-plane solution is available due to a lack of seismic data for the time (Camelbeeck et al., 2007). Predominantly E-W oriented isoseismals from this event have been deduced from historical documents (Somville, 1939), which led Ahorner (1975) to conclude that this event resulted from strike-slip faulting along a WNW-ENE-trending shear zone. Nguyen et al. (2004), however, suggested that the E-W oriented isoseismals are related to regional site effects in the 1938 epicentre area rather than to the mechanism of faulting.

The only independent method that can be used to evaluate the derived local stress field is calculation of the spatial variation of the differences in gravitational potential energy from the method of Camelbeeck et al. (2013). This method shows that local depth-integrated stress sources can be inferred from the second spatial derivative of the geoid height, which is used as a proxy for the gravitational potential energy. The inversion of the geoid height applied to Belgium is indicated in Figure 9c. As only local differences in the gravitational potential energy are applied, the resulting stress tensor is also local. Interestingly, the applied geoid method shows a local stress field with a WNW-ESE  $\sigma_H$  direction in the 2008-2010 epicentral area. This similarity of the geoid independent stress tensor ( $N280^\circ$ ; Figure 9c) and the stress field inferred from inversion of the ten calculated focal mechanisms ( $N289^\circ$ ; Figure 9b) suggest that our strike-slip stress tensor is reliable, even when considering the uncertainty of  $30^\circ$  of the local stress tensor given by the Win-Tensor programme.

When considering the uncertainty in the estimation of the local stress field (error of  $30^\circ$ , Figure 9c) with the regional stress tensor, there is only a small overlap between both stress tensors but the mechanisms are different (strike-slip versus extensional; Figure 9c). Stress inversion carried out in this study thus shows for the first time that a local left-lateral strike-slip regime is currently present within the studied southern part of the Brabant Massif and that the local stress configuration was presumably the main driver of the 2008-2010 seismicity.

#### **4.3. General implications for intraplate earthquake activity**

The geometry of the 2008-2010 seismic activity indicates an active fragmented fault structure within the Caledonian Brabant Massif. Also other kilometre-long, NW-SE aeromagnetic lineaments are present in the southern part of the Brabant Massif (Figure 11c). Due to their NW-SE orientation these lineaments might have a similar reactivation potential in the current stress field as the causative structure of the 2008-2010 seismicity. The limited size of the causative fault studied in this work however suggests that such long lineaments may be more fragmented than previously thought and that they thus may have a lower potential to generate large earthquakes in an intraplate setting as their full length cannot be considered.

To investigate this statement, magnetic lineaments that highlight fault structures in old geological massifs need to be studied in more detail by the aeromagnetic methods presented in this work. This will reveal their continuation at depth and their reactivation potential, even though no seismicity has taken place along them in the past.

## Conclusions

In this chapter A, a comprehensive seismological and seismotectonic analysis of the 2008-2010 earthquake swarm that took place near the city of Court-Saint-Etienne (Belgium) within the basement rocks of the Anglo-Brabant Massif, and multidisciplinary analysis of the available seismological, geological and potential geophysical data emphasise the importance of inherited fault structures and their reactivation potential in an intraplate seismotectonic setting. In particular:

1. Application of seldomly-used cross-correlation tools resulted in significant refinement of the first P-wave arrival times. Relocation in HypoDD showed that the original locations of the 2008-2010 seismic events can be improved to a fault structure that is limited to a horizontal length of 1.5 km and width of  $\sim 200$  m, and is restricted in the vertical direction between 5 and 7 km depth. The analysis of time history of events shows that the swarm occurred in several bursts of activity, with dominant phases in the summer and autumn of 2008 and in the spring of 2009. Neither depth migration, nor any horizontal rupture propagation can be demonstrated by the time occurrence of events. This indicates a rather slow and diffuse energy release during the two year swarm activity. The low b-value of the seismic catalogue indicates a dominance of small events over large events in a magnitude range between  $M_L$  0.4 and  $M_L$  3.2.
2. Comparison between the NW–SE oriented epicentral distribution and the fault plane solution of the largest events shows that the NW–SE nodal plane can be interpreted as the true fault plane. The focal mechanisms of ten events define left-lateral oblique to purely left-lateral strike-slip movements on a subvertical fault structure.
3. The waveform of the 1953  $M_L$  4.0 seismic event that took place near the 2008–2010 epicentral area shows a pronounced similarity in the asymmetry of the first S-wave arrival compared to the largest events of the 2008–2010 seismic swarm. Based on this comparison we speculate that the 1953–1957 events may have occurred along the same fault structure.
4. To find a relevant tectonic structure that may correspond to the seismic swarm, we applied a systematic filtering approach in which the magnetic field was bandpass matched-filtered to generate magnetic anomaly maps that highlight sources at equivalent depths. Filtering results and their comparison to the local geological structure strongly suggest that the causative fault is situated in a slaty rock body and is bordered at its both ends by magnetic anomalies with significant different orientations representing a different and stronger rock type. This analysis suggests that the fault along which seismicity took place is an isolated structure with an orientation that is consistent with the structural grain of this part of the Brabant Massif and that the limited spatial extent of the seismic swarm is due to limited length of the corresponding fault.
5. Stress inversion of the focal mechanisms indicates a local strike-slip stress regime with a WNW–ESE oriented maximum horizontal stress orientation. This local WNW-ESE stress orientation agrees with the local stress orientation independently inferred from the second spatial derivative of the geoid height and differs slightly from estimates of the regional stress field. Based on this comparison, local stresses are likely the cause of the seismicity.

## B. Identification of the fault in the field – Relationship between seismicity and (sub)surface geology?

### TASK 5 – Data collection

In order to deduce if the fault zone structure responsible for the 2008-2010 seismic sequence is potentially visible near the surface, all available cartographic documents about topography (satellite data, aerial photos), geomorphology geology, hydrogeology and soil characteristics were collected. This task has been completed at the onset of the project. All available data can be consulted on request at [www.seismology.be](http://www.seismology.be).

#### 5.1. Topography

The Royal Observatory uses a detailed 20 m data spacing Digital Elevation Model (DEM) from the Nationaal Geografisch Instituut (NGI). For this project a c. 200 km<sup>2</sup> (14 x 14 km) area around the different epicentres was used. The Lambert coordinates of the selected area are: x: 139140 to 153120 and y: 156320 to 170340. The WGS84 coordinates are: x: 4.456188 to 4.655158 and y: 50.563547 to 50.689134. The *Region Wallonne* additionally provides a DEM of the valley floors of the Dyle and Thyle valleys. Also the ASTER satellite provides free DEM models but as its resolution (60 m spacing) is lower than the NGI DEM, it is not further used in this study. The aerial photos of the area are available from the *Region Wallonne*. Combined with the DEM they can be of great use to conduct the geomorphological investigation in Task 5.

#### 5.2. Geomorphological data

No geomorphological studies have previously been performed in this part of the Walloon Brabant Province. A geomorphological study of the topography is briefly conducted in Task 6.

#### 5.3. Geology

There is a large record of the geology of the Brabant Massif and the local geology around the Dyle and Thyle valleys. A literature study on the tectonic grain has already been performed in section A to describe the seismotectonic framework (see Task 3). All relevant published maps have been geolocated in a GIS (MapInfo) to study and compare the cartographic data properly. Especially the new Walloon geological maps (see simplified geological map in Figure 5) and their explicatory notes are very useful as they provide cartographic information on

- (i) the Lower Palaeozoic geology of the incised Brabant Massif in the Dyle and Thyle valleys,
- (ii) the Quaternary alluvial deposits in these valleys,
- (iii) the Quaternary and Cenozoic cover of the surrounding hill tops.

Studied maps are: 39/3-4, 40/1-2, 39/7-8 and 40/3-4 (Blockmans et al., accepted; Delcambre and Pingot, 2002; Herbosch and Blockmans, 2012; Herbosch and Lemonne, 2000). Also detailed structural analyses and mapping projects (Debacker, 2012; Debacker et al., 2004a) are taken into account in the geological interpretation of the area.

A large effort has also been put in the data collection of existing borehole descriptions in the study area. By consulting the explicatory notes of the geological maps, the website of the Databank Ondergrond Vlaanderen (DOV) and the [Gisel online](#) databank of the Geological Survey of Belgium (GSB) numerous borehole and outcrop descriptions are collected and are further used to analyse and specify the local geological structure of the study area. The borehole information is used for the site effect analysis in Task 9. All these data are interpreted to construct a palaeotopographical map of the top of the Brabant Massif (see Task 9).

#### 5.4. Hydro(geo)logical data

HCOV (*Hydrogeologische Codering voor de Ondergrond Vlaanderen*) is an official numerical code in which all Paleozoic, Cenozoic and Quaternary hydrogeological units are ordered in an hierarchical way. The code has been developed to standardise all info on the present aquifers in the Flanders Region (Meyus et al., 2000). In general, the HCOV strongly correlates with the national stratigraphical units in Belgium. After all, the hydrogeological properties of a layer (or a unit in HCOV) are determined by the geological composition of the layer, which on its turn is captured in the stratigraphical classification. In the HCOV a full mapping of the subsurface of Flanders is included in which the base and thickness of each unit can be consulted as a grid layer. Fortunately for our research, these grid layers have been constructed until the southern Dyle River watershed and can thus be used.

Thanks to the databank of the GSB, we are in the possession of those HCOV grids that cover the Dyle/Thyle study area, i.e. the Quaternary alluvial (0140) and Pleistocene (0160) deposits, the Cenozoic Lede (0612) and Brussels (0620) Formations, the Cretaceous (1100) and the Cambro-Silurian Paleozoic basement (1340). These codes are used for constructing a sediment thickness map above the Brabant Massif, which is necessary to link the results of the macroseismic inquiries with the local geology (Task 9).

Additionally, in order to investigate the possibility that groundwater flow has been increased due to fault activity, we also checked all available hydrological data on groundwater extraction in the Court-Saint-Etienne region in an area around the fault. This data is provided on the [Dixsous](#) website (Property of the Walloon Ministry). Also the rainfall data of the nearest capture point at Chastre has been studied in order to check the possibility if the seismic swarm can be related to the infiltration of rainwater. However, no correlation exist between the timing of seismicity and rainfall data (Figure 19).

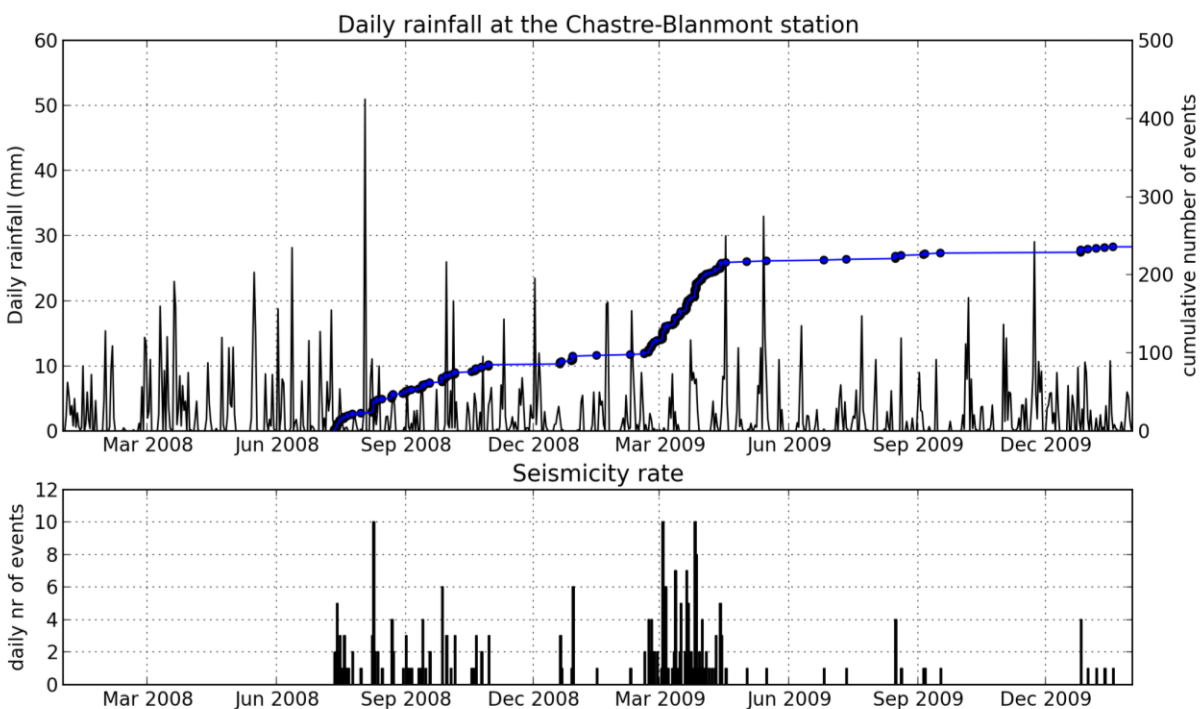


**Figure 19:** Comparison between daily rainfall at the Chastre station and time history of seismicity. No obvious correlation between seismicity, cumulative number of events or rainfall can be deduced.

## **5.5. Geophysical data**

Potential geophysical data such as the Bouguer gravity anomaly (Figure 20b) and the aeromagnetic map of Belgium (Figure 20c) were already in the possession of the ROB and have been discussed elaborately in Chapter A.

Geo-electric prospection data is quite limited. Tavernier et al. (1967) performed a full geo-electrical survey in the Lessines area in Hainaut. Resistivity values of the Quaternary deposits published in this work can be used for comparison with our work.

In the past the ROB has also invested in the development of a methodology in performing H/V ambient-noise seismic measurements (Rosset and Petermans, 2007). Several campaigns in central Belgium (Nguyen et al., 2004; Petermans et al., 2007), in the Brussels area (Rosset et al., 2005) and in Luxemburg (Rosset, 2006) have been performed and they will serve as guideline to successfully plan and perform our H/V campaign (Tasks 6 & 8).

## **5.6. Low-risk nuclear data**

Radon (Rn) is an inert gas that is produced by the radioactive decay of uranium and other elements in rocks. Radon in the atmosphere can occur due to the natural radioactive decay in rocks or can be related to rock deformation, e.g. during earthquakes, that forces the radon out of the earth. Newly formed microcracks related to earthquakes can serve as potential pathways for radon present in the groundwater.

We contacted the FANC (Federale Agentschap voor Nucleaire Controle) in order to have the cartographic information on radon emissions in Brabant Walloon (Figure 20). From these maps it is clear that soils and rocks are the predominant source for indoor radon in Belgium. The spatial distribution of the different sediments and rocks often correlates very well with the indoor concentrations of the geogenically distributed radon, especially in Brabant Walloon and in the southern Ardennes (Cinelli et al., 2009; Tondeur et al., 2001; Tondeur et al., 1994; Tondeur et al., 1996; Zhu et al., 2001; Zhu et al., 1998). The radon emission map shows a strong correlation between higher radon concentrations and the presence of Cambro-Ordovician rocks in the incised river valleys in Brabant. The highest potential of risk of encountering high concentrations of radon, i.e. > 10% chance to pass > 400 Bq/m<sup>3</sup>, is measured in the Dyle and Thyle valleys, more specifically in those areas of the Court-Saint-Etienne community at which the Cambrian Mousty Formation is present at the surface. River alluvium is expected to have low radon concentration, even when they are developed above older bedrocks characterised by higher Rn values. However, the thin alluvium in the Dyle/Thyle valleys (< 10 m) does not decrease the radon risks much.

We checked the 2008 to 2010 radon emissions measured at the Ernage, Beauvrechain and Braine l'Alleud radon stations and which can be consulted on the [Telerad website](#) of the Federal Government of Belgium. On those specific days during which the earthquakes with highest magnitude occurred, i.e. at 13/7/2008 (M<sub>L</sub> 3.2) and 03/03/2009 (M<sub>L</sub> 2.8), no significant increases of radon emission have been detected. This absence of changes in radon concentration does not necessarily needs to have a scientific meaning as the radon stations are probably too far away from the actual epicentres to detect any changes. Further analyses on the radon emission data are beyond the scope of this research project and will not be addressed further but we would like to address its importance towards seismology.

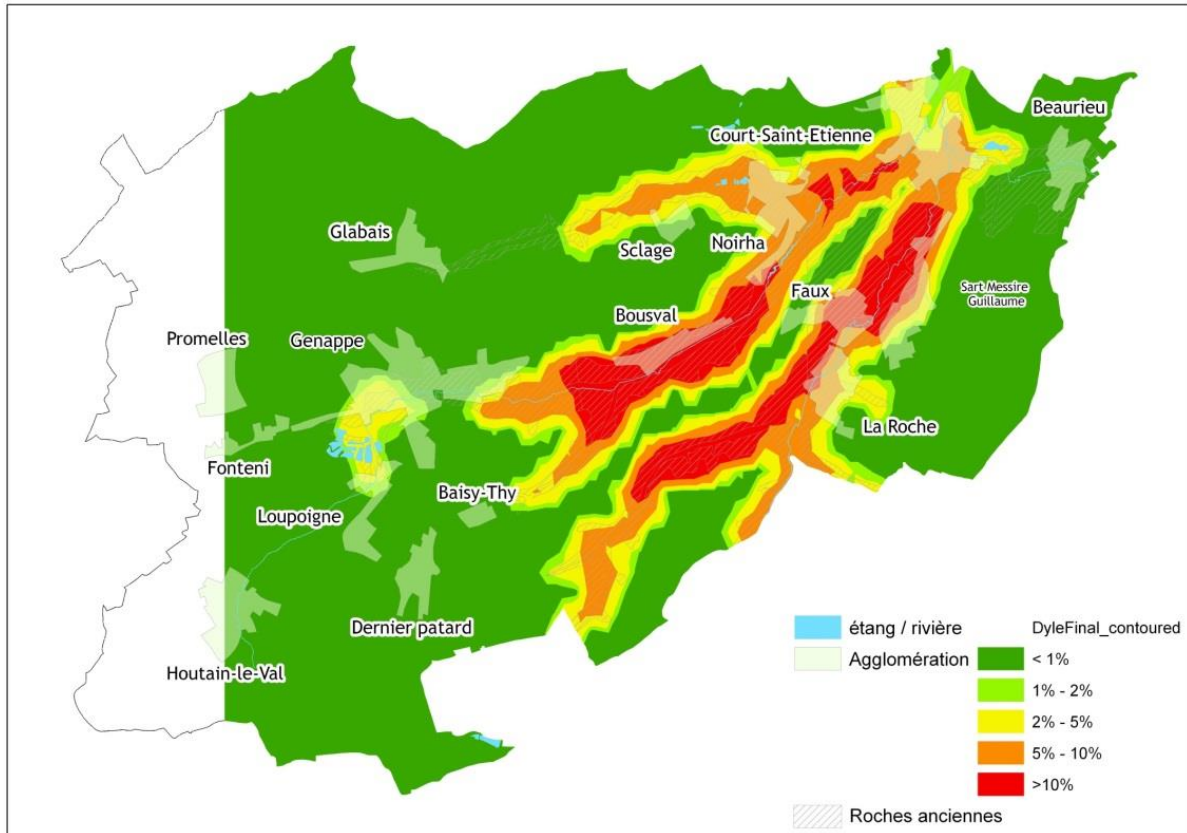


**Figure 20:** Radon emission map of the Dyle and Thyle valleys (©FANC2009). Higher radon emission (> 10% chance to pass > 400 Bq/m<sup>3</sup>) corresponds to the Mousty Formation and the presence of shallow Palaeozoic rocks. Low radiation emission (< 1% chance to pass > 400 Bq/m<sup>3</sup>) occurs at the hill tops around the valleys.



## TASK 6 – Geomorphological study on field and on the DEM to evaluate the relationship between geomorphology and the underlying geological structure

A detailed mapping of a possible fault trace based on geomorphological evidence is very difficult owing to the fact that outcrops are scarce and impede observing possible fault scarps. Especially the observation that the top of the Brabant Massif is strongly fractured (the fractured upper 5 m of the Brabant Massif serves as an aquifer in the HCOV code) complicates the goal of Task 6. Observing a clear fault scarp can, probably, be excluded because of the fact that the fault acted as a left-lateral strike-slip fault (see Task 2), a geometry which does not necessarily results in any vertical displacement. Based on the 3D hypocentre analysis (Task 1), the 2008-2010 sequence did not affect the surface; after all, the hypocentres are densely located between 5 km and 7 km and only a few doubtful events have occurred in the subsurface.

Despite these constraints, we performed a geomorphological analysis of all lineaments visible on the DEM. After all, it might be possible that the fault could have been active in the seismological history of the Quaternary of which palaeoseismological evidence might be found. The orientation of rivers and valleys has often been used as a morphological presence of faults. From the 3D hypocentral distribution (Figure 6) we calculated the position where the fault could have affected the surface, providing that the fault dip remains constant (c. 87°N) towards the surface. This calculation lead to hypothesis that the fault could hit the surface north of the hamlet of Faux. On the DEM map, several small stream valleys align NW-SE in this region (Figure 21). Especially the NE-SW curvature of the Dyle valley at La Motte (2.5 km SSW of Court-Saint-Etienne) is an interesting valley orientation that could correspond to the fault trace at Faux. However, after a careful investigation in the field, we noticed that many lineaments can be related to the local Cenozoic cover geology. The presence and the competence of the calcified sandstones in the Eocene Brussels Formation plays an important role in the geomorphology of the area as they are resistant to erosion and will stand out in the topography. This is for instance the case at La Motte.

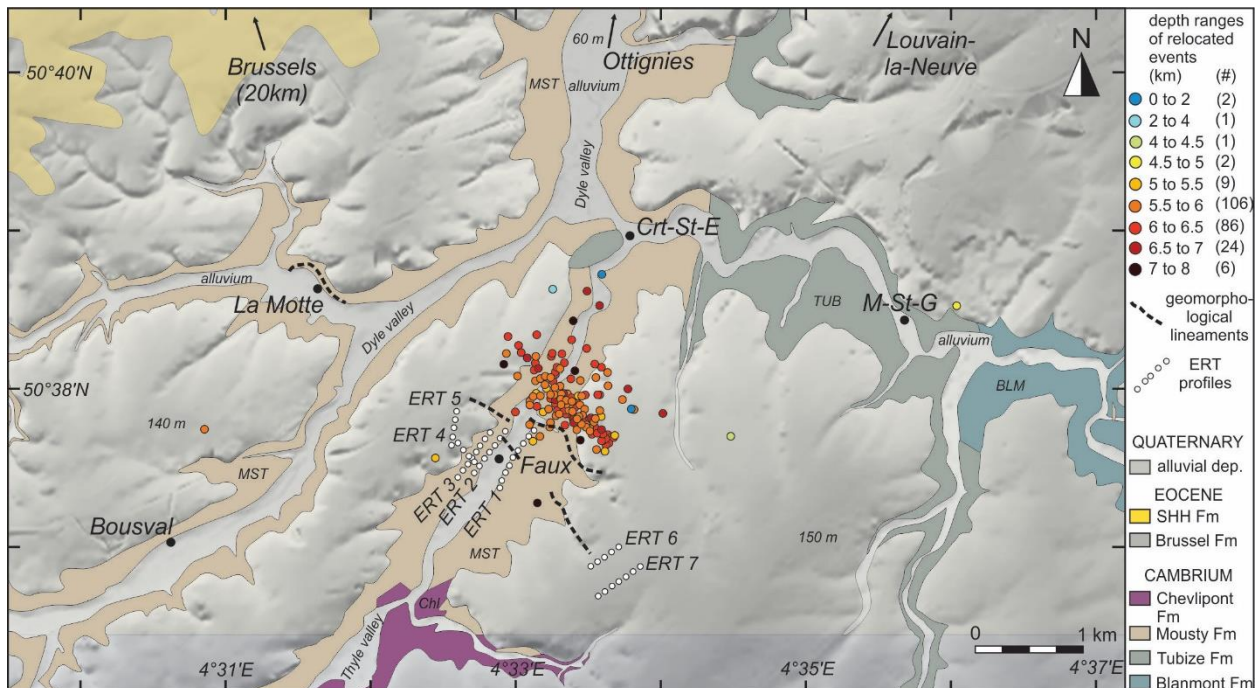


**Figure 21:** Geomorphological lineaments (dashed lines) in the epicentre area. Lineaments often correspond to the orientation of small streams and river valleys. Few lineaments have been investigated by Electrical Resistivity Tomography profiling (ERT) and are discussed in Task 7.

## TASK 7 – Geophysical survey by Electrical Resistivity Tomography

Based on the selected site in the Faux area at which a fault trace could have affected the surface (identified in Task 5) several electrical resistivity tomography (ERT) profiles are conducted. Ambient noise measurements by H/V are performed in Task 8.

### 7.1. Methodology

In two-dimensional ERT, a spread of 64 electrodes is laid out along a straight line with all electrodes equally spaced in distance. Resistivity measurements are then carried out using a specific electrode layout or array (e.g. Wenner-Schlumberger or dipole-dipole array) that is best suited for the objectives of the study. For each array, different array separation factors are chosen depending on the desired vertical resolution and penetration. The Wenner-Schlumberger (WSC) array is more sensitive for detecting vertical changes in resistivity whereas dipole-dipole (DDP) is better for visualising horizontal changes in resistivity. Compared to the DDP, the WSC has a slightly larger depth of penetration and a better signal/noise ratio (Loke, 2004). For each array, all possible measurements are carried out sequentially down the line of electrodes. In this way a large number of independent apparent resistivity measurements are performed that afterwards need to be inverted to obtain a two-dimensional model of the true resistivity of the subsurface.

Depending on the spacing of the electrodes different depths can be investigated. An electrode spacing of 5 m corresponds to a maximum investigation depth of 40 m, whereas a smaller spacing results in a more shallow depth but a higher resistivity resolution. The ERT profiles were conducted using an LS Terrameter (ABEM) and using four cables of 16 electrodes each, branched to the resistivity meter. Using a roll-along technique, the length of the profile (but not the depth) can be extended by multiples of 16 m. Visualising the true resistivity profiles can be performed by inverting the apparent data, visualised in a pseudosection, in the RES2DINV program (©Geoelectrical). This program iteratively calculates a resistivity model section, trying to minimise the difference between the observed apparent resistivity and those calculated in the model. Based on different models of inversion, i.e. normal, robust-blocky or combined, different end results are visualised in the resistivity profile. A python script developed by Dr. K. Vanneste (ROB) has been used and allows a flexible manipulation of the RES2DINV program.

### 7.2. Conducted ERT profiles

In the autumns of 2012 and 2013 seven ERT profiles were conducted in the Faux hamlet (Figure 22 and Figure 23). Six profiles are oriented at high angle to the suspected NW-SE oriented fault and are taken parallel to the NE-SW oriented Thyle valley. Only profile 4 was conducted in an NW-SE orientation, perpendicular to the valley orientation (Figure 22). These profiles are very useful to gain insight in the topography of the basement, i.e. the top of the Brabant Massif, in order to derive sediment/soil thicknesses (see also Tasks 8 and 9) and to derive a possible fault trace, taking into account the serious limitation that the fault may not have affected the (sub)surface.

From the resulting profiles in the Thyle valley (Profiles ERT1 and ERT2), an uppermost low-resistivity layer (blue coloured,  $< 97.7 \Omega\text{m}$ ) can be distinguished that corresponds to the alluvial clays in the valley. In the southeastern part of profile 1, this layer is more or less 10 m thick which corresponds to the 8.8 m soil thickness that has been described in Borehole 130W0267, situated close to the Faux station. At lower depths, the resistivity increases to a higher value ( $< 134.2 \Omega\text{m}$ ), indicative of the top of the Brabant Massif basement rocks. The very low resistivity at lower depths in profile ERT1 is probably an artificial effect due to the fact that electrical resistivity tomography cannot be performed below a higher resistivity layer.

An interesting feature is visible in the middle part of profile 1 and at about  $2/3^{\text{th}}$  of profile 2. There, a low resistivity vertical structure is present between a higher resistivity horizontal layer. Up to now, this structure is not yet understood and it is unclear whether or not it might reflect a fault. However, one



argument against a fault structure is the local structural orientation of folds and cleavage of the basement rocks in this area. In the outcrops visible in the railroad section, Debacker et al. (2004a) and Van Tassel (1986) both mapped NE-SW oriented bedding and fold axis, an orientation that fits to the linked structure between ERT profiles 1 and 3. Hence, this structure likely represent bedding variation.

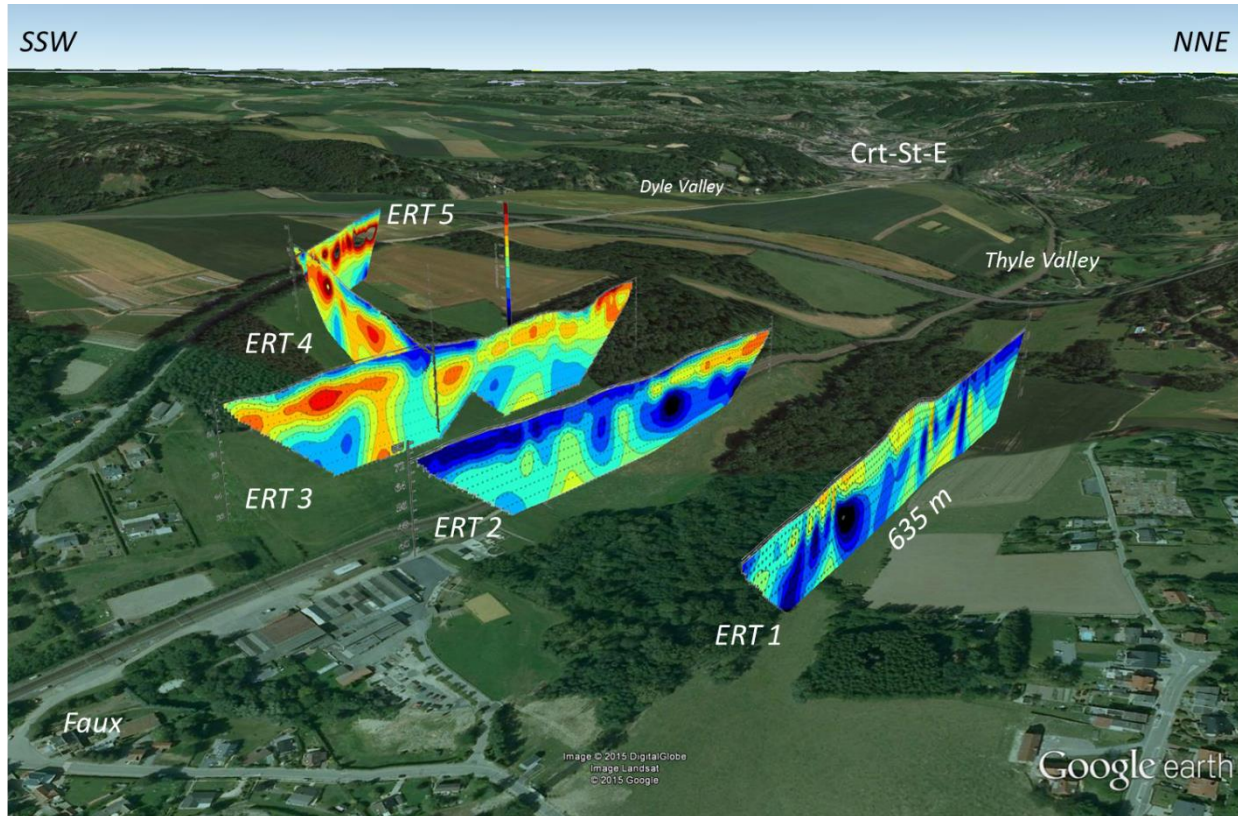


**Figure 22:** Electrical Resistivity Tomography profiles (WSC array) conducted in the Faux area and visualised in Google Earth. Profiles ERT1, ERT2, ERT3 and ERT5 are oriented parallel to the Thyle valley, profile ERT4 is perpendicular to the valley structure. The low resistivity layer (blue) at the top of each top likely corresponds to the presence of alluvial clays in the Thyle valley. These alluvial deposits disappear along the valley flank (profile ERT4).

The northern part of profile 3 is taken in a dense forest where the roots probably mix up the resistivity measurements and display an unrealistic high resistivity.

In profile 4, perpendicular to the valley floor, the alluvial clays disappear towards higher ground. The high resistivity ( $> 253.0 \Omega\text{m}$ ) in profile 4 reflects the shallow presence of the basement rocks of the Brabant Massif along the valley flank.

Whereas the ERT profiles in the valley show only thin alluvial clays on top of the basement rocks, two other ERT profiles, conducted on the hill top south of Faux, show a clear increase of thickness of sediments overlying the Brabant Massif (Figure 23). In profile 7 a rather flat topography of the Brabant Massif is visible. 15 m of Brussels sands are present above the basement. Similar as to ERT 7, also in ERT 6 the sharp contrast in resistivity visualises the contact of the bedrock with the overlying Brussel Sands. Thickness ranges from 10 m in the NE to a few metres in the SW (Figure 23). No faults can be deduced from both profiles.

Although we could not find clear evidence for a fault trace, the ERT profiles are still very useful for objective 3 to estimate the local site effects related to the seismic swarm. From the ERT profiles a better insight can be gained into the topography of the basement, i.e. the Brabant Massif, and the lateral

sediment thickness variation. The results of the ERT profiles are, moreover, useful to understand the ambient noise measurements (Objective 3).

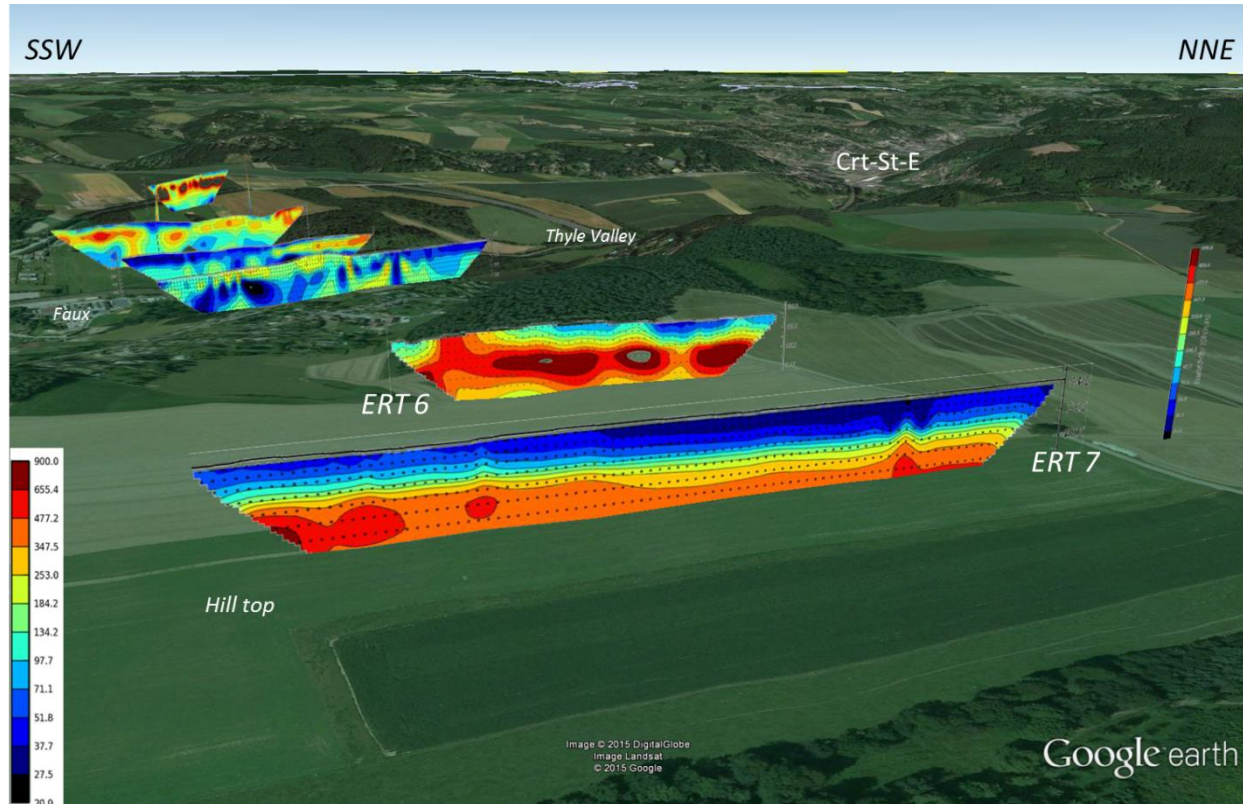


**Figure 23:** ERT 1 to 5 are located in the Thyle valley, ERT 6 and 7 are conducted on the hill top east of Faux (close to the roundabout at Arbre de la Justice). The low resistivity layer (blue) at the top of each top corresponds to Quaternary loess sediments. Light-blue to yellow colours represent the Brussels sands. Red = basement rocks. Depth of the basement estimated at 15m.

## TASK 8 – Interpretation of data in Tasks 4, 5 & 6: the relationship between faults and the shallow geological structure

Although we spend a considerable amount of time in the detection of a possible fault structure at the subsurface, a clear relationship between seismicity, fault structure, geomorphology and the shallow geological structure cannot be established. After all, geomorphological and geophysical analysis did not lead to any obvious or detectable continuous fault structure. The 2008-2010 seismicity did not have any shallow events that allowed to refine the search area. Also, the rather low magnitudes, the limited length of the fault and the absence of reported damage during the different earthquakes (see further) are not in favour to have created a surface rupture, now or during the 1953-1957 sequence. Moreover, due to the fractured nature of the top of the Brabant Massif, the NW-SE orientation of local fold structures and the mostly E-W oriented cleavage within the basement rocks, it is also unlikely to pinpoint a specific structure that could correspond to the surface expression of the fault. Even if a continuous structure can be found, we will be never sure whether this structure corresponds to a local feature related to variation in the local geology or to a fault structure. During this project, it was therefore chosen to spend more time in other objectives than into the identification of a potential structure in the subsurface.



## C. Site effects and S-wave attenuation in the Brabant Massif

### TASK 9 – Resonance frequency maps determined by H/V ambient noise recording

Investigations on the geological site conditions provide evidence that the local geological structure of a site can modify the characteristics of the ground motions produced by earthquakes in such way that ground motions can be amplified or attenuated. The third objective therefore aims to study the local site effects and attenuation of S-waves inside the Brabant Massif.

Taking into account the pronounced hilly topography of the research area, sites can be described by the resonance frequency of the soil that varies according to the thickness of the soil above the bedrock. These are important aspects to quantify the impact of the earthquakes in the region of Court-Saint-Etienne and to evaluate the seismic hazard in the future.

#### 9.1. Methodology

Estimating the sediment thickness and the geometry of the bedrock is a key component of many hydrogeological and seismic studies and can be of major importance to understand how earthquake waves are transferred or attenuated through the upper crust (Petermans et al., 2007; Rosset, 2006; Rosset and Petermans, 2007). The horizontal- to vertical (H/V) ambient noise seismic method is a novel, non-invasive technique that has been used to estimate the depth of the bedrock below sedimentary layers. The H/V method (Nakamura, 1989) uses a single, broad-band three-component seismometer to record ambient vibrations produced by local surface sources such as traffic and other human activities or from far-distance sources such as oceanic waves and wind structures. The seismic noise recorded are signals of low-amplitude motions of the ground. Periods from noise associated to wind and human activities are predominantly below 0.1 Hz, whereas noise generated by near-shore oceanic waves and current is at higher periods (SESAME, 2005).

For the measurement of the ambient noise we used the equipment available at the ROB: one 24-bit Cityshark II acquisition system (LEAS) connected to a 3-component LE-3D/5s Lennartz seismometer (Figure 24). The seismometer allows recording ambient noise measurements between 0.2 Hz and 50 Hz and adjustment of the sampling rate. Data are stored on a Compact Flashcard which

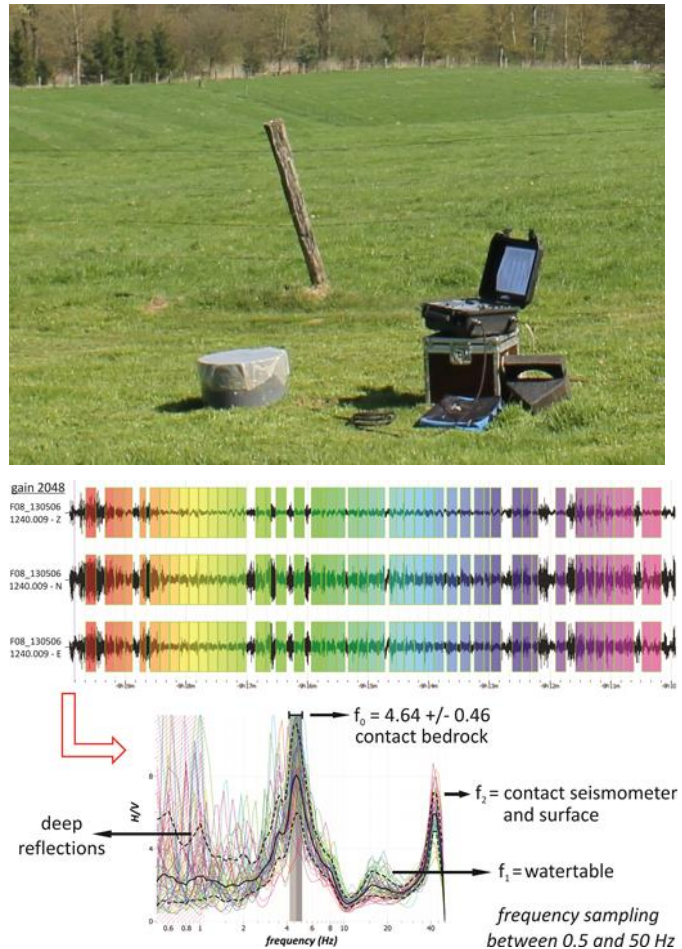


**Figure 24:** (above) Cityshark II (black box) connected to a seismometer that is protected from the wind by the grey box. (below) Ambient noise analysis, windows selection and  $f_0$ -calculation in GEOPSY. Semi-automatic STA/LTA triggering rejects windows with too much noise (e.g. cars passing) for the H/V calculation.

can be downloaded and further analysed. Duration of the ambient noise recordings are between 10 and 20 minutes. The gain level can be adapted to the local conditions and mostly varies between 128 (noisy traffic) and 2048 (calm rural environment). Position of the measurement is recorded by a handheld Garmin GPS.

The spectral analysis is performed by using the open source GEOPSY software (Wathelet, 2005). In the H/V module, the program calculates the Fourier spectra of the horizontal, with H as the mean of E-W and N-S components, over the vertical (V) component of ambient noises (Figure 25). The obtained spectral ratio generally exhibits a maximum amplitude peak and its corresponding frequency that generally corresponds to the fundamental resonance frequency  $f_0$  of the site. Other minor peaks can correspond to other contact that show a significant acoustic impedance contrast such as the groundwater level. Data analysis occurs by selecting overlapping (usually 5%) windows of 30 seconds that move over the seismic signal (Figure 24). Windows in which too much noise is generated, e.g. cars passing, electrical equipment running, are rejected by a semiautomatic anti-triggering tool as these windows will disturb the general H/V curve. The resulting curve is smoothed by a Konno and Omachi (1998) smoothing effect of 40%.

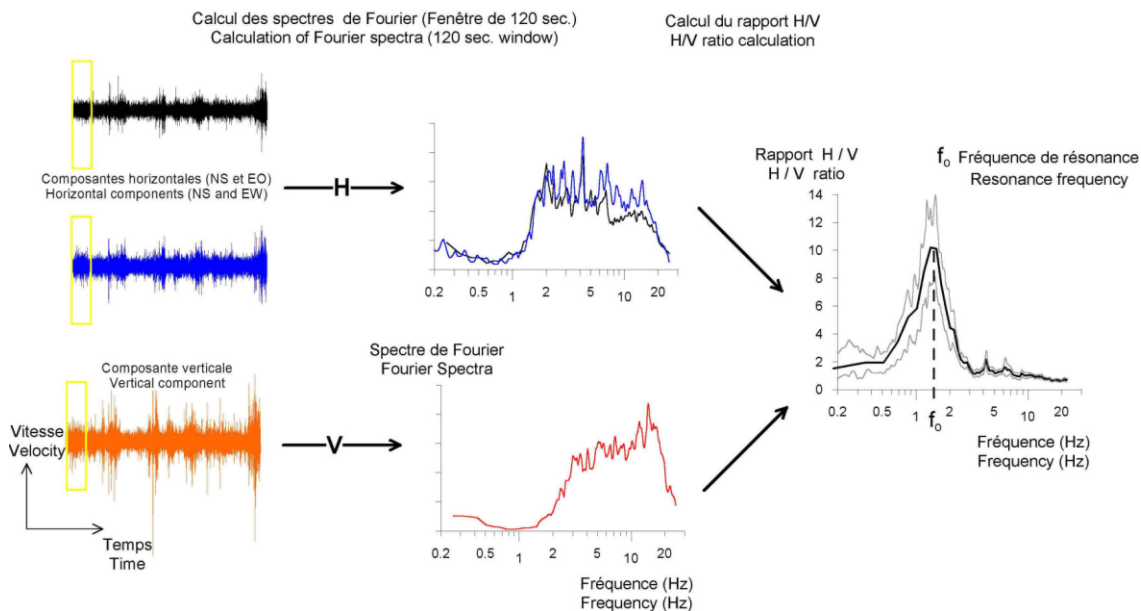


**Figure 25:** Procedure for H/V ambient noise analysis (Rosset and Petermans, 2007). Fourier analysis of the horizontal and vertical components of ambient noise allows determining the resonance frequency  $f_0$  of a certain site.

The ratio of the averaged horizontal-to-vertical frequency spectrum, that is used to determine  $f_0$ , can then be interpreted using regression equations to estimate depth to the bedrock and eventually also sediment thickness. The relationship between the thickness of the soil and the resonance frequency is given by following linear relationship (Bard, 1985):

$$f_0 = V_s/4h \quad (\text{Equation 2})$$

with  $h$  = soil thickness and  $V_s$  = shear wave velocity of the soft soil layer. Importantly, if the resonance frequency of the soil equals the resonance frequency of buildings due to site effects or site amplification, damage could arise during earthquakes. So by using the H/V method we can estimate the influence of the soft deposits on ground shaking and we can construct detailed maps of the local site effects in which the spatial variation of the ground response is estimated through field measurements.

In specific sites where the bedrock depth is known, equation 2 provides an estimation of the average  $V_s$  of all layers above the bedrock. This equation is useful for simple, one-layer-over-halfspace configurations, e.g. alluvium above bedrock, as the average  $V_s$  can be used to estimate  $h$  for sites at which bedrock depth is unknown. However, in more complex configurations, the average  $V_s$  of multiple soft-sediment layers

overlying bedrock is not always truly representative of the real  $V_s$ . However, case studies of the H/V method show that for a sufficiently large impedance contrast between bedrock and soft sediments, the fundamental peaks in the H/V spectra can be empirically correlated to the overall thickness of sediments by a power-law equation (Benjumea et al., 2011; Hinzen et al., 2004; Ibs-von Seht and Wollenberg, 1999).

An empirical relationship applicable for the Court-Saint-Etienne area can be calculated by conducting HVSR analysis of ambient noise measurements above boreholes with known bedrock depth. Borehole information is retrieved from the [GISEL](#) application of the Geological Survey of Belgium and the [DOV](#)-website. Additional H/V measurements above geophysical profiles such as created by Electrical Resistivity Tomography (ERT) furthermore allow training and improving the powerlaw relationship for sites with a shallow bedrock depth.

## 9.2. Results

### 9.2.1. Establishing the resonance frequency – sediment thickness powerlaw relationship

To estimate the response to ground shaking, numerous H/V-measurements are conducted. The HVSR measurements primarily concentrate on the region in which a large part of the population has felt/heard the seismic sequence as is derived from the macroseismic internet inquiries (see Task 10). H/V measurements were conducted above all boreholes that reach the bedrock in a region between Genappe in the south and Limal in the north (Figure 26).

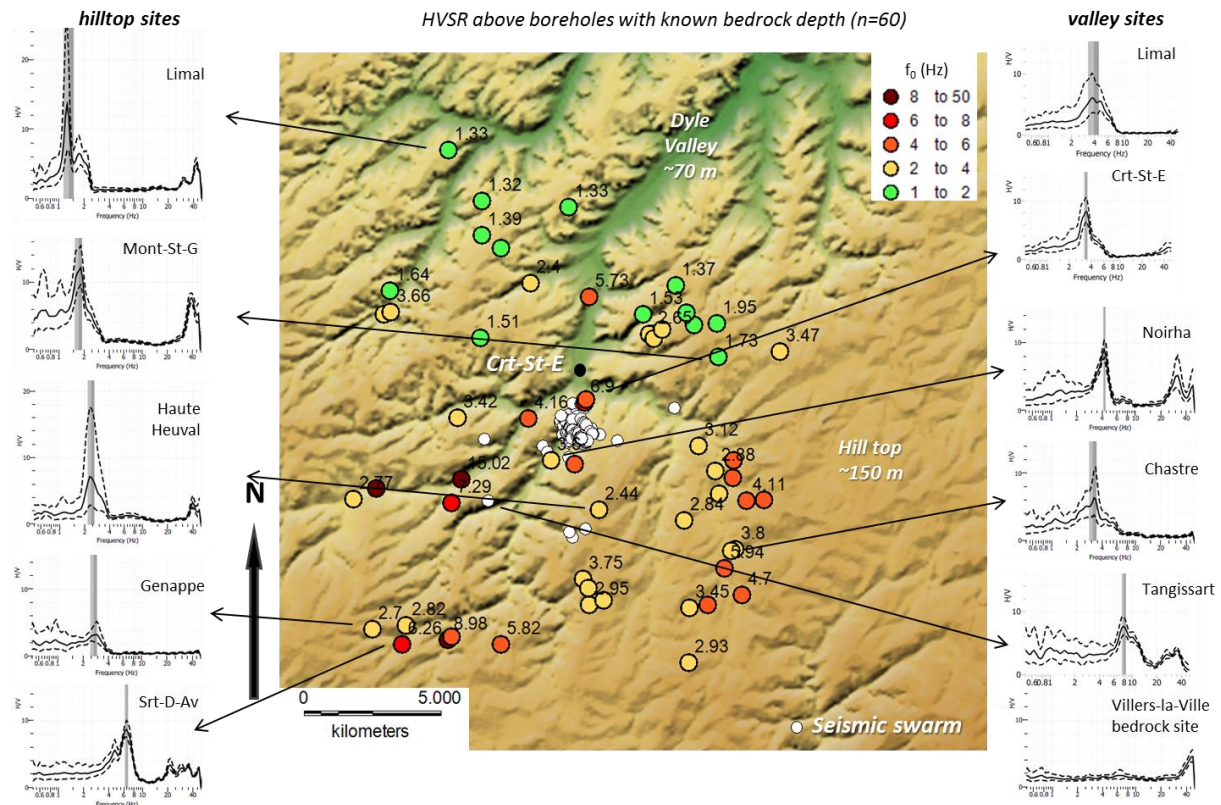


**Figure 26:** 60 H/V measurements conducted above all boreholes that reach bedrock depth. Fundamental frequency decreases towards the north as the bedrock depth increases. However, high  $f_0$  values are also measured in the incised Dyle and Thyle valleys due to shallow bedrock below the alluvium.

The H/V results in Figure 26 clearly show a general decrease of  $f_0$  towards the NW, both on the hill tops as in the valleys, conform the dip of the top of the bedrock. The flanks of the eroded Dyle and Thyle



valleys, however, exhibit higher  $f_0$  values because of a considerable decrease of sediment thickness due to river erosion. On the valley floor,  $f_0$  is slightly lower than on the flanks as a Quaternary clayey alluvium has been deposited in Dyle and Thyle valleys (~15 m thick at Court-Saint-Etienne).

From this survey an empirical powerlaw relationship of

$$h = 129.29(\pm 19) \cdot f_0^{(-1.733 \pm 0.03)} \quad (\text{Equation 3})$$

was established that explains the relationship between resonance frequency  $f_0$  and sediment thickness  $h$  (Figure 27). The error estimation in the equation results from the error estimation of the  $f_0$ -peak calculated in GEOPSY (see grey bars in Figure 24). Corresponding the error, a maximum and minimum powerlaw equation can be calculated (see grey curves in Figure 27A). We however note that this empirical relationship can only be used for a depth interval between 5 m and 85 m and for an area in which the geological structure is similar as the investigated area. Comparing the sediment thickness calculated by the powerlaw with the true sediment thickness retrieved from the borehole reports shows that the powerlaw equation slightly underestimates true sediment thickness between 20 m and 40m (Figure 27B). Nevertheless, with this powerlaw relationship, we can now perform additional ambient noise measurements at sites with an unknown bedrock depth to calculate resonance frequency and to derive sediment thickness.

Based on equation 2, the powerlaw also allows estimating the variation of  $V_s$  with depth. Figure 27C shows that the variation in  $V_s$  of the Quaternary alluvial clays in the valleys and the Quaternary loess deposits on the hill tops ranges between 100 m/s and 200 m/s and that this variation depends on the thickness of sediments. Similarly,  $V_s$  of the Brussel Sands covering the basement varies between 350 m/s and 450 m/s. It can be concluded that this  $V_s$  variation is more representative for a given area than an average  $V_s$  established from equation 2 as compaction is now included in the velocity profile.

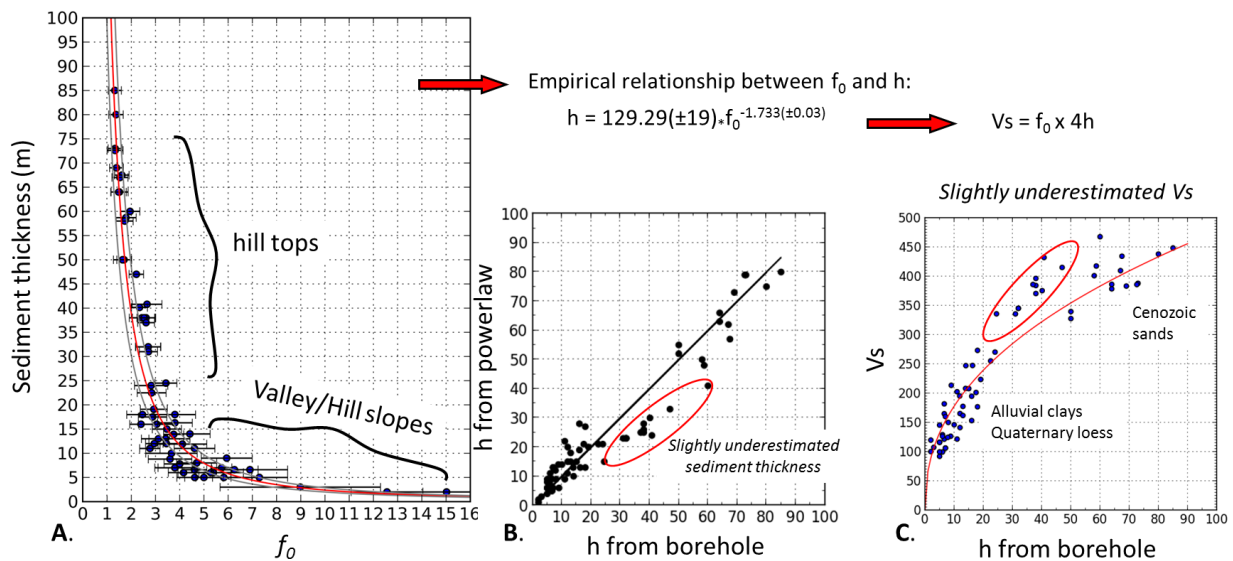


**Figure 27:** (a) Empirical relationship between fundamental frequency and sediment thickness established from H/V measurements above boreholes. Red curve: powerlaw of mean  $f_0$ , grey curves: powerlaw curves of minimum and maximum error on  $f_0$ . (b) Comparison between true  $h$  with  $h$  from empirical relationship. The powerlaw slightly underestimates the true thickness between 20 m and 40 m. (c) Powerlaw relationship between thickness and  $V_s$  as indicated by the relationship  $V_s = f_0 \times 4h$ .

9.2.2. Additional H/V measurements & applying the powerlaw equation

From the calculated H/V ratio and the resulting resonance frequency, the powerlaw will give a proper estimation of the sediment thickness of that site. To train the powerlaw, H/V measurements were performed above the ERT profiles that have been conducted in Task 7 (see Figure 28). Two examples are give in Figure 28: one ERT profile measured at the hill top site E of Faux (ERT 7) and one in the Thyle valley at Faux (ERT 1). In both cases, the bedrock depth established from ERT imaging more or less (with a variation of 2m) predicts the same depth as when the powerlaw is used on the measured  $f_0$ -peak.

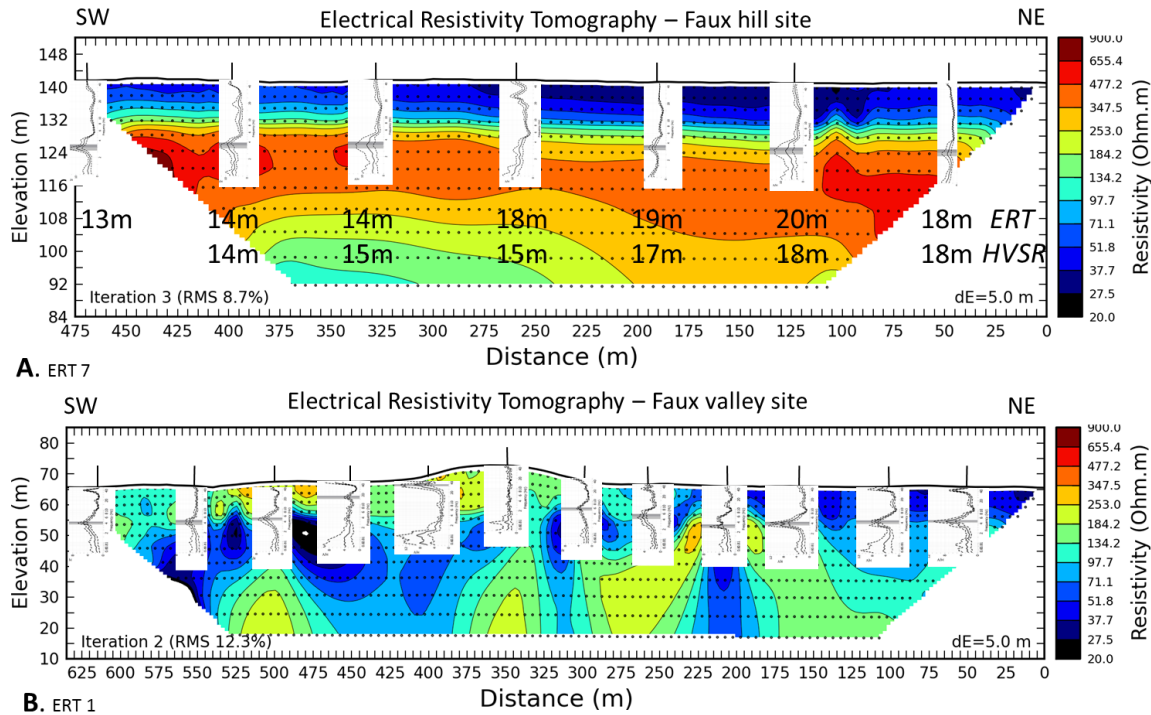


**Figure 28:** Comparison of bedrock depth estimated from ERT measurements and calculated from the established powerlaw relationship. With an error of a few metres, both techniques result in the same depth estimation. A) ERT 7 – hill top site. B) ERT 1 – Faux valley.

To understand and visualise the geological structure of the Court-Saint-Etienne area, we first performed several H/V cross-sections oriented parallel and perpendicular to the Thyle valley in the epicentral area of the seismic swarm. In particular, the valley sites at Faux and La Roche, and the hill tops E and W of the Thyle valley are investigated in detail. H/V measurements along these profiles are regularly spaced between 50 m and 150 m. Each H/V measurement is analysed in GEOPSY to derive the  $f_0$  of this site. The results of this microzonation are shown in Figure 29 and few representative individual H/V analyses are shown in Figure 30. GEOPSY also provides a module to create a profile in which the individual H/V spectral ratio is shown as function of the distance along the profiles. The value of the amplitude spectra between individual H/V points results from linear interpolation.

As example Profile L and Profile J are shown. Profile L was taken along the hill site west of the Thyle valley and continues through the Thyle valley. Because of the high acoustic impedance between soft sediment and bedrock, the bedrock geometry can be visualised by the amplitude variation of the H/V peak (purple = high amplitude, green/oranje = low amplitude) as amplitude variations are sensitive to buried topographic variations. Both Profiles L and M show similar features: on the hill sites,  $f_0$  varies between 2.6 and 3.5 Hz, corresponding to a sediment thickness of 25 m and 15 m, respectively. Along the valley flank,  $f_0$  rapidly increases to values  $> 10$  Hz, representing a thin cover of 2 m caused by the erosion of the valley flanks.



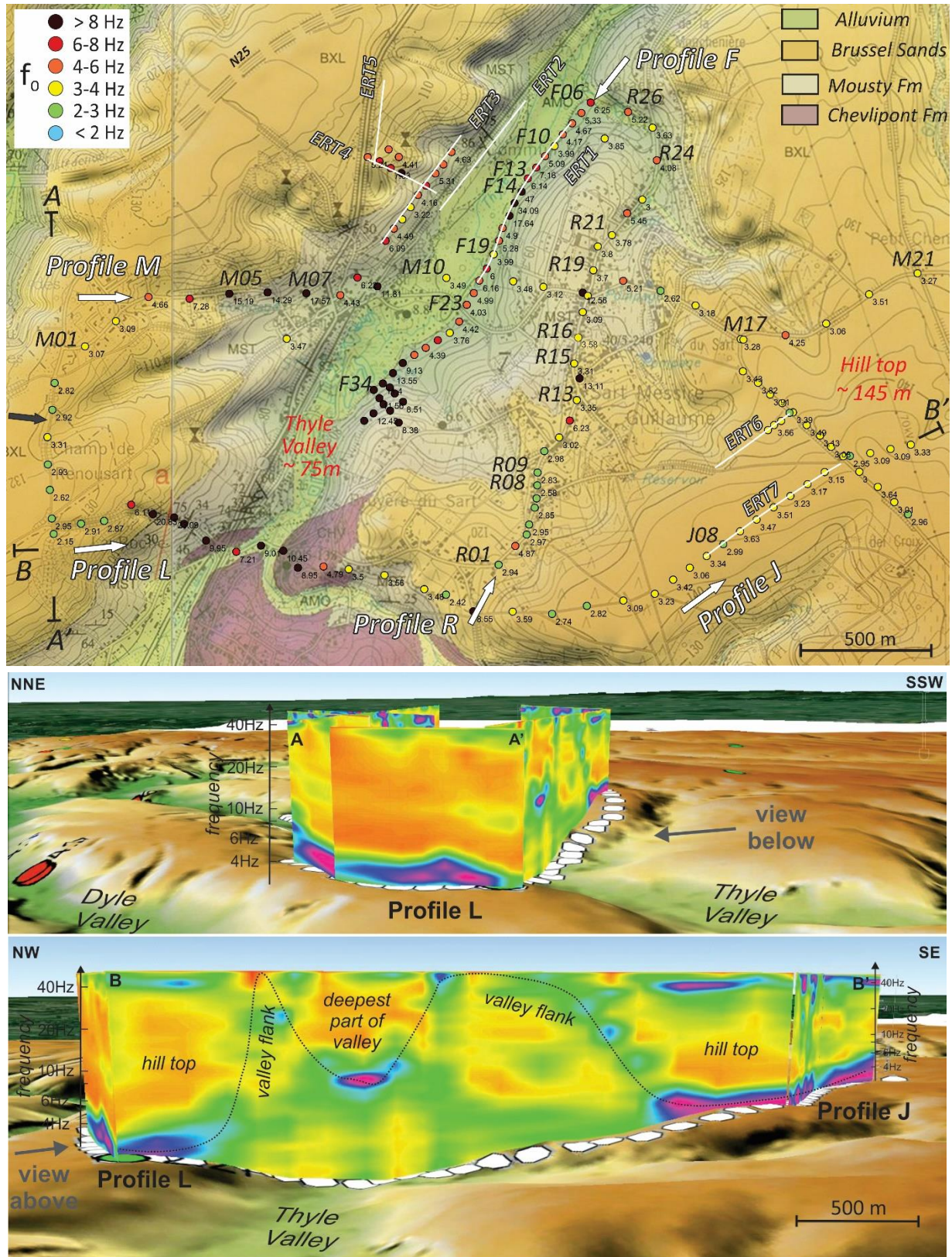


**Figure 29:** H/V measurements performed at Faux. Numbers correspond to  $f_0$ . Cross-sections illustrate numerical interpolation between individual H/V points and indicate how the H/V results can be used to map bedrock depth variation through a valley. Hill top site ~20 m sediments. Valley site ~14 m. Increase of  $f_0$  along valley flanks.



**Figure 30 (right):** Individual spectra of single ambient noise measurements in the Faux – La Roche area. See Figure 29 for location of the measurements.

Detailed profiling leads to the following observations/conclusions.

**Profile F:** varying  $f_0$  values due to irregular bedrock morphology in the Thyle valley. Note the absence of a peak in F14 as this measurement is performed at a rock site (see also Figure 28b).

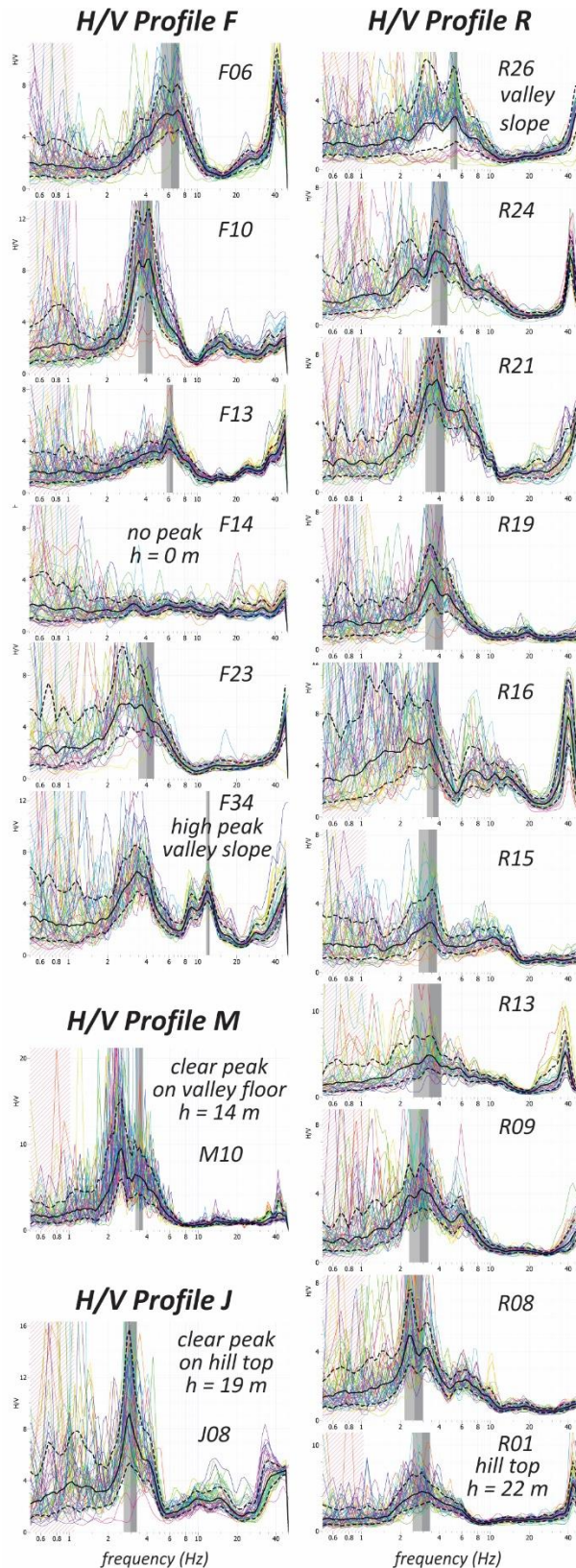
**Profiles M & L:**  $f_0$  increases from the W hill top towards the valley and is the highest at the valley slope (M05-M07). In the centrum of the valley (see M10,  $f_0$ : 3.49 Hz = 14 m),  $f_0$  is higher and reflects the accumulation of the Quaternary alluvium.  $f_0$  gradually decreases towards the E hill top. Sediment thickness in the valley floor increases from south to north.

**Profile R:** S - N profile from hill top (R01) to valley floor (R26) along the valley slope:  $f_0$  increases due to thickness decrease of 20 m (R01) to 7 m (R26) along the valley flank.

**Profile J:** Profile on the hill top showing a constant  $f_0$  and sediment thickness of 19 m.

The cross-sections and individual H/V spectra show that  $f_0$  is not always that obvious along valley flanks as not enough energy might be excited to detect a reliable  $f_0$ . In addition it has to be noted that the H/V peak has a tendency to become broader when the slope of the buried bedrock increases: compare the broad peaks in profile R versus the relative small peak in Profile J.

Detailed H/V profiling eventually results in understanding the shape of the weathered bedrock geometry and will be used as an additional input for sediment thickness modelling executed in Task 10.



## TASK 10 – Macro seismic investigation of internet earthquake inquiries

### 10.1. The transferability of the Brabant Massif

The shallow presence of the Brabant Massif in the Walloon Brabant, but also in southern Limburg and Liège provinces, plays a prominent role in how earthquake vibrations are experienced by the people in central Belgium. On 8 September 2011 19:02:50 a  $M_L$  4.3 earthquake occurred at Goch (NL) on one of the basinbounding faults of the Venlo Graben and caused minor damage in The Netherlands. In contrast to the NE part of Belgium, where the event was barely felt, many macroseismic reports were submitted in central Belgium at larger epicentral distances (Figure 31). The peculiar shape of the intensity distribution cannot be explained by a traditional geometrical amplitude attenuation, relating energy decay to the increasing epicentral distance.

In central Belgium, the Brabant Massif is present at the surface in incised river valleys and it gradually deepens towards the north where it is covered by soft sediments. The macroseismic distribution of the 2011 Goch earthquake exemplifies that the area over which this event was felt might be related to the thickness of the sediment column above the Brabant Massif and that sediments might have a significant influence on earthquake strong ground motions. To the north of Brabant (Limburg & Antwerp provinces) vibrations are probably attenuated due to the thick Cenozoic sediment cover. In central Belgium, the E-W elongated shape of the felt shaking or damage is not due to a better transfer of seismic waves in the E-W direction, but rather to an E-W elongated zone with sediment thicknesses that amplify seismic waves in the frequency range to which humans and buildings are susceptible. The reported damage from the 1932 Oudenaarde earthquake ( $M_S$  5.0) shows a similar E-W damage distribution (Nguyen et al., 2004) illustrating the importance of the shallow presence of the Brabant Massif. Also on a local scale and for low-magnitude earthquakes such as for the Walloon Brabant seismic swarm, the shallow presence of the Brabant Massif might play a prominent role on the perception of the felt events of the seismic swarm. Macro seismic maps illustrating the earthquake perception are herein valuable tools to analyse the spatial impact of felt events.

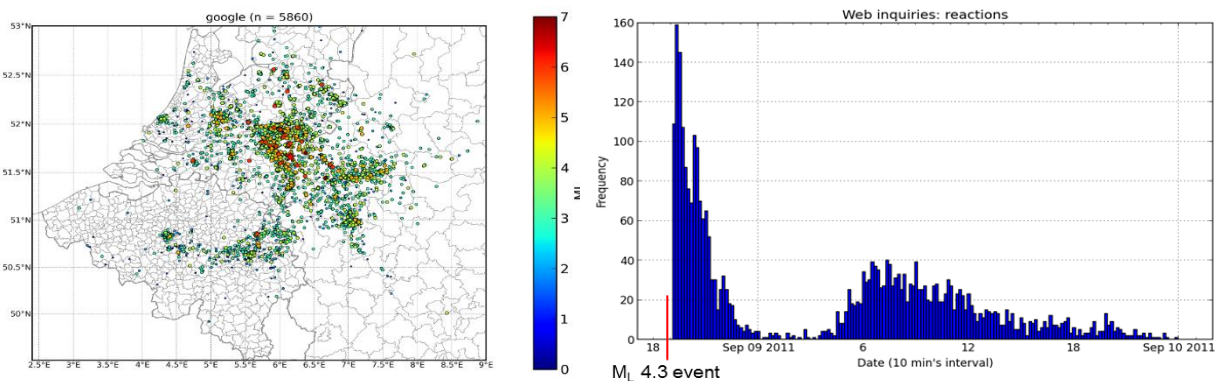


**Figure 31:** Macro seismic intensity map and responsiveness of the people to the Goch  $M_L$  4.3 earthquake (08-09-2011). The thick pile of sediments covering the Brabant Massif in the north of Flanders probably attenuates vibrations that are felt in central Belgium.

### 10.2. Macro seismic internet inquiries related to the Walloon Brabant seismic swarm

The Royal Observatory of Belgium cooperates with the Cologne University on a trans-border web-based macroseismic data acquisition on the seismology website. Community Internet Intensity (CII) and Macro seismic Intensity (MI) evaluation estimated from ‘Did You Feel It’ (DYFI) inquiries (Wald et al., 1999) are useful tools to quickly analyse the area over which an earthquake was perceived. The reported macro seismic intensities are conform to the official European intensity scale (EMS-98 scale) which denotes how strongly an earthquake was felt in a specific place. In addition to being extremely useful for rapid post-earthquake information, ‘Did You Feel It’ data are also robust and of surprisingly high utility.



They offer the potential to not only describe ground-motion effects qualitatively, but also to be used in quantitative scientific studies. DYFI data make up in quantity what they lack in quality and can thus provide a estimation of earthquake ground motion (Atkinson and Wald, 2007).

The macroseismic internet inquiries of the Walloon Brabant sequence were a great success. Owing to the high responsiveness of people, 60 events of the total 239 events of the seismic swarm have been reported to be felt or heard. Consequently, the seismology section has now a large databank of testimonies on how strong and where people have felt the earthquakes in the Walloon Brabant. Their contribution is very import for us as we can study the local seismic impact by investigating each earthquake in detail. In a community internet intensity (CII) map all the reported macroseismic intensities (MI) of one community zip code are averaged and an average intensity value is assigned to the zip code area. Only if three or more responses are located in the same zip code, then the zip code will be coloured in the CII map. The CII maps of all the 60 felt events of the Walloon Brabant seismic are shown in Figure 33, Figure 34 and Figure 35. These CII maps illustrate the distance over which the earthquake has been felt. If a sufficient amount of total responses are submitted and if the earthquake has a sufficiently large magnitude, a macroseismic intensity decay with epicentral distance will be apparent. However, a variety of factors, such as the type of earthquake, rupture direction, local geography, soil conditions, and type and age of buildings, result in an often complicated pattern of varying intensities from place to place.

Thanks to the high and quick responsiveness of the people (Figure 32), we are quite confident that the very low earthquakes of the Walloon Brabant sequence that were reported were really felt and were not a only a reaction of the public to the news spread by the media and on the internet. After all, the histogram on Figure 32 for example shows that several tens of DYFI?-webforms had already been submitted even before any information was published on the seismology website or on the media. It is thus valuable to use the macroseismic information. Especially the fact that some earthquakes, sometimes with very low magnitudes down to  $M_L$  0.4, are heard rather than felt is of special interest. When the perception of such earthquake occurs in the human audible range, then this perception is indicative of the high frequency of the local earthquake source. This contrasts to far-away earthquakes of which the high-frequency content of the earthquake signal will be attenuated by the time/at the place where the perception took place.

Unfortunately, due to the large amount of testimonies and earthquake events, performing a detailed macroseismic study is a very time-consuming task. Also, as we hardly have any experience with how to handle all the macroseismic data, a considerable amount of time of the project was spend on developing a proper methodology to investigate the macroseismic intensity distribution properly.

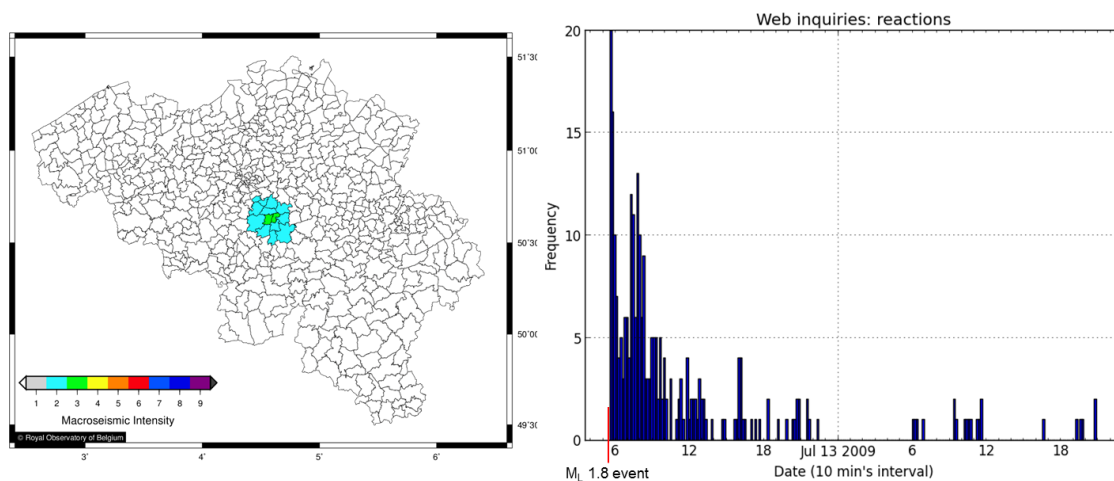


**Figure 32:** Community internet intensity map of a  $M_L$  1.8 event (12-07-2009) and the responsiveness of the people after the earthquake took place. Ten minutes after the event took place (05:29:34) already more than 20 inquiries were submitted to the seismology website. The second response peak between 8h-9h might be related to the effect of the media, or to the information that was placed on the seismology website.



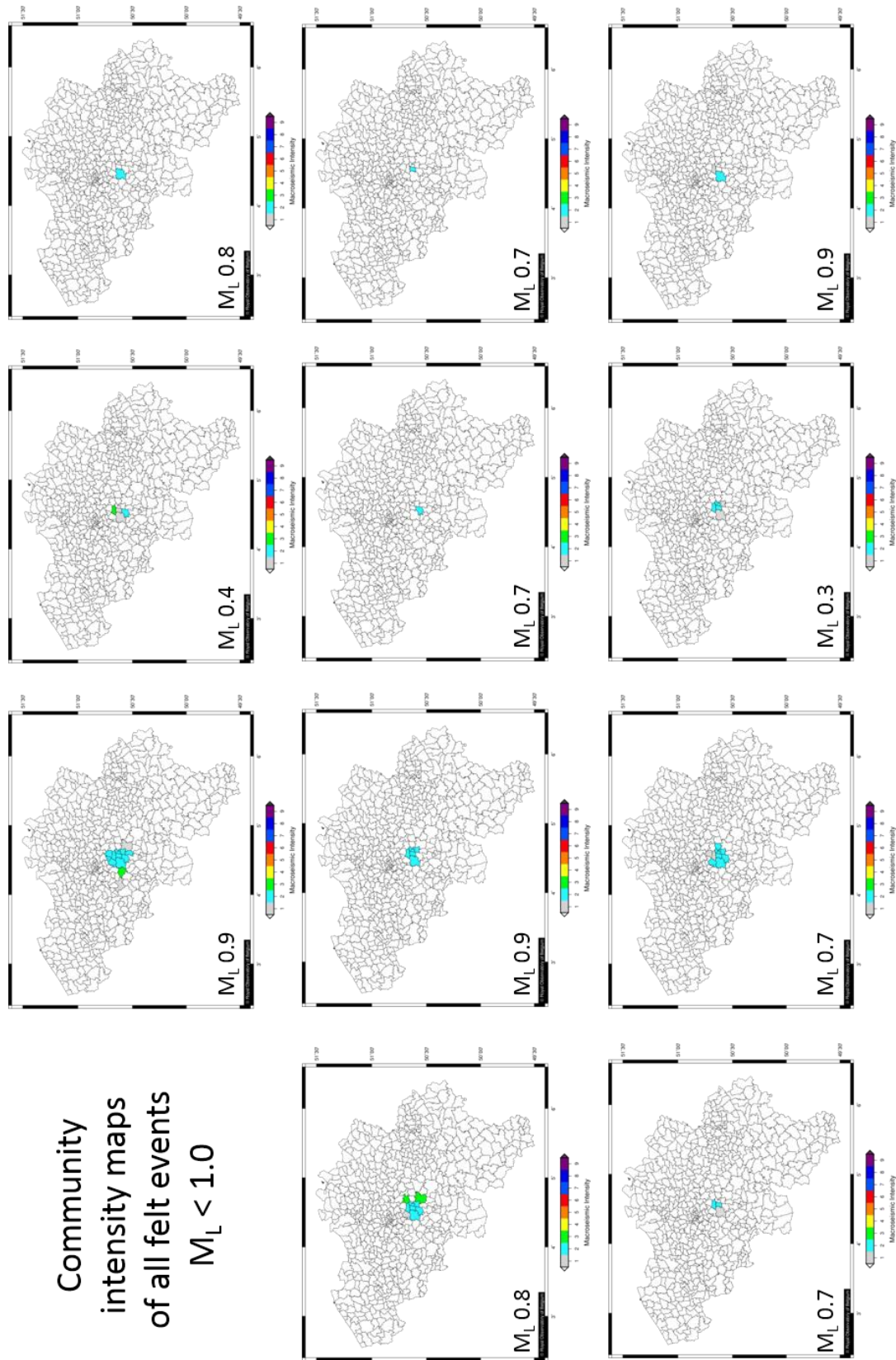
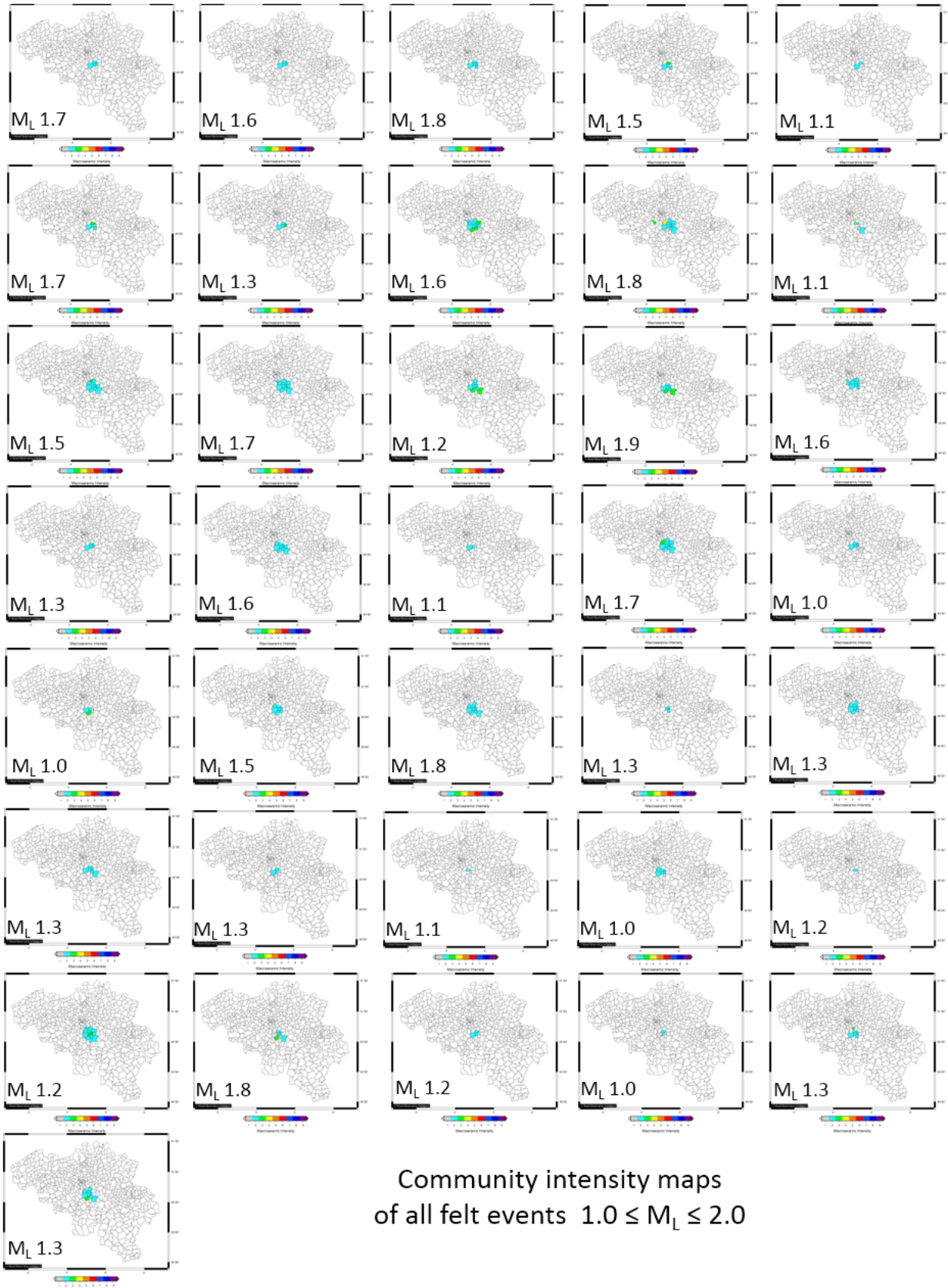


Figure 34: Community internet intensity maps of all felt events ( $n=11$ )  $M_L < 1.0$ . Note the felt  $M_L 0.4$  event.





**Figure 35:** Community internet intensity maps of all felt events ( $n = 36$ ) between  $M_L 1.0$  and  $M_L 2.0$ .

### 10.3. Developing a proper research methodology

In addition to being extremely useful for rapid post-earthquake information, ‘Did You Feel It’ data are also robust and of surprisingly high utility. They appear to offer the potential to not only describe ground-motion effects qualitatively, but to be used in quantitative scientific studies. The key to the usefulness of the data is simply this: they make up in quantity what they lack in quality and can thus provide a reliable relationship between DYFI data and earthquake ground motion (Atkinson and Wald, 2007).

The averaged MI’s of all 60 felt events range between non-damaging intensities of I and IV (EMS-98 scale). A few times intensity V has been reported, but without damage. For larger magnitudes  $M_L > 2.0$ , a gradual decrease of the average MI away from the epicentre can be observed. However, within a single community the reported MI’s locally often vary ranging between I and VI (Figure 36). The average macroseismic intensity decay is thus only useful for larger magnitude earthquakes affecting a large region, but when considering the impact of low-magnitude earthquakes affecting a small area, the averaged MI of a zip code often oversimplifies the local intensity how the people experienced the earthquake. Especially in the hilly area around Court-Saint-Etienne, the geomorphology and local geology might have an influence on the local perception of the people.

In order to provide an answer to the question why the reported MI’s of the small earthquakes have such a large spread in a single community, we thus need to investigate if the perception of the people (sounds or vibrations) was influenced by local site effects.

A site effect study has already been performed in Task 9 and detailed H/V measurements helped to understand the local geology in the Thyle and Dyle valleys. The methodology of tackling this macroseismic research question is as follows:

(i) Currently on the *seismology.be* website only CII maps are displayed. These maps are based on the provided zip code in the inquiry. The true location of observation is not considered in these maps. To overcome this problem, all the individual observations need to be plotted in a GIS to digitise and analyse the macroseismic data. Although people are obliged to give their resident ZIP code in the inquiry, they do not need to submit their detailed address. Consequently, only for a reduced number of people detailed information on the local intensity is available. Usually about 80% of the people provide their street name and number. In order to geolocate the exact position of their observation a new algorithm needs to be developed from which individual addresses can be **geocoded** into their geographical coordinates. Geocoding the location of the individual respondents will lead to a spatial refinement of intensity variation and allows to analyse the felt events in more detail.

(ii) To deduce if macroseismic intensity is influenced by local geology and thickness of sediments covering the Brabant Massif, a **sediment thickness map** of the Cenozoic and Quaternary cover has to be constructed in a 200 km<sup>2</sup> area around the different epicentres. Such sediment thickness map can be constructed by subtracting the height of the top of the Brabant Massif, i.e. the **palaeotopomap** of the top

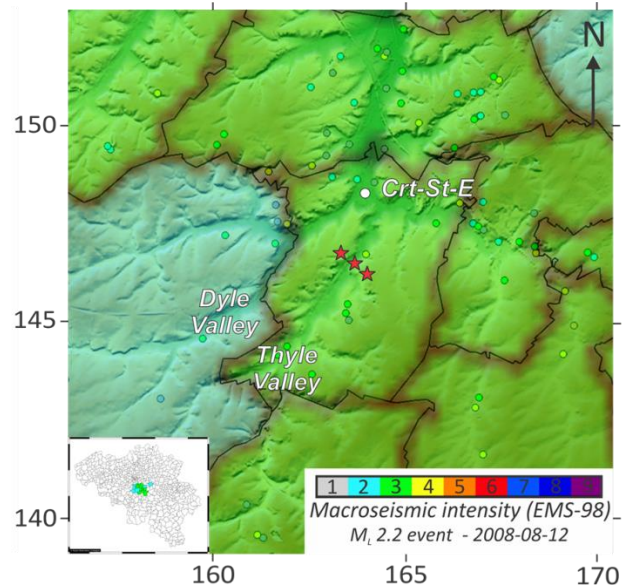


**Figure 36:** Detail of the community internet intensity map of a  $M_L$  2.2 event. The red stars indicate the epicentral position of the seismic swarm. Despite an average II or III intensity for each zip code, higher intensities are reported within each zip code.



of the Brabant Massif constructed from borehole and outcrop data, from the topographic height, available from a Digital Elevation Model. A detailed methodology is explained in Figure 37.

(iii) To improve the sediment thickness map, additional H/V geophysical measurements are performed from which new info on the sediment thickness can be added to the model. Especially on the hill tops borehole information is often lacking and geophysical data from the H/V and ERT prospection (see previous tasks) will add value and decrease the uncertainty.

iv) To study the individual macroseismic intensities and deduce if intensity variation can be linked to local geomorphology or local site effects, the reported MI's need to be compared to the local sediment thickness and the distance to the epi-/hypocentre for each earthquake of the seismic sequence. This will allow deducing if there is a link between the perception of the people and their location above the Brabant Massif (expressed by the sediment thickness). It will be of interest to investigate if the MI is highest on the hill tops, on the slopes or in the valleys.

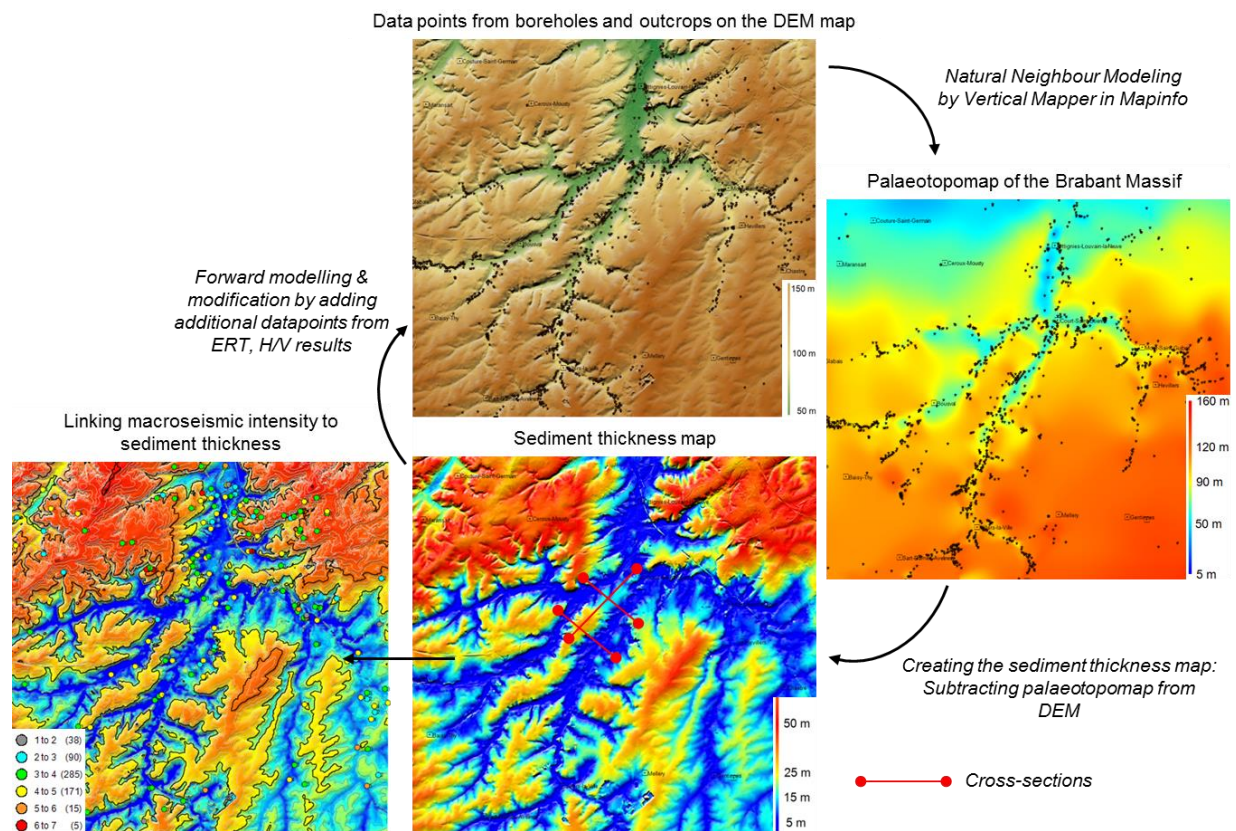


**Figure 37:** Methodology of the creation of a sediment thickness map of the 200 km<sup>2</sup> area around Court-Saint-Etienne. Based on the gathered borehole and outcrop data, a numerical model of the top of the Brabant Massif is created. A draft version of the sediment thickness results from subtracting the height of the top of the Brabant Massif from the present topographic height. Results of geophysical surveying in Tasks 6 and 9 allow to improve the sediment thickness map by adding additional datapoints from which bedrock depth is known. Finally, we will try to link macroseismic intensity to the local sediment thickness. The cross-sections through the Dyle and Thyle valleys are illustrated in Figure 47.

## 10.4. Research results

### 10.4.1. Geocoding addresses for individual macroseismic intensity maps

People that submit an online inquiry often abbreviate street names (e.g. str, st = street, av. = avenue, blv = boulevard,...) and also will not correct any written mistakes on their address. To account for these inconveniences, a new python code was developed to correct mistakes on addresses and to geocode individual addresses into their geographical coordinates. Although Google Earth Pro provides a geocoding service, an address correction and a quality control on the geocoded address is currently absent in the Google Earth module. In our python geocode application, however, we send the address to a [Google API](#) which automatically corrects any written mistakes in the submitted address and also gives a quality control on the geocoded address. Quality control includes a description how well the address was geocoded and is listed with the following terms with decreasing precision: *rooftop*, *range interpolated*, *geometric center* and *approximate*. Whereas the first three qualities are sufficient to study macroseismic effects, the *approximate* quality control only gives the center location of a community and its accuracy is thus insufficient for detailed macroseismic analysis.

In 2014, the developed geocode module was first tested and applied. On 3 January 2014, 301 macroseismic internet inquiries were submitted by people that reacted to the perception of an air blast caused by the accidental explosion of a WOII bomb at Euskirchen (Germany) (Hinzen, 2014). From the 301 inquiries, 235 observations could be geocoded to the street level or better for those addresses for which the respondents provided their house number. Almost all observations were made in a northeasterly direction with respect to the origin of the air blast. **Distribution of individual macroseismic observations proved to be much better suited to interpret the macroseismic distribution than the zip code distribution.** Seismological analysis and macroseismic intensity variation allowed

Hinzen (2014) to conclude that strong directivity of this felt event was related to source directivity of the air blast, population density, effects of the wind field and topography.

After this successful cooperation with K. Hinzen (Seismological Institute Bensber, University of Cologne), the geocoding module has been applied to the felt events of the Brabant Walloon seismic sequence and also to larger earthquakes such as the 2011  $M_L$  4.3 Goch (Figure 31), 2011  $M_L$  4.4 Nassau (Koblenz) and the 2002  $M_L$  4.9 Alsdorf earthquakes. Given its usability, the geocoding module will soon be implemented in the daily routine of the seismology section.

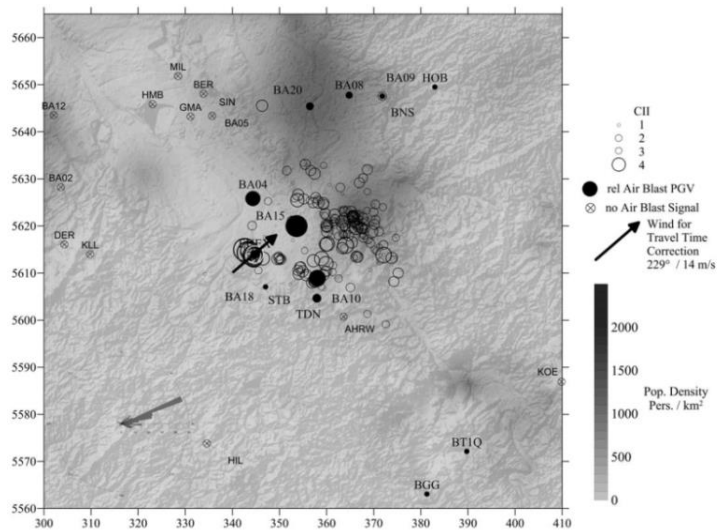


**Figure 38:** People's responses to the 2014 Euskirchen (Germany) WOII Bomb explosion. Distribution of felt events result from our developed geocode module. Circles show the variation in Community Intensity. After Hinzen (2014).

10.4.2. *Macro seismic intensity analysis of the seismic swarm*

Previous investigations of other felt events in Belgium has shown that macro seismic data and observed damage reports are useful data and a real source of information on earthquake ground motion (Camelbeeck et al., 2014; García Moreno and Camelbeeck, 2013).

The geocoded maps of the Walloon Brabant seismic swarm and improvement of the location of individual observations by geocoding will therefore serve as a great dataset for future research at the seismology section for seismic hazard of the Walloon Brabant region. As an example, the comparison of a CII and an individual macro seismic map of the  $M_L$  3.2 earthquake is shown (Figure 40). In this particular example 1358 of the 1501 responses could be geocoded to the street level or better. Near the epicentre of the  $M_L$  3.2 event, the maximal municipality average CII is 3.8 (Lecocq et al., 2009) (Figure 39).

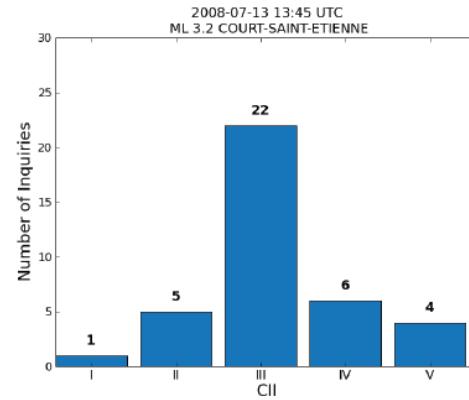


**Figure 39:** *Distribution of the intensities at the municipality of Court-Saint-Etienne. Values are rounded down to the nearest unit. The distribution corresponds to an average intensity of 3.8. (see also Figure 42).*

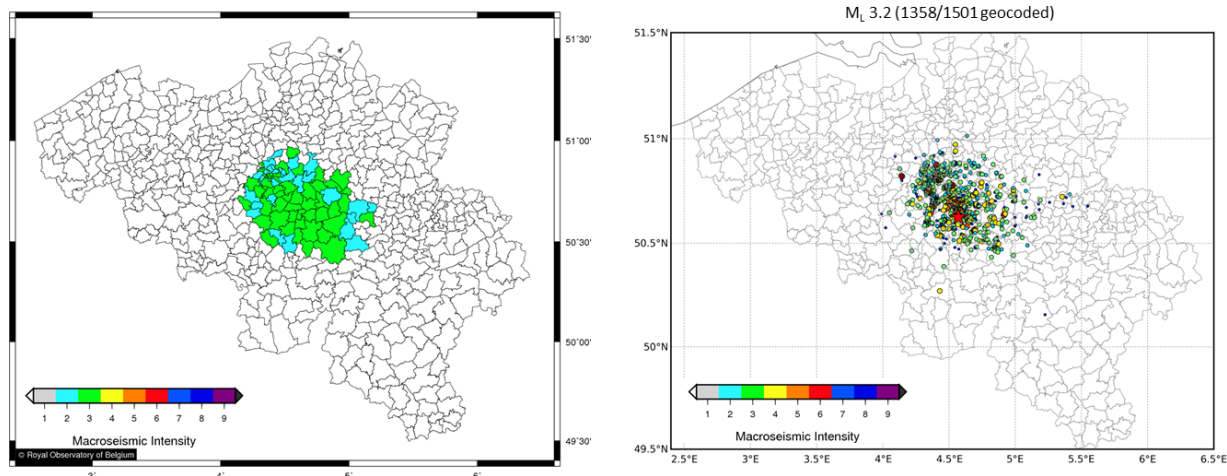


**Figure 40:** *Macro seismic analysis of the  $M_L$  3.2 earthquake. A(Left): Community internet intensity map illustrating the distribution of the average intensity of each zip-code. A zip code is coloured if three or more responses are submitted for that zip code. B(Right): Macro seismic map of individual macro seismic intensities after geocoding. Red star = epicentre location. Zip code areas for far-distance observations are not coloured as observations < 3.*

From the individual macro seismic response maps of the two largest  $M_L$  3.2 and  $M_L$  2.8 earthquakes and the rose diagrams illustrating the number of responses in function of azimuth and epicentral distance (Figure 41), it is clear that these events are farther (larger epicentral distance) felt in an E-W direction than in a N-S direction. This is more apparent on the macro seismic map than on the community internet intensity map. For the  $M_L$  3.2 earthquake, the felt observation with largest epicentral distance was reported at Bressoux (Liège), 71 km E from the epicentre, whereas farthest report north was only at 42 km (Zemst). Figure 41 moreover shows that the felt distribution of the  $M_L$  3.2 event is not concentric but slightly elliptical. This observation confirms what was hypothesised above, namely that events are farther felt in an E-W direction in the Henegouwen, Walloon Brabant and Liege provinces and that this is related to the thickness of the sediment column above the Brabant Massif. This confirms the similar findings of Nguyen et al. (2004) and Molron (2015).



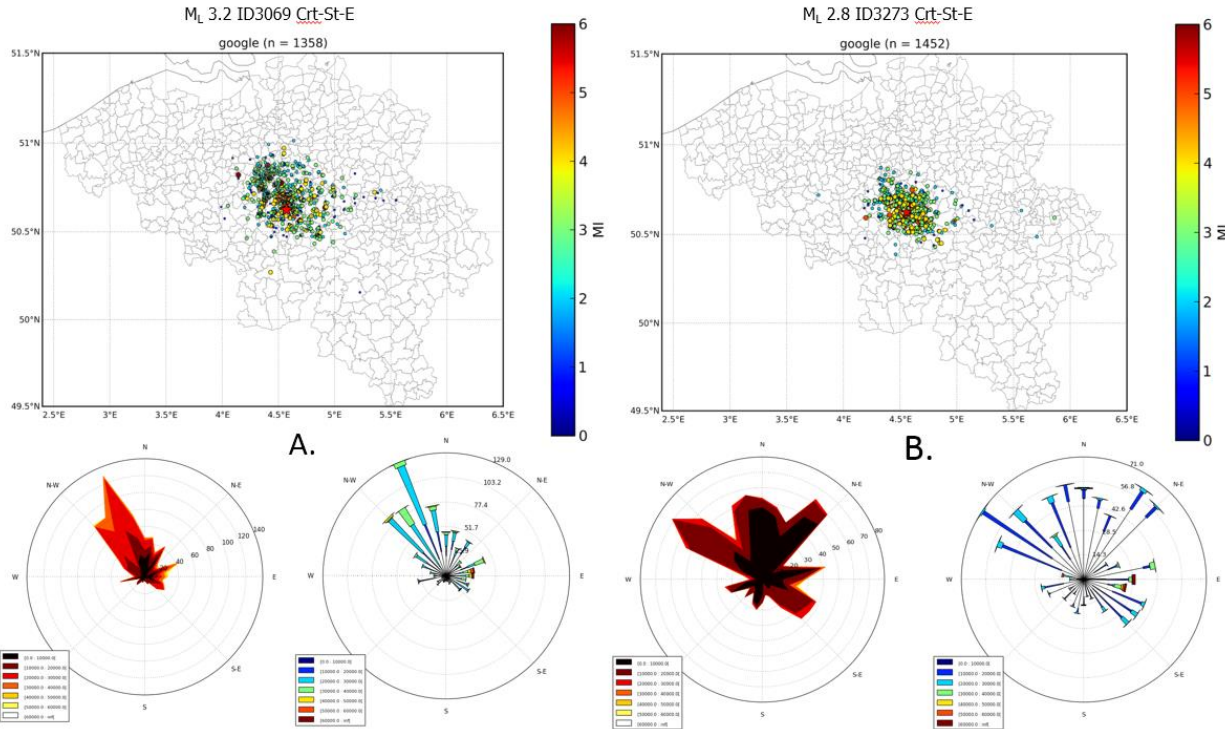


**Figure 41:** Rose diagrams illustrating the number of responses to the  $M_L$  3.2 and  $M_L$  2.8 earthquakes in function of the epicentral distance and azimuth to the epicentre location. Colours represent distance bins (in m). Note the yellow contour in the both rose diagrams which indicates that for both earthquakes the farthest responses came from the E. Rose diagrams in A. and B. have different maxima. The rose diagram in A. is clearly biased by the high population density north of the epicentre location (Ottignies – Brussels).

Rose diagrams illustrating the number of responses, the azimuth to epicentre location and epicentral distance are a useful tool to estimate the variance in the amount of responses. However, it has to be noted that DYFI data is clearly biased by the high population density. Especially the towns of Ottignies and Louvain-la-Neuve north of the epicentres, and Brussels, northeast of the seismic swarm bias the macroseismic maps of larger events. Calculating a barycentre, i.e. the centre point of observations, for these events would be useless as the barycentre would be strongly affected by population density.

As the exact location of individual observations is known after geocoding, macroseismic intensity decay will be more apparent using the individual observations than if the average intensity of the zip codes would be used, especially when small-magnitude earthquakes are considered. To evaluate if macroseismic data are reliable and if an average intensity decay can be deduced, only individual DYFI data of  $M_L > 2.0$  events are analysed and only when the amount of responses to these earthquakes is high enough. Subtle changes of intensity decay are better visible when epicentral distance is displayed in a logarithmic scale. Figure 42 plots the individual CII values, coloured by reliability of the response, versus hypocentral distance. Average CII values are calculated in distance bins that are 5 km in width, with a moving window of 1 km (coloured lines in Figure 42). In blue, the Atkinson & Wald (2007) regression relationship is plotted. This relationship analyses the dependence of the macroseismic intensity on the earthquake magnitude and distance from the fault (expressed in hypocentral distance). Shaking in Europe can be compared to these regression curves constructed for eastern US.

Comparison between our calculated average intensity decrease and the Atkinson & Wald regression line allows deducing if a sufficient amount of macroseismic reports of a felt seismic event are submitted in each distance bin.

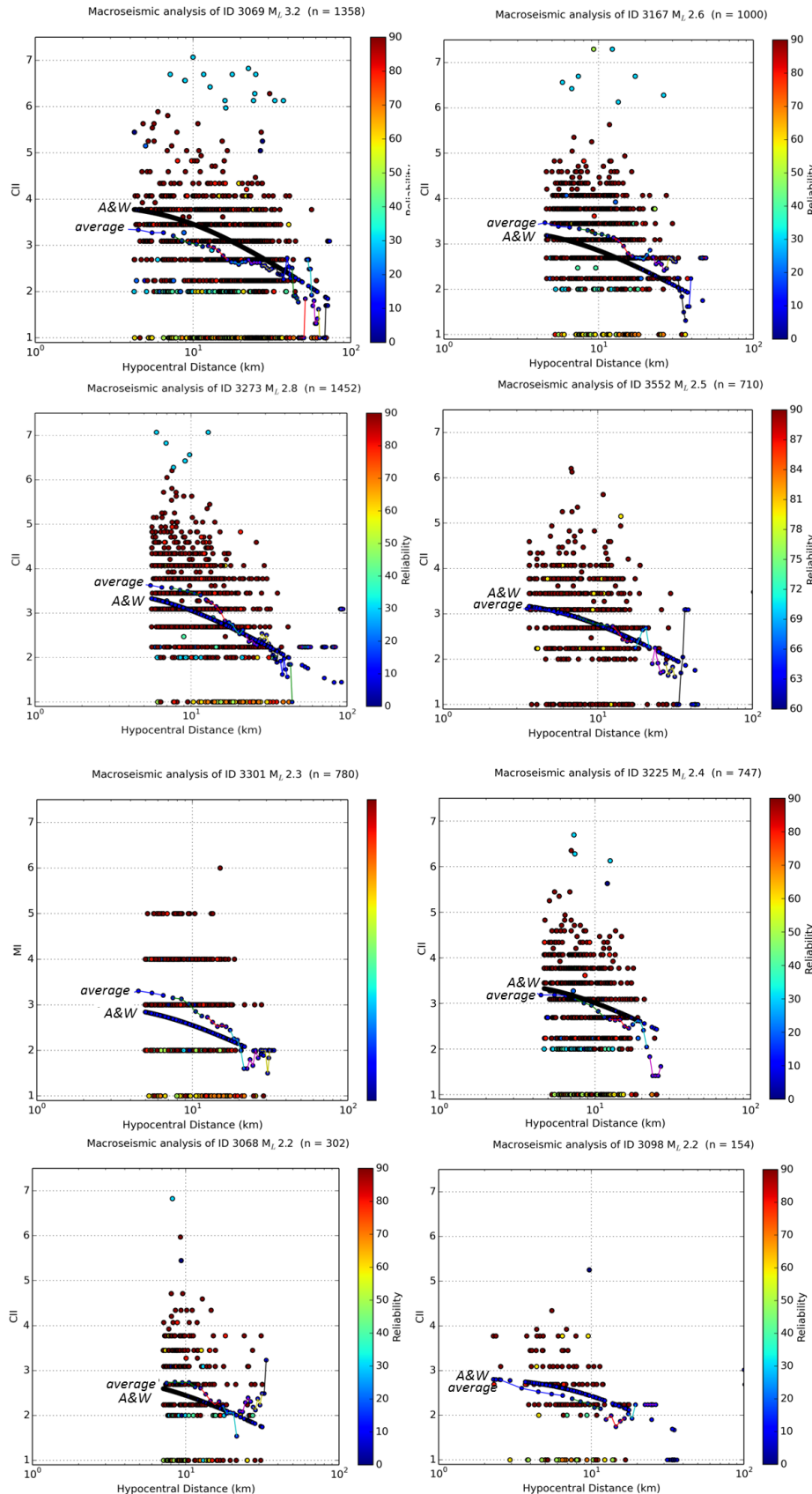


**Figure 42:** Community internet intensity (CII) decay of individual responses ordered by hypocentral distance to the felt event.

The blue line represents the predicted intensity decay by the Atkinson & Wald (2007) (A&W) regression line whereas the coloured curve shows the averaged intensity decay after intensity binning for each 5 km and with a moving window each 1 km.

Typically higher average macroseismic intensities are observed at closer hypocentral distances. High  $M_L$ 's such as intensity VI and VII are not considered to be reliable.

Average intensities at the epicentre vary between non-damaging intensities 3.8 and 2.6 from  $M_L$  3.2 to  $M_L$  2.2 events respectively.



The intensity values show a well-behaved progression of decreasing intensity with increasing distance. Despite the fact that the average curve is sometimes messy at larger distances due to the fact of too low amount of responses, the intensity decay holds trend with the predicted values of Atkinson & Wald (2007). For  $M_L$  3.2 and  $M_L$  2.2 average intensities at the epicentres are between intensity 3.8 and 2.6 respectively.

#### 10.4.3. Thickness map of cover sediments

To study local site effects, a sediment thickness map of the epicentral area has been constructed following the methodology explained in Figure 37. First, a **palaeotopomap of the Brabant Massif** has been modelled by using all available boreholes that reached bedrock depth and outcrops from which the absolute height of the Brabant Massif could be deduced. Modelling was performed by using Vertical Mapper in the Mapinfo GIS program. Vertical Mapper contains a Natural Neighbour (NN) Interpolation Method which allows the creation of grid files based on the availability of datapoints. The NN interpolation makes use of an area-weighting technique to determine a new value for every grid node. A natural neighbour region is first generated for each data point. Then, a new natural neighbour region is generated at every node in the new grid which effectively overlies various portions of the surrounding natural neighbour regions defining each point. The new grid value is calculated as the average of the surrounding point values proportionally weighted according to the intersecting area of each point. By continuous forward modelling, the input file is repeatedly adapted in order to improve the end result.

The available datapoints, visualised as black dots on the DEM in , result from described outcrops and boreholes. In the incised valleys numerous outcrops of the Lower Palaeozoic rocks of the Brabant Massif are present at the surface. The topographic height of these outcrops is used as input for the model. If the model predicts a BM height that is above the present topography, then the model was adapted and the actual topography was used as height of the BM. On the hill tops, however, the only information on the height of the BM is derived from borehole descriptions.

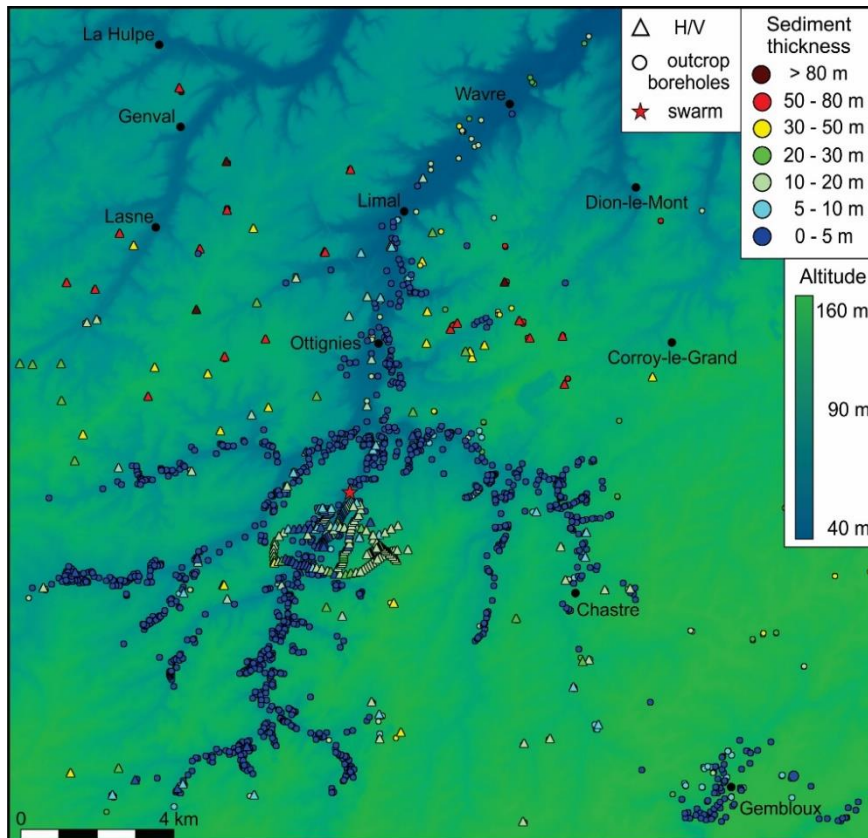


**Figure 43:**

Available outcrop and borehole information combined with additional H/V measurements performed in this study (Task 9). The sediment thickness of the individual H/V points is calculated with powerlaw equation of Figure 27.

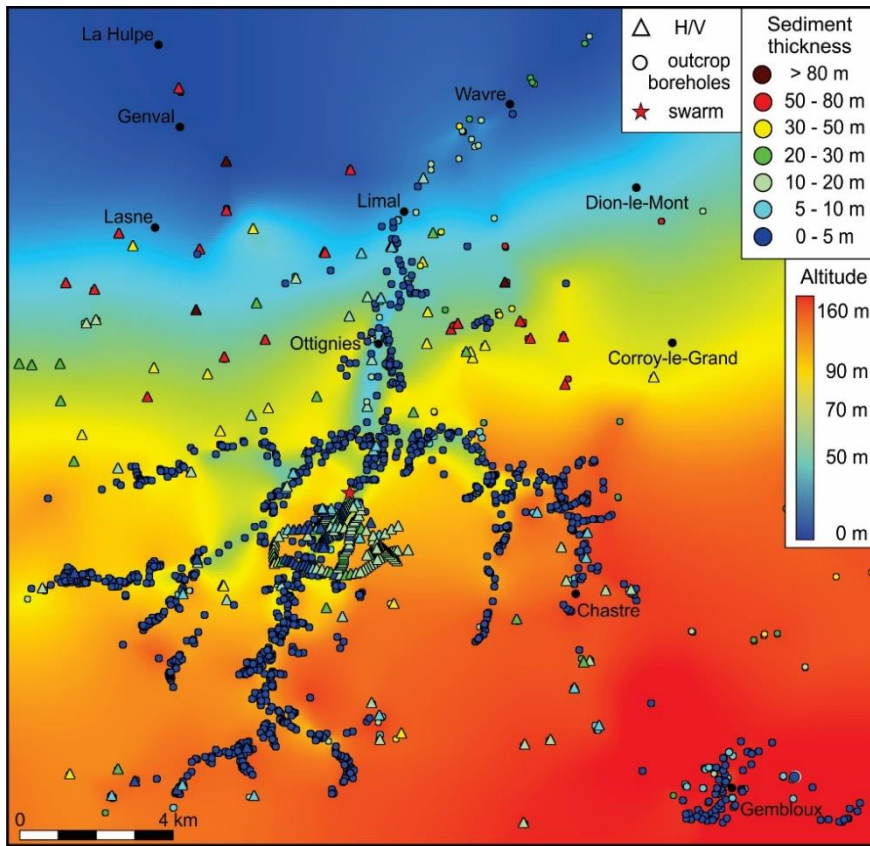


**Figure 44:**  
*Paleotopomap of the studied area. The top of the Brabant Massif dips towards the NE with an altitude of +160 m at Gembloux to 0 m at La Hulpe. River erosion has incised the Brabant Massif only south of Limal.*

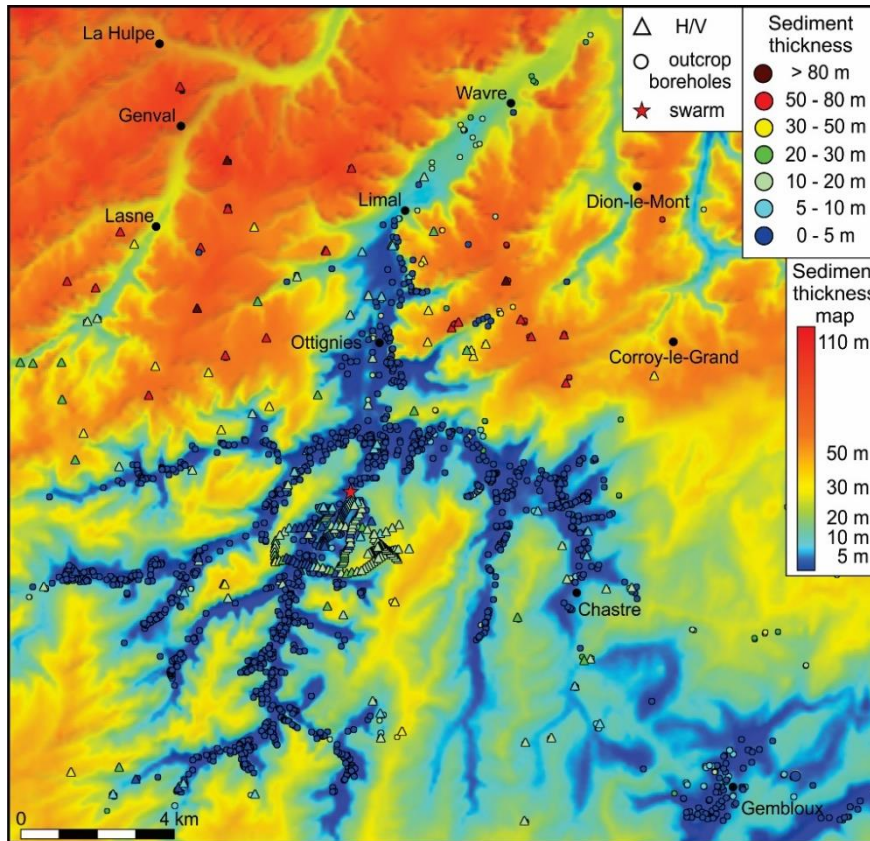


**Figure 45:**  
*Sediment thickness map resulting from subtracting the modelled paleotopomap from the topography according to the methodology explained in Figure 37.*



Consequently, the uncertainty of the first model is higher at the hill tops due to lack of information. To overcome this problem we used the results of geophysical data (ERT & H/V) gathered in Tasks 6 & 8 to improve the sediment thickness map. As highlighted in Task 6, several electrical resistivity tomography (ERT) profiles are conducted in the Faux area (Thyle valley). In all the profiles, we were able to identify the contact between alluvial sediments and the bedrock of the BM. The absolute height of these contacts (e.g. Figure 28) have been added to the datapoints to improve the model of the palaeotop of the BM and consequently to improve the sediment thickness map.

The modelled paleotopography of the Brabant (Figure 44) results shows that the top of the BM gradually dips to the NE, from +160 m in the south at Gembloux to 0 m in the north at La Hulpe. Interestingly, this map also suggests that the most northern point where the Dyle river has incised the Brabant Massif is situated somewhere between Limal and Ottignies.

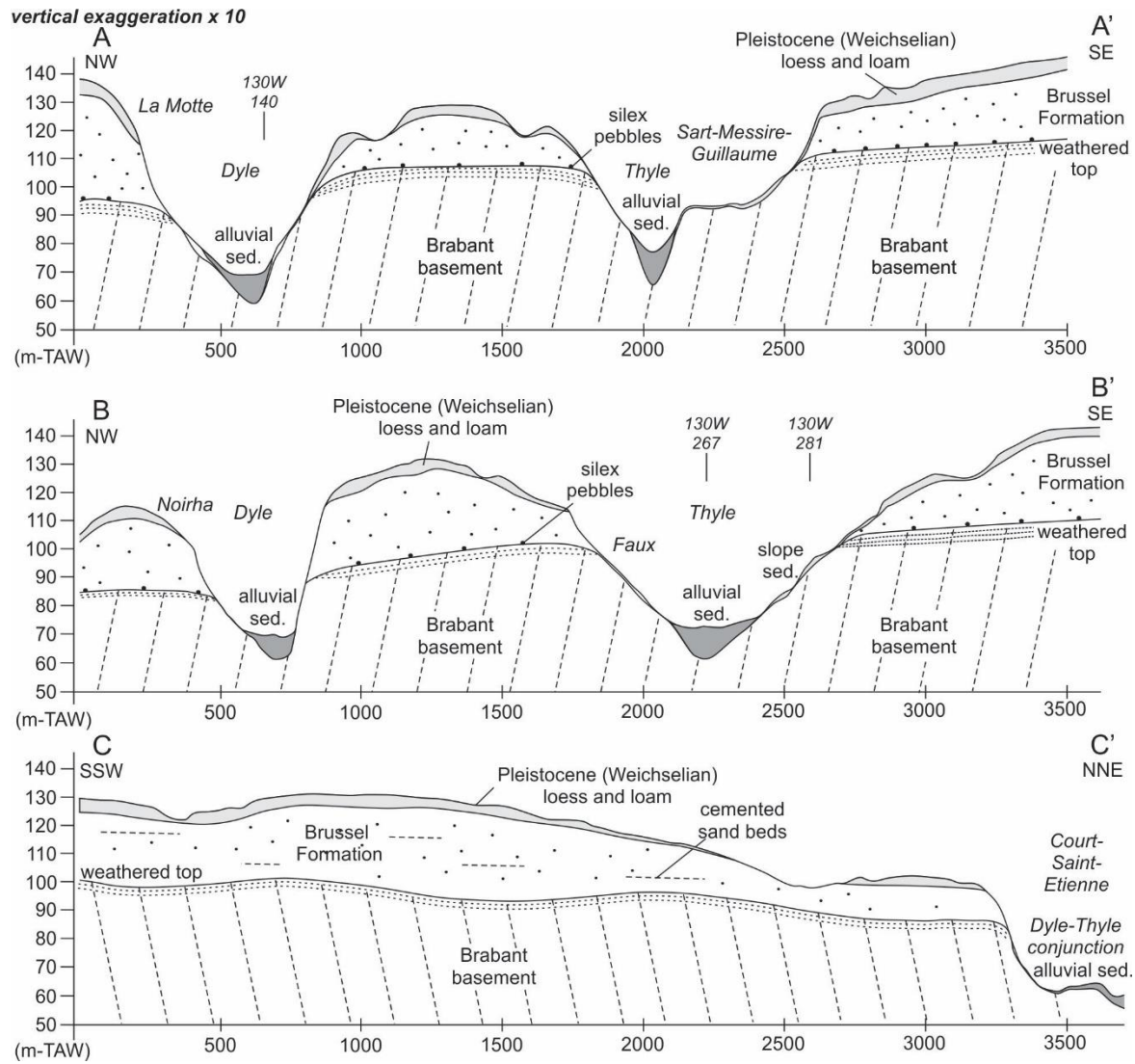


**Figure 46:** NW-SE and SSW-NNE cross-sections through the Dyle-Thyle valleys with indication of major lithological units: Quaternary loess, Brussel sands & Brabant Massif. Depth of the basement rocks has been determined by a cross-section through the model of the top of the Brabant Massif (Figure 37). Topography is taken from the DEM. Quaternary and Cenozoic deposits have been interpreted from representative boreholes (e.g. 130W267) in the valleys. Note the vertical exaggeration of 10.

Finally, based on all gathered data, a **sediment thickness map** of the Cenozoic and Quaternary cover above the basement rocks of the Brabant Massif has been created (Figure 45). As explained in the methodology, this map results from subtracting the height of the modelled paleotopography (Figure 44) of the Brabant Massif from the DEM (Figure 43:). The increasing sediment thickness to the NE clearly results from the dip of the Brabant Massif to the NE.

There are several anomalies illustrating the irregularity of the top of the BM. Especially the Lower Palaeozoic formations and lithology play an important role how the top of the BM is expressed. The Cambrian slaty Mousty Formation, that is exposed in the region of the epicentres of the seismic swarm, has a low resistance to erosion. It is clear from the palaeotopomap that everywhere the Mousty slates are present, the palaeotopography is lower. The DEM also shows that the incised Dyle and Thyle valley is wider in this area, than compared to their incision in Ordovician sandstone units to the south, or in the Cambrian quartzitic sandstone units (Tubize and Blanmont Formations) in the east (see also Figure 5).

Despite these minor anomalies, sediment thickness on the hill tops generally increases to the northeast. In the epicentre area, sediment thickness varies from 30 m on the hill tops. On the slopes and in the incised Dyle and Thyle river valleys, however, sediment thickness is minor and does not exceed 10 m (see Figure 47).

To conclude, the variation of sediment thickness is primarily controlled by dip of Brabant Massif and the incision of the rivers into the sandy Brussels Formation and the thin Pleistocene loess and loam deposit.

#### 10.4.4. Link between macroseismic intensity and sediment thickness?

As a final task, the macroseismic intensity of some larger-magnitude earthquakes was compared to sediment thickness. As we have the availability to geocode every individual macroseismic response, it is possible to extract the depth to the basement, i.e. the sediment thickness, below each of these responses.

Unfortunately, both parameters (macroseismic intensity and thickness) do not behave as a 1:1 relationship. Figure 47 shows an example of an the 13 September 2008  $M_L$  2.6 earthquake. The absence of correlation suggests that many other parameters such as earthquake directivity, path ways and site effects may control the macroseismic intensity reported by people and thus that intensity is not only controlled by depth to bedrock.

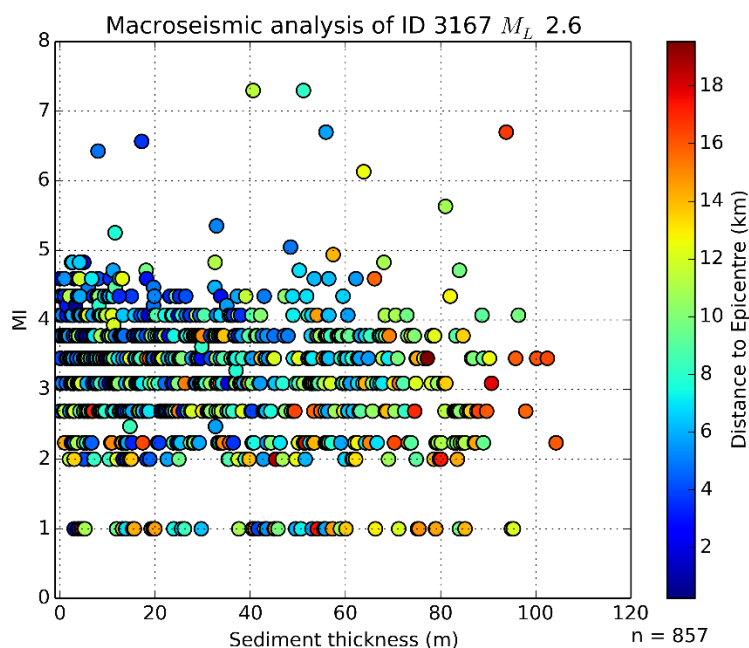


**Figure 47:** Variation of macroseismic intensity with sediment thickness of 857 responses to the  $M_L$  2.6 earthquake (13 September 2008). Sediment thickness has been derived from Figure 45 after geocoding each individual macroseismic address. Epicentral distance corresponds to the distance of the individual response to the epicentre. There is hardly any correlation with macroseismic intensity variation and sediment thickness.



## General conclusions

The results of BELSPO project MO/33/028 led to some important insights regarding source detection of intraplate seismicity and seismic swarms. Between 12 July 2008 and 10 January 2010 a seismic swarm occurred close to the town of Court-Saint-Etienne (Walloon Brabant, Belgium). Seismological earthquake data were gathered by the permanent stations in Belgium and by a locally-installed temporary seismic network. Detailed relocation of events by waveform cross-correlation allowed to improve the location of the 237 events in the seismic swarm considerably. The distribution of relocated events demonstrates the presence of a fault that has been active for 1.5 years at a depth between 5 and 7 kilometre. The 13 July  $M_L$  3.2 earthquake contributed to the largest displacement, i.e. several centimetres along a fault surface with a maximum dimension of  $0.01 \text{ km}^2$ , whereas events smaller than  $M_L$  2 only caused millimetre displacement along a fault surface with a dimension of a few  $\text{m}^2$  to some ten  $\text{m}^2$ .

Intraplate seismic swarms are frequently linked to volcanic or geothermal activity in the Earth's crust. The Walloon Brabant seismic swarm is defined as a continental intraplate seismic swarm. The absence of any correlation between the depth of the different earthquake events in the swarm and the time history of events suggests that this swarm was not an expression of a large-scale fluid movement through the crust such as is frequently the case in volcanic and geothermal settings. As the events have occurred randomly along a 1.5 km long fault (zone) situated between 5 and 7 km depth, no clear rupture propagation through time has been observed. It is hypothesised that the 2008-2010 Walloon Brabant seismic swarm was triggered by the (local) stress-state conditions in the crust which caused small-scale, millimetre- to centimetre-scale displacements along the fault.

To investigate the relationship between the fault and the local geology at epicenter depths, we relied on a systematic filtering approach in which the magnetic field was bandpass matched-filtered to generate magnetic anomaly maps that highlight sources at earthquake depths. The results of this methodology showed that the causative fault along which seismicity took place is limited in size as it is placed in a low-magnetic body (equivalent to the Mousty Formation, a shaly rock unit) surrounded at both sides by high-magnetic bodies. This source detection implicates that the fault is an isolated structure and that the limited spatial extend of the individual events in the swarm is related to the limited length of the fault. The limited dimension of the fault thus explains why no large magnitude earthquakes have occurred along this structure in Walloon Brabant. This finding does not exclude the fact that elsewhere in the Brabant Massif large magnitude earthquakes could not occur. After all, the magnetic maps shows that long NW-SE oriented lineaments do occur in the Brabant Massif and that they may favourably oriented for reactivation. The multidisciplinary methodology developed in this project offers some interesting insights for future research in detecting potential active faults along old geological structures.

Although a considerable amount of time has been spend on identifying a potential fault in the field, a surface expression of the causative fault has not been found. The facts that cleavage and bedding orientation is mostly parallel to the swarm's orientation, that the top of the Brabant Massif is strongly fractured (it serves as an aquifer) and that the swarm occurred in the Mousty Formation explain why it was very difficult to separate primary and secondary tectonic features and to find a surface fault (if any). However, the numerous ERT profiles are useful for detecting the depth of the basement.

Evaluating the powerlaw relationship between the fundamental frequency and sediment thickness has a great potential for future collaborations between Belgian or international institutes. If both parameters are calibrated by conducting ambient noise measurements above boreholes or by applying any other geophysical technique (such as ERT) that allows detecting bedrock depth, the thickness of sediments at any unknown place, e.g. in a valley, in a cave, or in a large-scale region, can be calculated by HVSR analysis. Furthermore, it was shown by HVSR analysis that the variability of the eroded top of the Brabant Massif is strongly affected by the capability of rock formations to resist erosion.

The “Did You Feel It?” inquiries during the seismic swarm showed that 60 of the 237 events have been felt by the local population. In order to analyse the macroseismic results, a new methodology was developed to geocode the location of individual responses based only on the address that was provided by the respondents. This developed geocoding service will be used at the Royal Observatory of Belgium for future macroseismic research and will be combined by additional existing national Geocoding tools (e.g. Geocoding NGI).

The macroseismic maps of the larger-magnitude earthquakes all show a decentred barycentre due to the larger population density north of the seismic swarm. An intensity evaluation of the community intensity, i.e. the average intensity value of a community, demonstrates that the depth to bedrock is an important factor that controls where people have felt an earthquake. The largest  $M_L$  3.2 earthquake has caused slightly E-W oriented elliptical isoseismals because of the fact that sediment thickness in Belgium above the Brabant Massif increases towards the North. This confirms the observation of the E-W elongated isoseismals related to the 11 June 1938  $M_L$  5.6 Zulzeke-Nukerke earthquake..

It was also hypothesised that the variation in macroseismic intensity could be related to the local variation of the sediment thickness above the Brabant Massif. However, after sediment thickness modelling this statement could not be confirmed. Macroseismic intensity and depth to bedrock do not behave as simply as a 1:1 relationship. Nevertheless, all the geophysical work (electrical resistivity tomography and H/V spectral ratio analysis (HVSr)) which was performed to generate a sediment thickness map will help in future to evaluate site effects related to ground motions of larger earthquakes in Belgium.

## D. Scientific publications and attendance to (inter)national conferences

### Published and planned Peer reviewed publications

- Van Noten, K., Lecocq, T., Shah, A.K., Camelbeeck, T., **2015**. Seismotectonic significance of the 2008-2010 Walloon Brabant seismic swarm in the Brabant Massif (Belgium). *Tectonophysics* 656, 20-38. [doi:10.1016/j.tecto.2015.05.026](https://doi.org/10.1016/j.tecto.2015.05.026)
- Van Noten, K., Vleminckx, B., Lecocq, T., Vanneste, K. & Camelbeeck, T. **in prep**. Geocoding individual addresses for macroseismic intensity analysis of locally-felt earthquakes. *Computer and Geosciences*.
- Van Noten, K., Lecocq, T., Molron, J., Meyer, L. & Camelbeeck, T. **in prep**. The applicability of the powerlaw relationship between sediment thickness and fundamental frequency: a critical review. *Journal of Geophysical Research*

### Presentations at international conferences and national meetings

- Van Noten, K., Lecocq, T., Shah, A., Camelbeeck, T. **2015**. The seismotectonic significance of the 2008-2010 seismic swarm in the Brabant Massif, Belgium. Geophysical Research Abstracts 17, EGU2015-4229, 13 April - 17 May 2015, Vienna, Austria. [Oral presentation](#).
- Van Noten, K., Lecocq, T., Shah, A., Camelbeeck, T. **2015**. Deducing the seismotectonic significance of the 2008-2010 seismic swarm in the Brabant Massif by aeromagnetic bandpass filtering. Tectonic Studies Group, 6-8 January 2015, Edinburgh. *Poster presentation*. See [Appendix C](#).
- Van Noten, K., Lecocq, T., Shah, A., Camelbeeck, T. **2014**. Aeromagnetic bandpass filtering: applicable to seismology? Informal student meeting, 17 November 2014, KULeuven. *Oral presentation*
- Van Noten, K., Lecocq, T., Shah, A., Camelbeeck, T. **2014**. Deducing a seismic swarm's seismotectonic significance by aeromagnetic matched filtering. RMS meeting, 14 november 2014, ROB, Brussels. *Oral presentation*
- Van Noten, K., Lecocq, T., Watlet, A., Camelbeeck, T., **2014**. Modelling Sediment Thickness for Site-Effect Characterisation using H/V Spectral Ratio Analysis and Electrical Resistivity Tomography. Geophysical Research Abstracts 16, EGU2014-13252, 28 April - 2 May 2014, Vienna, Austria. *Oral presentation*.
- Van Noten, K., Lecocq, T., Vleminckx, B., Camelbeeck, T., **2014**. Geocoding individual 'Did You Feel It' addresses for macroseismic analysis. RMS Meeting, 14 March 2014, KNMI, Utrecht. *Oral Presentation*
- Van Noten, K., Lecocq, T. & Camelbeeck, T. **2013**. Using H/V Spectral Ratio Analysis to Map Sediment Thickness and to Explain Macroseismic Intensity Variation of a Low-Magnitude Seismic Swarm in Central Belgium. American Geophysical Union, AGU2013-S53B-2406, 9-13 December 2013, San Francisco, USA. *Poster presentation*. See Appendix B.
- Van Noten, K., Lecocq, T., Vleminckx, B., Camelbeeck, T., **2013**. Relationship between the 2008-2010 Brabant sequence and local geology. RMS Meeting, 8 October 2013, Seismological Institute Bensberg, Cologne. *Oral Presentation*
- Van Noten, K., Lecocq, T. & Camelbeeck, T. **2013**. The tectonic significance of the 2008-2010 seismic swarm in the Brabant Massif, Belgium. DRT2013, 16-18 September 2013, Leuven, Belgium. *Poster presentation*
- Van Noten, K., Lecocq, T., Vleminckx, B., Camelbeeck, T., **2013**. Macroseismic investigation of the 2008-2010 low magnitude seismic swarm in the Brabant Massif, Belgium. The link between macroseismic intensity and geomorphology. Geophysical Research Abstracts 15, EGU2013-4923, 7-12 April 2013, Vienna, Austria. *Poster presentation*
- Lecocq, T., Camelbeeck, T., **2012**. The 2008-2010 Seismic Sequence in the Brabant Massif 20 km South of Brussels, Belgium, AGU Fall Meeting, 3-7 December 2012, San Francisco, USA. *Poster presentation*

Van Noten, K., Lecocq, T., Verbeeck, K., Vanneste, K., Camelbeeck, T., **2012**. Modelling the palaeotopography of the Brabant Massif: a necessity to understand the site effects of the 2008-2011 seismic activity in the Brabant Walloon. *4th International Geologica Belgica Meeting 2012. Moving Plates and Melting Icecaps – Processes and Forcing Factors in Geology*. 11-14 September 2012, Brussels. *Oral presentation*

*People (days) involved in field work:* Koen Van Noten (28), Thomas Lecocq (6), Justine Molron (4), Lauriane Meyer (4), Arnaud Watlet (3), Koen Verbeeck (2), Bart Vleminckx (2), Kris Vanneste (1), Devy Natamanggala (1), Dimitri Kusters (1).



## References

- Ahorner, L., 1975. Present-day stress field and seismotectonic block movements along major fault zones in Central Europe. *Tectonophysics* 29, 233–249.
- Ahorner, L., 1983. The general pattern of seismotectonic dislocations in Central Europe as the background for the Liège earthquake on November 8, in: P., M. (Ed.), *Seismic Activity in Western Europe*. Springer Netherlands, 41–56.
- Angelier, J., Mechler, P., 1977. Sur une méthode graphique de recherche des contraintes principales également utilisable en tectonique et en séismologie: la méthode des dièdres droits. *Bulletin de la Société géologique de France* (7)19, 1309-1318.
- Archief, Geodoc, 2012. Koninklijk Belgisch Instituut voor Natuurwetenschappen, Belgisch Geologische Dienst.
- Atkinson, G.M., Wald, G.J., 2007. "Did you feel it?" Intensity Data: A Surprisingly Good Measure of Earthquake Ground Motion. *Seismological Research Letters* 78, 3.
- Bard, P.-Y., 1985. Les effets de site d'origine structurale: Principaux résultats expérimentaux et théoriques, in: Davidovici, V. (Ed.), *Genie Parasismique*, Presses de l'Ecole Nationale des Ponts et Chaussées, pp. 223–238.
- Benjumea, B., Macau, A., Gabàs, A., Bellmunt, F., Figueras, S., Cirés, J., 2011. Integrated geophysical profiles and H/V microtremor measurements for subsoil characterization. *Near Surface Geophysics* 9, 413-425.
- Beyreuther, M., Barsch, R., Krischer, L., Megies, T., Behr, Y., Wassermann, J., 2010. ObsPy: A Python Toolbox for Seismology. *SRL* 81, 530-533.
- BGS, 1994. Aeromagnetic map of the Brabant Massif: residual total field reduced to the pole. 1:100 000.
- Blakely, R.J., Wells, R.E., Weaver, C.S., Johnson, S.Y., 2002. Location, structure, and seismicity of the Seattle fault zone, Washington: Evidence from aeromagnetic anomalies, geologic mapping, and seismic-reflection data. *GSA Bulletin* 114, 169-177.
- Blockmans, S., Dumoulin, V., Herbosch, A., accepted. Carte Waterloo - La Hulpe, n° 39/3-4, Carte géologique de la Wallonie, échelle 1/25000, Namur: Ministère de la Région Wallonne.
- Bott, M.P.H., 1959. The mechanics of oblique-slip faulting. *Geological Magazine* 96, 109–117.
- Camelbeeck, T., 1993. Mécanisme au foyer des tremblements de terre et contraintes tectoniques : le cas de la zone intraplaque belge. Louvain-la-Neuve: Université Catholique de Louvain, PhD Thesis, 344 pp.
- Camelbeeck, T., Alexandre, P., Sabbe, A., Knuts, E., Moreno, D.G., Lecocq, T., 2014. The impact of earthquake activity in Western Europe from the historical and architectural heritage records, in: Talwani, P. (Ed.), *Intraplate earthquakes*. Cambridge University Press, pp. 198-230.
- Camelbeeck, T., van Eck, T., 1994. The Roer Valley Graben earthquake of 13 April 1992 and its seismotectonic setting. *Terra Nova* 6, 291-300.
- Camelbeeck, T., Vanneste, K., Alexandre, P., Verbeeck, K., Petermans, T., Rosset, P., Everaerts, M., Warnant, R., Van Camp, M., 2007. Relevance of active faulting and seismicity studies to assessments of long-term earthquake activity and maximum magnitude in intraplate northwest Europe, between the Lower Rhine Embayment and the North Sea. *The Geological Society of America Special Paper* 425, 193-224.
- Chacksfield, B.C., De Vos, W., D'Hooge, L., Duser, M., Lee, M.K., Poitevin, C., Royles, C.P., Verniers, J., 1993. A new look at Belgian aeromagnetic and gravity data through image-based display and integrated modelling techniques. *Geological Magazine* 130, 583-591.
- Charlier, C., Van Gils, J., 1953. Liste des stations séismologiques mondiales. L'association internationale de séismologie, Observatoire Royal de Belgique.
- Cinelli, G., Tondeur, F., Dehandschutter, B., 2009. Statistical analysis of indoor radon data for the Walloon region (Belgium). *Radiation Effects & Defects in Solids* 164, 307-312.

- Daniel, G., Prono, E., Renard, F., Thouvenot, F., Hainzl, S., Marsan, D., Helmstetter, A., Traversa, P., Got, J.L., Jenatton, L., Guiguet, R., 2011. Changes in effective stress during the 2003–2004 Ubaye seismic swarm, France. *Journal of Geophysical Research: Solid Earth* 116, B01309.
- de Magnée, I., Raynaud, J., 1944. Etude magnétique de la tectonique du Cambrien du Brabant à l'est de Court-St-Etienne. *Annales de la Société Géologique de Belgique* 67, 495-546.
- De Vos, W., Chacksfield, B.C., D'Hooge, L., Dusaar, M., Lee, M.K., Poitevin, C., Royles, C.P., Vandendorgh, J., Van Eyck, J., Verniers, J., 1993a. Image-based display of Belgian digital aeromagnetic and gravity data. *Belgian Geological Survey Professional Paper* 263, 1-20.
- De Vos, W., Poot, B., Hus, J., El Khayati, M., 1992. Geophysical characterization of lithologies from the Brabant Massif as a contribution to gravimetric and magnetic modelling. *Bulletin de la Société belge de Géologie* 101, 173-180.
- De Vos, W., Verniers, J., Herbosch, A., Vanguetstaine, M., 1993b. A new geological map of the Brabant Massif, Belgium. *Geological Magazine* 130, 605-611.
- Debacker, T.N., 2012. Folds and cleavage/folds relationships in the Brabant Massif, southeastern Anglo-Brabant Deformation Belt. *Geologica Belgica* 15, 81-95.
- Debacker, T.N., Dewaele, S., Sintubin, M., Verniers, J., Muchez, P., Boven, A., 2005. Timing and duration of the progressive deformation of the Brabant Massif, Belgium. *Geologica Belgica* 8, 20-34.
- Debacker, T.N., Herbosch, A., Sintubin, M., 2004a. The supposed thrust fault in the Dyle-Thyle outcrop area (southern Brabant Massif, Belgium) re-interpreted as a folded low-angle extensional detachment. *Geologica Belgica* 8, 53-69.
- Debacker, T.N., Herbosch, A., Sintubin, M., Verniers, J., 2003. Palaeozoic deformation history of the Asquempont-Virginal area (Brabant Massif, Belgium): large-scale slumping, low-angle extensional detachment development (the Asquempont Fault redefined) and normal faulting (the Nieuwpoort-Asquempont fault zone). *Memoirs of the Geological Survey of Belgium* 49, 1-30.
- Debacker, T.N., Sintubin, M., Verniers, J., 2004b. Transitional geometries between gently plunging and steeply plunging folds: an example from the Lower Paleozoic Brabant Massif, Anglo-Brabant deformation belt, Belgium. *Journal of the Geological Society, London* 161, 641-652.
- Deichmann, N., Garcia-Fernandez, M., 1992. Rupture geometry from high-precision relative hypocentre locations of microearthquake clusters. *Geophysical Journal International* 110, 501-517.
- Delcambre, B., Pingot, J.-L., 2002. Carte Chastre-Gembloux n° 40/5-6, Carte géologique de la Wallonie, échelle 1/25000, Namur: Ministère de la Région Wallonne.
- Delvaux, D., Sperner, B., 2003. Stress tensor inversion from fault kinematic indicators and focal mechanism data: the TENSOR program, in: Nieuwland, D. (Ed.), *New Insights into Structural Interpretation and Modelling*. Geological Society, London, Special Publications, 212: 75-100.
- Everaerts, M., De Vos, W., 2012. Gravity acquisition in Belgium and the resulting Bouguer anomaly map, *Memoirs of the Geological Survey of Belgium*. Koninklijk Belgisch Instituut voor Natuurwetenschappen. Belgische Geologische Dienst, Brussels, p. 39 p.
- Everaerts, M., Poitevin, C., De Vos, W., Sterpin, M., 1996. Intergrated geophysical/geological modelling of the Western Brabant Massif and structural implications. *Bulletin de la Société belge de Géologie* 105, 41-59.
- Fischer, T., Horálek, J., Hrubcová, P., Vavryčuk, V., Bräuer, K., Kämpf, H., 2014. Intra-continental earthquake swarms in West-Bohemia and Vogtland: A review. *Tectonophysics* 611, 1-27.
- García Moreno, D., Camelbeeck, T., 2013. Comparison of ground motions estimated from prediction equations and from observed damage during the M = 4.6 1983 Liège earthquake (Belgium). *Natural Hazards and Earth System Sciences* 13, 1983-1987.
- Gutenberg, B., Richter, C.F., 1956. Earthquake magnitude, intensity, energy and acceleration. *Bulletin of the Seismological Society of America* 46, 105-145.
- Hainzl, S., 2004. Seismicity patterns of earthquake swarms due to fluid intrusion and stress triggering. *Geophysical Journal International* 159, 1090-1096.

- Hainzl, S., Fischer, T., 2002. Indications for a successively triggered rupture growth underlying the 2000 earthquake swarm in Vogtland/NW Bohemia. *Journal of Geophysical Research* 107, 2338, doi:10.29/2002JB001865.
- Herbosch, A., Blockmans, S., 2012. Carte Wavre-Chaumont-Gistoux, n° 40/1-2, Carte géologique de la Wallonie, échelle 1/25000, Namur: Ministère de la Région Wallonne.
- Herbosch, A., Lemonne, E., 2000. Carte Nivelles-Genappe n° 39/7-8, Carte géologique de la Wallonie, échelle 1/25000, Namur: Ministère de la Région Wallonne.
- Herbosch, A., Verniers, J., 2013. Stratigraphy of the Lower Palaeozoic of the Brabant Massif, Belgium. Part I: The Cambro-Ordovician from the Halle and Ottignies groups. *Geologica Belgica* 16, 49-64.
- Hiemer, S., Toessler, D., Scherbaum, F., 2012. Monitoring the West Bohemian earthquake swarm in 2008/2009 by a temporary small-aperture seismic array. *J Seismol* 16, 169-182.
- Hinzen, K.-G., 2003. Stress field in the Northern Rhine area, Central Europe, from earthquake fault plane solutions. *Tectonophysics* 377, 325-356.
- Hinzen, K.-G., Reamer, S.K., 2007. Seismicity, seismotectonics, and seismic hazard in the Northern Rhine Area, in: Stein, S., Mazzotti, S. (Eds.), *Continental Intraplate Earthquakes: Science, Hazard, and Policy Issues*. Vol. Special Paper 425:225-242, Geological Society of America.
- Hinzen, K.G., 2014. Seismic Analysis of the Accidental WWII Bomb Explosion in Euskirchen, Germany, on 3 January 2014. *Seismological Research Letters* 85, 825-835.
- Hinzen, K.G., Weber, B., Scherbaum, F., 2004. On the resolution of H/V measurements to determine sediment thickness, a case study across a normal fault in the lower rhine embayment, Germany. *Journal of Earthquake Eng.* 8, 909-926.
- Hofmann, R.B., 1996. Individual faults can't produce a Gutenberg-Richter earthquake recurrence. *Engineering Geology* 43, 5-9.
- Ibs-von Seht, M., Plenefisch, T., Klinge, K., 2008. Earthquake swarms in continental rifts — A comparison of selected cases in America, Africa and Europe. *Tectonophysics* 452, 66-77.
- Ibs-von Seht, M., Wollenberg, U., 1999. Microtremor Measurements Used to Map Thickness of Soft Sediments. *Bull. Seis. Soc. Am.* 89, 250-259.
- Konno, K., Omachi, T., 1998. Ground-motion characteristics estimated from spectral ratio between horizontal and vertical components of microtremor. *Bull. Seism. Soc. Am.* 88, 228-241.
- Krischer, L., 2015. hypoDDpy: hypoDDpy 1.0. Zenodo. <http://dx.doi.org/10.5281/zenodo.18907>.
- Leclère, H., Fabbri, O., Daniel, G., Cappa, F., 2012. Reactivation of a strike-slip fault by fluid overpressuring in the southwestern French–Italian Alps. *Geophysical Journal International* 189, 29-37.
- Lecocq, T., 2011. L'activité sismique en Ardenne et sa relation avec la tectonique active, Département des Sciences de la Terre et de l'Environnement. Université Libre de Bruxelles, PhD Thesis, pp. 265, Brussels, p. 265.
- Lecocq, T., Rapagnani, G., Martin, H., De Vos, F., Hendrickx, M., Van Camp, M., Vanneste, K., Camelbeeck, T., 2009. B-FEARS: The Belgian Felt Earthquake Alert and Report System. *Cahiers du Centre Européen de Géodynamique et de Séismologie*.
- Lee, M.K., Pharaoh, T.C., Williamson, J.P., Green, C.A., De Vos, W., 1993. Evidence on the deep structure of the Anglo-Brabant Massif from gravity and magnetic data. *Geological Magazine* 130, 575-582.
- Lee, W.H.K., Lahr, J.C., 1972. HYPO71: A computer program for determining hypocenter, magnitude, and first motion pattern of local earthquakes. *U.S. Geol. Surv. Open-file Report* 72-224, 100 pp.
- Legrand, L., 1968. Le Massif du Brabant. Mémoires pour servir à l'explication des cartes géologiques et minières de la Belgique. Service Géologique de Belgique, Bruxelles.
- Leynaud, D., Jongmans, D., Teerlynck, H., Camelbeeck, T., 2000. Seismic hazard assessment in Belgium. *Geologica Belgica* 3, 67-86.
- Lindenfeld, M., Rumpker, G., Link, K., Koehn, D., Batte, A., 2012. Fluid-triggered earthquake swarms in the Rwenzori region, East African Rift—Evidence for rift initiation. *Tectonophysics* 566–567, 95-104.

- Loke, M.H., 2004. Tutorial: 2-D and 3-D electrical imaging surveys. Geotomo Software: Penang, Malaysia.
- Mansy, J.L., Everaerts, M., De Vos, W., 1999. Structural analysis of the adjacent Acadian and Variscan fold belts in Belgium and northern France from geophysical and geological evidence. *Tectonophysics* 309, 99-116.
- Meyus, Y., De Smet, D., De Smedt, F., Walraevens, K., Batelaan, O., Van Camp, M., 2000. Hydrogeologische codering van de ondergrond van Vlaanderen (HCOV). *Water* 8, 1-13.
- Mogi, K., 1963. Some discussions on aftershocks, foreshocks and earthquake swarms—the fracture of a semi-infinite body caused by an inner stress origin and its relation to the earthquake phenomena. *Bulletin of the Earthquake Research Institute* 41, 615–658.
- Molron, J., 2015. Thickness estimation of sediments overlying the Brabant Massif by H/V spectral ratio analysis in central Belgium. Université libre de Bruxelles. M.Sc. Thesis. Promotors: Dr. T. Lecocq & Dr. K. Van Noten (Royal Observatory of Belgium).
- Nakamura, Y., 1989. A method for dynamic characteristics estimation of subsurface using microtremor of the ground surface. *Quarterly Report of RTRI* 30, 25-33.
- Nguyen, F., Van Rompaey, G., Teerlynck, H., Van Camp, M., Jongmans, D., Camelbeeck, T., 2004. Use of microtremor measurement for assessing site effects in Northern Belgium – interpretation of the observed intensity during the MS = 5.0 June 11 1938 earthquake. *J Seismol* 8, 41-56.
- Parotidis, M., Rothert, E., Shapiro, S.A., 2003. Pore-pressure diffusion: A possible triggering mechanism for the earthquake swarms 2000 in Vogtland/NW-Bohemia, central Europe. *Geophysical Research Letters* 30, 1-4.
- Petermans, T., Rosset, P., Camelbeeck, T., 2007. Evaluation of site effects and local seismic hazard in Belgium. Final internal report of contract MO/33/016. Royal Observatory of Belgium, Brussels.
- Phillips, J.D., 1997. Potential-field geophysical software for the PC, version 2.2 (<http://pubs.usgs.gov/of/1997/ofr-1997-0725/>). U.S. Geological Survey Open-File Report 97-725, 34p.
- Phillips, J.D., 2001. Designing matched bandpass and azimuthal filters for the separation of potential-field anomalies by source region and source type, Australian Society of Exploration Geophysicists, 15th Geophysical Conference and Exhibition, Expanded Abstracts CD-ROM, 4p.
- Piesens, K., Vancampenhout, P., De Vos, W., 2005. Geologische subcropkaart van het Massief van Brabant in Vlaanderen. Schaal 1:200.000. Opgemaakt door de BGD in opdracht van ANRE, Ministerie van de Vlaamse Gemeenschap, project VLA/03.1-1.
- Reamer, S.K., Hinzen, K.-G., 2004. An Earthquake Catalog for the Northern Rhine Area, Central Europe (1975-2002). *Seismological Research Letters* 75, 713-725.
- Rosset, P., 2006. Site effect in the Grand-Duche of Luxembourg. Preliminary study. Report for the Council of Europe, EUR-OPA Major Hazards Agreement.
- Rosset, P., Petermans, T., 2007. Guidelines of used and developed tools for ambient noise analysis. Internal methodological report. Royal Observatory of Belgium.
- Rosset, P., Petermans, T., Devleeschouwer, X., Pouriel, F., Camelbeeck, T., 2005. Identifying the influence of the local geology in case of earthquake for urban planning: case study in Brussels, Les journées Géographiques Belges, Mobilité, Société et Environnement en Cartes, pp. 9 novembre 2005, T.II, 2171-2177.
- Schaff, D.P., Waldhauser, F., 2005. Waveform Cross-Correlation-Based Differential Travel-Time Measurements at the Northern California Seismic Network. *Bulletin of the Seismological Society of America* 95, 2446-2461.
- Schenk, V., Schenková, Z., Jechumtálová, Z., Pichl, R., 2012. Crustal deformations in the epicentral area of West Bohemia 2008 earthquake swarm in central Europe. *Journal of Geophysical Research* 117, 1-19.
- SESAME, 2005. Guidelines for the implementation of the H/V spectral ratio technique on ambient vibrations - measurements, processing and interpretations. SESAME European research project, deliverable D23.12.2005.



- Shah, A., Horton, J.W., Burton, W.C., Spears, D.B., Gilmer, A.K., 2015. Subsurface geologic features of the 2011 central Virginia earthquakes revealed by airborne geophysics, in: Horton, J.W., Chapman, M.C., Green, R.A. (Eds.), *The 2011 Mineral, Virginia earthquake and its significance for seismic hazards in Eastern North America*. Geological Society of America Special Papers 509, pp. 295-304.
- Sibson, R., 1985. A note on fault reactivation. *Journal of Structural Geology* 7, 751-754.
- Sintubin, M., 1997. Structural implications of the aeromagnetic lineament geometry in the Lower Paleozoic Brabant Massif (Belgium). *Aardkundige Mededelingen* 8, 165-168.
- Sintubin, M., 1999. Arcuate fold and cleavage patterns in the southeastern part of the Anglo-Brabant fold Belt (Belgium): tectonic implications. *Tectonophysics* 309, 81-97.
- Sintubin, M., Debacker, T.N., Van Baelen, H., 2009. Early Palaeozoic orogenic events north of the Rheic suture (Brabant, Ardenne): A review. *Comptes Rendus Geoscience* 341, 156-173.
- Sintubin, M., Everaerts, M., 2002. A compressional wedge model for the Lower Paleozoic Anglo-Brabant Belt (Belgium) based on potential field data, in: Winchester, J.A., Pharaoh, T., Verniers, J. (Eds.), *Paleozoic Amalgamation of Central Europe*. Geological Society, London, Special Publication, London, pp. 327-343.
- Somville, O., 1939. Le tremblement de terre belge du 11 juin 1938. Publication de l'Observatoire Royal de Belgique, Imprimerie Duculot, Gembloux, 16 pp.
- Špičák, A., 2000. Earthquake Swarms and Accompanying Phenomena in Intraplate Regions: A Review. *Studia geophysica et geodaetica* 44, 89-106.
- Tavernier, R., de Breuck, W., De Moor, G., 1967. Geo-elektrisch onderzoek in de streek van Lessines. *Palais der Academien*. 64 p.
- Tondeur, F., Gerardy, I., Couwenberg, C., Herbosch, A., Festraets, M., 2001. Search and mapping of small radon-prone areas in Walloon Brabant (Belgium) on a geological basis. , Third Eurosymposium on Protection against Radon (Liège). Extended Abstract, 4pp.
- Tondeur, F., Gerardy, I., Licour, C., Dubois, N., 1994. Repartition géographique et géologique du risque 'radon' en Belgique Francophone. *Annales de l'association Belge Radioprotection* 19, 205-226.
- Tondeur, F., Zhu, H.-C., Charlet, J.M., Gerardy, I., Perreux, R., 1996. Radon from the subsoil to the dwelling in southern Belgium. *Environment International* 22.
- Van Noten, K., Lecocq, T., Shah, A.K., Camelbeeck, T., 2015. Seismotectonic significance of the 2008-2010 Walloon Brabant seismic swarm in the Brabant Massif (Belgium). *Tectonophysics*.
- Van Noten, K., Van Baelen, H., Sintubin, M., 2012. The complexity of 3D stress-state changes during compressional tectonic inversion at the onset of orogeny, in: Healy, D., Butler, R.W.H., Shipton, Z.K., Sibson, R.H. (Eds.), *Faulting, Fracturing, and Igneous Intrusion in the Earth's crust*. Geological Society, London, Special Publications 367, pp. 51-69.
- Van Tassel, R., 1986. Contribution a la lithologie du segment Caledonien des vallées de la Dyle et de la Thyle, Brabant, Belgique. *Aardkundige Mededelingen* 3, 239-268.
- Vander Auwera, J., André, L., 1985. Sur le milieu de dépôt, l'origine des matériaux et le faciès métamorphique de l'Assise de Tubize (Massif du Brabant, Belgique). *Bulletin de la Société belge de Géologie* 94, 171-184.
- Vanneste, K., Camelbeeck, T., Verbeeck, K., 2013. A Model of Composite Seismic Sources for the Lower Rhine Graben, Northwest Europe. *Bulletin of the Seismological Society of America* 103, 984-1007.
- Verbeeck, K., Vanneste, K., Camelbeeck, T., 2009. Seismotectonic zones for probabilistic seismic-hazard assessment in Belgium. *NIROND TR-2008-31 E*, pp. 1-47 pp.
- Verniers, J., Pharaoh, T.C., André, L., Debacker, T.N., De Vos, W., Everaerts, M., Herbosch, A., Samuelsson, J., Sintubin, M., Vecoli, M., 2002. The Cambrian to mid Devonian basin development and deformation history of eastern Avalonia, east of the Midlands Microcraton: new data and a review, in: Winchester, J.A., Pharaoh, T.C., Verniers, J. (Eds.), *Paleozoic Amalgamation of Central Europe*. Geological Society, London, Special Publications, pp. 49-93.
- Wald, D.J., Quitoriano, V., Dengler, L.A., Dewey, J.W., 1999. Utilization of the internet for rapid community intensity maps. *Seismological Research Letters* 70, 680- 697.

- Waldhauser, F., Ellsworth, W.L., 2000. A Double-Difference Earthquake Location Algorithm: Method and Application to the Northern Hayward Fault, California. *Bulletin of the Seismological Society of America* 90, 1353-1368.
- Wallace, R.E., 1951. Geometry of shearing stress and relation to faulting. *Journal of Geology* 69, 118–130.
- Wathelet, M., 2005. GEOPSY: GEOPhysical Signal database for noise arraY processing. ISTerre, Grenoble. <http://www.geopsy.org/>.
- Zhu, H.-C., Charlet, J.M., Poffijn, A., 2001. Radon risk mapping in southern Belgium: an application of geostatistical and GIS techniques. *The Science of the Total Environment* 272, 203-210.
- Zhu, H.-C., Charlet, J.M., Tondeur, F., 1998. Geological controls to the indoor radon distribution in southern Belgium. *The Science of the Total Environment* 220, 195-214.
- Zoback, M.L., 1992. First- and second-order patterns of stress in the lithosphere: the world stress map project. *Journal of Geophysical Research* 97, 11703–11728.

## Appendix A: Catalogue of events of the 2008-2010 seismic swarm

The table shows the epicentre location of the different events after location improvement by cross-correlation. Location is available in longitude/latitude and in local Belgium Lambert 1972 coordinates (in m-scale).  $M_L$ : local magnitude.

Nr	ID ROB-ID	Date			Time h:min:s	Longitude (°N)	Latitude (°E)	Belgian Lambert 1972		Depth (km)	$M_L$
		Year	Month	Day				Northing (m)	Easting (m)		
1	3068	2008	7	12	17:47:18	50.6296	4.5633	146570	163764	5.90	<b>2.2</b>
2	3082	2008	7	12	20:45:12	50.6316	4.5645	146788	163852	8.73	0.4
3	3069	2008	7	13	13:45:49	50.6259	4.5653	146153	163910	7.74	<b>3.2</b>
4	3084	2008	7	13	18:14:45	50.6395	4.5682	147671	164105	1.40	0.0
5	3071	2008	7	14	02:07:38	50.6272	4.5614	146305	163630	5.89	1.3
6	3083	2008	7	14	03:42:53	50.6357	4.5644	147243	163843	7.93	0.5
7	3085	2008	7	14	05:19:17	50.6321	4.5554	146847	163207	7.10	0.6
8	3073	2008	7	14	18:57:32	50.6298	4.5623	146595	163692	6.48	0.8
9	3074	2008	7	14	23:23:34	50.6301	4.5624	146622	163702	6.50	0.9
10	3075	2008	7	15	03:58:07	50.6302	4.5614	146633	163627	6.50	0.5
11	3089	2008	7	15	20:51:10	50.6299	4.5623	146605	163697	6.38	0.2
12	3086	2008	7	16	04:01:08	50.6290	4.5631	146506	163748	6.31	0.6
13	3087	2008	7	16	04:07:29	50.6330	4.5629	146945	163737	6.47	0.0
14	3088	2008	7	16	18:57:08	50.6286	4.5596	146460	163505	6.12	0.0
15	3092	2008	7	17	10:20:33	50.6289	4.5631	146488	163751	6.47	0.4
16	3114	2008	7	19	01:16:39	50.6293	4.5638	146529	163802	6.52	0.7
17	3115	2008	7	19	01:16:52	50.6283	4.5611	146427	163613	5.75	0.0
18	3116	2008	7	19	04:31:04	50.6283	4.5648	146423	163872	6.07	0.4
19	3117	2008	7	21	21:10:22	50.6281	4.5644	146397	163842	6.02	0.5
20	3118	2008	7	22	23:25:09	50.6270	4.5633	146280	163766	6.04	0.3
21	3120	2008	7	25	16:21:22	50.6264	4.5667	146210	164007	6.05	0.2
22	3119	2008	7	25	20:10:49	50.6308	4.5641	146707	163818	6.25	0.2
23	3121	2008	7	31	18:06:33	50.6381	4.5662	147518	163967	6.64	0.4
24	3091	2008	8	8	09:40:19	50.6284	4.5641	146436	163819	6.00	1.6
25	3090	2008	8	8	09:54:40	50.6341	4.5643	147070	163833	6.34	1.7
26	3094	2008	8	8	17:52:02	50.6282	4.5605	146408	163567	5.47	1.8
27	3095	2008	8	9	03:33:42	50.6369	4.5678	147384	164081	6.95	1.5
28	3096	2008	8	9	14:18:56	50.6335	4.5662	146997	163968	6.46	<b>2.2</b>
29	3101	2008	8	9	14:39:56	50.6289	4.5620	146488	163675	6.17	1.0
30	3105	2008	8	9	17:20:37	50.6298	4.5621	146592	163677	6.06	0.3
31	3098	2008	8	9	18:31:41	50.6321	4.5672	146846	164041	6.41	<b>2.2</b>
32	3100	2008	8	9	18:34:14	50.6280	4.5761	146396	164669	6.68	0.4
33	3108	2008	8	9	18:34:36	50.6300	4.5715	146616	164343	6.67	1.3
34	3099	2008	8	9	18:35:15	50.6257	4.5591	146137	163468	5.20	0.7
35	3109	2008	8	9	18:35:42	50.6319	4.5680	146823	164099	6.46	1.6
36	3110	2008	8	9	18:37:41	50.6264	4.5677	146218	164074	6.16	0.0
37	3111	2008	8	10	00:27:58	50.6267	4.5648	146246	163873	5.88	0.2
38	3112	2008	8	10	04:04:00	50.6279	4.5621	146377	163680	5.86	0.1
39	3177	2008	8	12	13:38:26	50.6271	4.5658	146287	163940	5.75	0.6
40	3178	2008	8	12	13:39:49	50.6293	4.5642	146536	163827	6.01	0.9
41	3179	2008	8	15	10:07:41	50.6307	4.5653	146691	163907	5.85	0.5
42	3137	2008	8	22	13:26:57	50.6297	4.5625	146576	163707	6.00	1.1
43	3138	2008	8	22	15:38:47	50.6300	4.5622	146613	163684	6.05	0.7

44	3139	2008	8	22	15:38:48	50.6299	4.5625	146606	163707	6.06	1.0
45	3140	2008	8	22	15:38:58	50.6302	4.5621	146631	163681	6.09	1.7
46	3180	2008	8	23	00:16:52	50.6273	4.5656	146310	163926	6.36	0.4
47	3181	2008	8	23	00:46:13	50.6305	4.5618	146672	163659	6.03	0.3
48	3161	2008	8	30	22:30:11	50.6296	4.5630	146563	163743	5.97	0.5
49	3182	2008	9	1	01:46:14	50.6283	4.5678	146419	164084	5.88	-0.2
50	3183	2008	9	1	01:59:42	50.6273	4.5646	146307	163857	6.53	-0.4
51	3184	2008	9	1	02:00:47	50.6276	4.5670	146349	164030	5.64	0.2
52	3188	2008	9	3	19:16:10	50.6323	4.5633	146868	163762	6.28	0.7
53	3213	2008	9	5	20:25:53	50.6278	4.5651	146364	163890	6.26	0.4
54	3164	2008	9	10	08:26:41	50.6273	4.5652	146313	163899	6.23	1.3
55	3165	2008	9	12	05:08:55	50.6300	4.5629	146607	163738	6.41	<b>2.2</b>
56	3167	2008	9	13	01:14:17	50.6251	4.5674	146065	164059	5.87	<b>2.6</b>
57	3185	2008	9	13	01:42:31	50.6322	4.5595	146861	163494	6.40	0.7
58	3186	2008	9	13	02:00:26	50.6283	4.5723	146430	164400	6.14	0.7
59	3187	2008	9	13	15:57:25	50.6302	4.5611	146633	163607	6.20	1.1
60	3200	2008	9	15	02:09:13	50.6285	4.5649	146443	163875	6.04	1.1
61	3169	2008	9	18	20:57:24	50.6317	4.5593	146801	163484	6.23	0.9
62	3214	2008	9	18	21:42:16	50.6327	4.5614	146915	163631	6.14	1.4
63	3215	2008	9	27	14:31:06	50.6308	4.5605	146698	163565	6.47	0.9
64	3216	2008	9	27	14:31:35	50.6270	4.5666	146281	163997	6.35	1.2
65	3171	2008	9	27	16:41:32	50.6309	4.5598	146716	163517	5.67	1.6
66	3217	2008	9	27	16:59:30	50.6266	4.5668	146231	164016	6.31	0.7
67	3218	2008	9	27	18:19:30	50.6269	4.5661	146270	163965	6.35	0.5
68	3219	2008	9	27	22:11:44	50.6272	4.5661	146299	163963	6.36	0.7
69	3220	2008	9	30	11:01:30	50.6265	4.5671	146225	164037	6.32	1.3
70	3221	2008	9	30	22:32:10	50.6262	4.5600	146187	163534	5.57	0.4
71	3222	2008	9	30	22:34:09	50.6260	4.5695	146172	164207	6.11	0.7
72	3223	2008	10	3	02:13:17	50.6261	4.5694	146183	164195	6.07	0.7
73	3176	2008	10	6	06:07:49	50.6280	4.5643	146388	163839	6.33	1.1
74	3175	2008	10	6	06:14:15	50.6295	4.5651	146558	163891	5.43	1.8
75	3224	2008	10	6	08:36:06	50.6267	4.5667	146245	164008	6.21	1.3
76	3241	2008	10	18	22:53:33	50.6271	4.5656	146294	163926	6.61	0.4
77	3242	2008	10	20	12:14:01	50.6274	4.5667	146323	164007	6.57	1.0
78	3243	2008	10	21	02:43:14	50.6274	4.5651	146319	163890	6.63	0.7
79	3203	2008	10	21	02:46:21	50.6297	4.5596	146578	163503	5.08	0.4
80	3245	2008	10	21	23:50:23	50.6267	4.5665	146242	163989	6.28	0.5
81	3246	2008	10	25	22:24:30	50.6303	4.5689	146643	164161	5.66	1.0
82	3247	2008	10	25	22:33:23	50.6290	4.5642	146497	163828	6.64	0.5
83	3248	2008	10	30	01:34:07	50.6255	4.5686	146112	164140	6.33	0.4
84	3249	2008	10	30	06:08:33	50.6258	4.5681	146147	164108	6.31	0.7
85	3204	2008	10	30	19:12:29	50.6297	4.5631	146576	163749	6.54	1.5
86	3259	2008	12	20	20:50:51	50.6278	4.5680	146367	164100	5.38	1.2
87	3225	2008	12	20	20:53:08	50.6269	4.5660	146274	163958	5.65	<b>2.4</b>
88	3260	2008	12	20	21:57:44	50.5946	4.5617	142676	163663	6.25	0.3
89	3261	2008	12	21	02:30:19	50.5973	4.5685	142973	164139	5.94	0.3
90	3262	2008	12	28	00:16:53	50.6330	4.5557	146945	163228	5.56	0.7
91	3232	2008	12	29	03:27:56	50.6271	4.5586	146288	163436	5.72	1.7
92	3263	2008	12	29	03:40:01	50.6243	4.5465	145980	162574	5.22	-0.1
93	3264	2008	12	29	04:01:32	50.5962	4.5602	142855	163553	6.28	0.0
94	3265	2008	12	29	04:25:14	50.6224	4.5488	145767	162738	6.85	0.0
95	3266	2008	12	29	04:50:10	50.6066	4.5182	144004	160578	9.95	0.6
96	3233	2008	12	29	14:01:14	50.6283	4.5644	146421	163841	5.00	1.2



97	3239	2009	1	15	12:02:25	50.6345	4.5596	147117	163505	6.46	1.9
98	3250	2009	2	8	19:33:02	50.6274	4.5659	146328	163948	5.77	1.6
99	3884	2009	2	18	04:04:23	50.6279	4.5653	146379	163908	6.00	0.2
100	3885	2009	2	18	10:23:04	50.6271	4.5661	146291	163966	5.78	0.5
101	3252	2009	2	21	13:21:21	50.6273	4.5661	146308	163961	6.06	<b>2.0</b>
102	3309	2009	2	21	21:52:22	50.6258	4.5682	146143	164115	6.14	-0.7
103	3310	2009	2	21	22:29:20	50.6314	4.5688	146769	164153	5.64	-0.6
104	3311	2009	2	21	22:29:22	50.6283	4.5652	146422	163897	5.76	0.0
105	3312	2009	2	22	01:41:47	50.6270	4.5670	146275	164030	5.83	0.0
106	3313	2009	2	22	22:35:41	50.6266	4.5667	146233	164009	5.83	0.0
107	3314	2009	2	23	02:48:06	50.6271	4.5670	146287	164029	6.16	0.4
108	3315	2009	2	23	04:49:11	50.6277	4.5654	146362	163916	5.97	0.5
109	3254	2009	2	23	19:31:43	50.6284	4.5641	146436	163823	5.73	1.3
110	3316	2009	2	23	22:59:04	50.6302	4.5611	146629	163608	6.79	0.6
111	3317	2009	2	24	02:08:47	50.6278	4.5657	146366	163935	6.23	0.5
112	3318	2009	2	24	02:15:25	50.6286	4.5636	146459	163790	5.77	0.6
113	3319	2009	2	25	04:54:14	50.6280	4.5639	146395	163806	6.30	0.2
114	3257	2009	2	25	07:26:37	50.6283	4.5647	146427	163866	5.74	1.6
115	3269	2009	2	27	15:21:04	50.6289	4.5632	146493	163760	5.68	1.1
116	3320	2009	2	27	22:49:09	50.6296	4.5676	146564	164068	6.07	0.3
117	3271	2009	3	2	08:47:19	50.6283	4.5648	146419	163872	5.76	0.8
118	3273	2009	3	3	03:23:32	50.6299	4.5614	146606	163630	6.26	<b>2.8</b>
119	3321	2009	3	3	03:23:50	50.6296	4.5679	146566	164087	6.07	1.6
120	3322	2009	3	3	03:26:12	50.6310	4.5674	146722	164052	5.87	0.3
121	3323	2009	3	3	03:27:23	50.6296	4.5659	146564	163951	6.36	0.3
122	3324	2009	3	3	03:57:08	50.6280	4.5626	146391	163715	5.57	-0.6
123	3325	2009	3	3	04:11:27	50.6368	4.6144	147383	167376	4.95	-0.4
124	3277	2009	3	3	04:29:57	50.6286	4.5652	146455	163899	5.68	1.0
125	3326	2009	3	3	04:33:58	50.6280	4.5648	146387	163873	5.71	0.4
126	3274	2009	3	3	19:25:20	50.6292	4.5620	146519	163671	6.82	0.8
127	3327	2009	3	3	23:41:37	50.6383	4.5617	147540	163650	2.09	-0.6
128	3328	2009	3	4	09:25:52	50.6273	4.5655	146317	163921	5.68	1.1
129	3329	2009	3	5	01:47:29	50.6288	4.5645	146477	163848	6.19	-0.6
130	3330	2009	3	5	01:49:02	50.6301	4.5618	146622	163660	6.23	-0.5
131	3331	2009	3	5	04:14:03	50.6268	4.5164	146248	160444	5.54	-0.6
132	3276	2009	3	5	04:21:42	50.6294	4.5614	146541	163629	6.09	1.7
133	3332	2009	3	5	04:21:48	50.6319	4.5623	146823	163691	6.44	0.0
134	3333	2009	3	5	04:24:42	50.6277	4.5653	146356	163905	5.78	0.5
135	3334	2009	3	5	22:03:00	50.6290	4.5635	146505	163782	5.74	0.5
136	3280	2009	3	7	19:40:50	50.6266	4.5672	146231	164045	5.93	1.0
137	3430	2009	3	10	02:15:36	50.6277	4.5646	146354	163855	5.63	-0.2
138	3284	2009	3	11	05:19:53	50.6287	4.5639	146469	163808	5.80	1.0
139	3432	2009	3	11	23:18:39	50.6277	4.5656	146360	163925	5.75	0.3
140	3433	2009	3	12	04:10:12	50.6302	4.5621	146637	163681	5.82	0.6
141	3285	2009	3	12	07:31:04	50.6296	4.5614	146572	163632	5.69	1.4
142	3288	2009	3	12	10:42:22	50.6288	4.5635	146475	163777	5.81	1.8
143	3434	2009	3	12	15:11:37	50.6288	4.5648	146485	163872	6.37	1.2
144	3289	2009	3	12	15:12:47	50.6280	4.5634	146387	163774	6.38	1.3
145	3435	2009	3	12	15:46:36	50.6288	4.5630	146481	163747	5.59	1.0
146	3436	2009	3	12	18:00:35	50.6288	4.5626	146481	163712	5.62	0.7
147	3437	2009	3	14	01:22:08	50.6279	4.5653	146384	163909	5.80	0.1
148	3438	2009	3	15	04:43:32	50.6303	4.5611	146642	163605	5.77	-0.2
149	3439	2009	3	15	05:33:21	50.6274	4.5669	146327	164023	5.93	-0.4

150	3440	2009	3	16	01:42:30	50.6284	4.5658	146437	163939	5.87	-0.6
151	3441	2009	3	16	09:22:06	50.6302	4.5626	146637	163712	5.77	0.4
152	3292	2009	3	16	22:40:43	50.6295	4.5627	146555	163722	6.47	0.9
153	3442	2009	3	16	22:41:28	50.6296	4.5625	146571	163707	6.24	-0.1
154	3443	2009	3	16	22:42:21	50.6288	4.5635	146476	163777	5.74	0.5
155	3444	2009	3	19	03:54:29	50.6315	4.5622	146778	163687	6.18	0.7
156	3445	2009	3	19	03:55:19	50.6293	4.5626	146532	163712	5.69	0.2
157	3446	2009	3	20	00:44:52	50.6290	4.5640	146497	163818	5.96	0.5
158	3293	2009	3	20	01:39:00	50.6274	4.5653	146327	163906	5.56	0.7
159	3447	2009	3	20	10:03:29	50.6284	4.5644	146439	163841	5.60	0.7
160	3448	2009	3	20	17:46:54	50.6256	4.5689	146119	164161	6.10	0.7
161	3449	2009	3	20	18:04:31	50.6256	4.5690	146122	164170	6.15	0.4
162	3296	2009	3	20	22:22:15	50.6276	4.5655	146343	163921	5.80	0.6
163	3295	2009	3	20	22:29:56	50.6306	4.5611	146674	163609	6.03	0.6
164	3450	2009	3	21	05:45:58	50.6259	4.5687	146158	164149	6.12	0.9
165	3451	2009	3	21	05:46:16	50.6259	4.5685	146155	164135	6.07	0.3
166	3294	2009	3	21	15:06:06	50.6302	4.5619	146629	163663	5.66	1.3
167	3452	2009	3	21	15:07:15	50.6305	4.5612	146665	163613	5.68	0.2
168	3453	2009	3	21	16:42:00	50.6295	4.5622	146559	163687	5.57	0.9
169	3454	2009	3	22	00:42:38	50.6295	4.5619	146553	163667	5.66	0.0
170	3456	2009	3	23	01:09:22	50.6311	4.5572	146739	163331	5.76	0.2
171	3455	2009	3	23	20:14:38	50.6263	4.5684	146203	164129	6.08	0.5
172	3457	2009	3	24	02:51:24	50.6299	4.5619	146596	163669	5.68	-0.4
173	3299	2009	3	26	14:30:28	50.6296	4.5616	146567	163642	5.68	1.3
174	3458	2009	3	26	14:30:41	50.6300	4.5615	146614	163636	5.73	0.9
175	3459	2009	3	26	14:30:52	50.6296	4.5619	146572	163666	5.71	0.8
176	3301	2009	3	26	19:42:55	50.6300	4.5610	146615	163598	5.66	<b>2.3</b>
177	3460	2009	3	26	21:32:37	50.6305	4.5606	146673	163572	5.72	0.3
178	3461	2009	3	26	22:18:49	50.6281	4.5569	146403	163310	6.38	0.2
179	3462	2009	3	26	22:28:32	50.6330	4.5617	146947	163653	6.38	0.6
180	3463	2009	3	26	22:31:19	50.6328	4.5596	146920	163500	5.85	0.1
181	3464	2009	3	26	23:07:21	50.6269	4.5613	146271	163627	5.82	0.1
182	3465	2009	3	26	23:37:12	50.6287	4.5587	146467	163441	5.87	-0.1
183	3466	2009	3	27	01:23:43	50.6295	4.5653	146554	163907	5.89	-0.1
184	3468	2009	3	27	01:29:07	50.6277	4.5652	146362	163899	5.95	0.1
185	3469	2009	3	27	01:57:12	50.6290	4.5587	146505	163442	5.91	-0.1
186	3470	2009	3	27	02:15:45	50.6308	4.5617	146705	163653	5.70	-0.3
187	3471	2009	3	27	03:44:14	50.6296	4.5619	146568	163664	5.71	-0.1
188	3472	2009	3	27	17:51:36	50.6331	4.5576	146953	163361	6.29	1.0
189	3473	2009	3	27	23:49:37	50.6303	4.5609	146644	163594	5.61	0.4
190	3474	2009	3	28	22:35:13	50.6300	4.5614	146614	163629	5.82	-0.1
191	3475	2009	3	29	00:02:59	50.6307	4.5595	146695	163499	5.73	1.0
192	3476	2009	3	29	21:58:21	50.6295	4.5594	146556	163486	5.74	0.0
193	3477	2009	3	30	02:20:02	50.6289	4.5639	146486	163810	5.71	0.4
194	3478	2009	3	31	01:34:08	50.6273	4.5652	146313	163899	6.03	0.8
195	3479	2009	3	31	01:46:57	50.6309	4.5601	146709	163536	5.91	0.4
196	3480	2009	3	31	02:15:16	50.6305	4.5605	146672	163567	5.91	0.1
197	3481	2009	3	31	03:17:16	50.6312	4.5620	146750	163673	6.07	0.0
198	3303	2009	4	1	18:58:44	50.6277	4.5649	146353	163876	5.60	0.7
199	3482	2009	4	2	21:03:31	50.6295	4.5622	146553	163689	5.71	0.4
200	3483	2009	4	3	00:10:26	50.6291	4.5707	146518	164292	5.80	-0.3
201	3484	2009	4	3	21:33:30	50.6337	4.5573	147025	163337	6.34	0.7
202	3485	2009	4	5	12:02:04	50.6272	4.5655	146306	163923	5.62	0.7

203	3486	2009	4	7	11:42:22	50.6287	4.5652	146469	163900	5.90	1.2
204	3305	2009	4	9	10:57:10	50.6317	4.5626	146800	163715	5.87	1.1
205	3487	2009	4	10	02:24:33	50.6312	4.5607	146740	163579	5.80	-0.3
206	3488	2009	4	10	13:31:01	50.6304	4.5609	146655	163595	5.86	0.7
207	3489	2009	4	10	16:29:08	50.6287	4.5636	146471	163788	5.62	0.7
208	3342	2009	4	13	03:38:01	50.6291	4.5628	146513	163727	5.53	0.5
209	3814	2009	4	13	03:50:18	50.6286	4.5638	146456	163799	5.63	-0.1
210	3815	2009	4	13	12:47:25	50.6276	4.5651	146350	163896	5.79	0.4
211	3343	2009	4	13	12:50:37	50.6295	4.5597	146559	163513	5.96	0.5
212	3816	2009	4	13	18:17:25	50.6283	4.5624	146424	163699	6.11	0.0
213	3817	2009	4	14	01:37:13	50.6283	4.5637	146420	163795	5.64	0.0
214	3818	2009	4	14	03:20:01	50.6266	4.5667	146230	164003	5.65	0.5
215	3308	2009	4	14	13:28:17	50.6285	4.5644	146444	163841	5.57	1.0
216	3819	2009	4	17	22:16:36	50.6345	4.5559	147108	163240	6.34	0.4
217	3898	2009	5	2	21:54:12	50.6268	4.5665	146260	163991	5.67	0.2
218	3346	2009	5	16	21:52:27	50.6297	4.5619	146578	163669	5.65	1.2
219	3422	2009	6	26	01:50:42	50.6283	4.5638	146425	163799	6.90	1.2
220	3426	2009	7	12	05:29:34	50.6301	4.5620	146625	163670	6.37	1.8
221	3506	2009	8	16	07:22:24	50.6301	4.5610	146618	163603	5.47	1.2
222	3507	2009	8	16	16:23:10	50.6276	4.5667	146350	164008	6.51	0.7
223	3908	2009	8	16	16:33:51	50.6304	4.5606	146654	163577	5.57	0.3
224	3508	2009	8	16	22:43:02	50.6304	4.5607	146656	163580	5.51	1.0
225	3909	2009	8	20	00:43:40	50.6276	4.5643	146340	163837	6.67	0.2
226	3511	2009	9	5	22:50:07	50.6283	4.5652	146424	163898	6.58	1.3
227	3911	2009	9	6	20:44:41	50.6285	4.5651	146448	163891	6.75	0.3
228	3912	2009	9	17	22:56:38	50.6274	4.5656	146327	163931	6.43	0.1
229	3552	2009	12	26	06:50:13	50.6249	4.5684	146045	164130	5.47	<b>2.5</b>
230	3806	2009	12	26	06:51:06	50.6262	4.5697	146196	164221	5.23	0.5
231	3807	2009	12	26	06:51:53	50.6261	4.5849	146183	165291	4.12	0.8
232	3808	2009	12	26	06:53:04	50.6327	4.5584	146909	163417	6.59	0.5
233	3555	2009	12	31	03:16:45	50.6317	4.5598	146804	163517	6.57	1.3
234	3560	2010	1	6	22:04:50	50.6307	4.5608	146692	163584	6.62	0.7
235	3565	2010	1	12	20:15:56	50.6284	4.5719	146437	164374	5.86	0.3
236	3568	2010	1	18	11:59:28	50.6267	4.5681	146243	164106	6.83	0.9
237	4057	2011	1	30	16:39:45	50.6230	4.5510	145832	162896	-	1.2
238	4058	2011	1	30	21:12:14	50.6290	4.5690	146502	164168	-	1.0
239	5027	2014	1	10	03:21:53	50.6206	4.5597	145570	163515	9.87	1.0

# Appendix B: AGU2013 poster presentation

**Using H/V spectral ratio analysis to map sediment thickness in order to explain macroseismic intensity variation related to a low-magnitude seismic swarm in central Belgium**

AGU FALL MEETING  
14-18 November 2013

S53B-2406  
Friday, 13 Dec - 1:40-6:00 PM  
Hall A-C (Moscow South)

koen.vannoten@oma.be  
http://www.seismology.be

Seismology-Gravimetry  
Royal Observatory of Belgium  
Ringlaan 3, 1180 Brussels, Belgium

Koen Van Noten, Thomas Lecocq & Thierry Camelbeek

**1. INTRODUCTION: THE 2008-2010 SEISMIC SWARM**

Between July 2008 and January 2010 a seismic swarm took place 20 km SE of Brussels (Belgium) at a depth range between 3 and 6 km. Thanks to the installation of a temporary seismic network more than 300 earthquakes with magnitudes  $-0.7 < M < 3.2$  have been recorded. Relocation by cross-correlation revealed a NW-SE oriented fault zone.

60 events, of which some as low as  $M 0.4$ , have been felt by the local population and are more often only heard which is indicative of a shallow high-frequency source.

Within a single community reported macroseismic intensity (MI) often strongly varies the average MI of a community therefore oversimplifies the local intensity, especially in hilly areas in which local site effects could have influenced the impact of the earthquakes at the surface.

Remarkably, the highest MI's have been reported at hill slopes, at which the bedrock is closest to the surface, instead of at hill top sites or at valley sites at which one would expect local amplification due to the presence of a thicker soft sediment pile.

**FIGURE 1:** Localisation of the seismic swarm illustrated on an aeromagnetic map showing prominent NW-SE oriented lineaments in the Lower Palaeozoic Brabant Massif. The seismic swarm is interpreted as a reactivation of an old Palaeozoic shear zone under the current local stress field.

**2. AIM OF THE RESEARCH & METHODOLOGY**

We want to investigate if the variability in macroseismicity (MI) is influenced by the thickness of soft sediments above the bedrock of the Loosdrecht Massif. Therefore, a reliable sediment thickness map needs to be created. This has been done by:

- 1) establishing an empirical relationship between sediment thickness (h) and fundamental frequency (f<sub>0</sub>) from H/V Spectral Ratio (HVSR) analysis above boreholes from which the depth to the bedrock is known;
- 2) performing a local HVSR survey at places at which sediment thickness is unknown but can be inferred by the determining f<sub>0</sub> and using the established empirical relationship.
- 3) constructing a numerical model of the top of the bedrock using regional borehole & outcrop data and the sediment thickness resulting from the numerical model of the top of the bedrock. The final sediment thickness map then results from subtracting the numerical model of the top of the basement from a digital elevation model. Subsequently MI's related to the different events of the 2008-2010 seismic swarm can be linked to the thickness map.

**3. HVSRINGEOPSY**

- measuring time = 10 minutes of ambient noise with a CityShark II connected to a seismometer
- semi-automatic window selection
- window length 5-10s
- 35 to 50 windows necessary for a reliable f<sub>0</sub>
- Konno and Ohmachi smoothing (0.40 constant)

**FIGURE 2:** Localisation of the seismic swarm on a topographic map. The red line indicates the NW-SE oriented fault zone. The map shows the distribution of the seismic swarm and the location of the boreholes used for the study.

**FIGURE 3:** (a) Local HVSR survey results showing the variability of f<sub>0</sub> and the sediment thickness. (b) ERT profiles in the valley illustrate the thickness of alluvial sediments and the bedrock. (c) ERT profiles in the valley illustrate the thickness of alluvial sediments and the bedrock. This result is in agreement with the HVSR results in (a).

**FIGURE 4:** (a) Relocated epicenter distribution of the 2008-2010 seismic swarm delimiting a NW-SE oriented fault zone. (b) Average community versus individual MI of a M 2.2 event. (c) MI of a M 2.6 event. The highest MI (MI 5) is reported from the hill tops.

**4. CONSTRAINING THE POWER-LAW RELATIONSHIP BETWEEN h AND f<sub>0</sub>**

- H/V measurements above 68 boreholes
- f<sub>0</sub> decreases from SW to NE because of the NW dip of the top of bedrock
- lowest f<sub>0</sub> on hill tops
- low f<sub>0</sub> on valley floor
- highest f<sub>0</sub> on valley slopes

Empirical power-law relationship between h and f<sub>0</sub>:

$$h = 142.64 f_0^{-2.386}$$

**FIGURE 5:** (a) Establishing a representative power-law relationship between f<sub>0</sub> and h. (b) Derived from power-law slightly overestimates the h in between 30 m and 50 m. (c) Positive power-law between h and f<sub>0</sub> owing to the relationship f<sub>0</sub> = V<sub>s</sub>/4h.

**5. HVSR ANDERT SURVEY TESTIMATES SEDIMENT THICKNESS AT UNKNOWN SITES**

**FIGURE 6:** (a) Resulting sediment thickness map. The map is constructed by using outcrop boreholes, HVSR and ERT data points (interpolated to create a numerical model of the top of the bedrock). Afterwards, the numerical model of the top of the bedrock is subtracted from the digital elevation model to calculate the local sediment thickness.

**FIGURE 7:** (a) Resulting sediment thickness map. The map is constructed by using outcrop boreholes, HVSR and ERT data points (interpolated to create a numerical model of the top of the bedrock). Afterwards, the numerical model of the top of the bedrock is subtracted from the digital elevation model to calculate the local sediment thickness.

**6. H/V DISCUSSION AND CONCLUSIONS**

Profile M: f<sub>0</sub> increases from the W hill top towards the valley, is the highest at the valley slope (M05-M07), is lower in the central part of the valley (M10) because of thicker alluvial sediments, f<sub>0</sub> finally decreases again towards the E hill top.

Profile R: S to N profile from hill top (R01) to valley floor (R26) along the valley slope, f<sub>0</sub> increases due to thickness decrease.

The MI related to a M 2.6 event is plotted on the map. Notice the link between the variability in MI and the sediment thickness. The highest MI 5 is reported on the valley slopes.

Linking macroseismic intensity (MI), related to the 2008-2010 seismic swarm, to the sediment thickness map shows that the highest MI, i.e. MI 5, is related to the thinnest sediment cover located on the valley slopes. The decrease in MI off the hill events on hill tops or on valley floors can therefore be explained by an absorption of high frequency seismic energy by the local sediment column.

**6. H/V DISCUSSION AND CONCLUSIONS**

Profile M: f<sub>0</sub> increases from the W hill top towards the valley, is the highest at the valley slope (M05-M07), is lower in the central part of the valley (M10) because of thicker alluvial sediments, f<sub>0</sub> finally decreases again towards the E hill top.

Profile R: S to N profile from hill top (R01) to valley floor (R26) along the valley slope, f<sub>0</sub> increases due to thickness decrease.

The MI related to a M 2.6 event is plotted on the map. Notice the link between the variability in MI and the sediment thickness. The highest MI 5 is reported on the valley slopes.

Linking macroseismic intensity (MI), related to the 2008-2010 seismic swarm, to the sediment thickness map shows that the highest MI, i.e. MI 5, is related to the thinnest sediment cover located on the valley slopes. The decrease in MI off the hill events on hill tops or on valley floors can therefore be explained by an absorption of high frequency seismic energy by the local sediment column.



# Appendix C: TSG2015 poster presentation

**Deducing the seismotectonic significance of the 2008-2010 seismic swarm in the Brabant Massif by aeromagnetic bandpass filtering**



ROYAL OBSERVATORY OF BELGIUM  
SEISMOLOGY - GRAVIMETRY

Koen VAN NOTEN<sup>1</sup>, Thomas LECOQ<sup>1</sup>, Anjana K. SHAH<sup>2</sup> & Thierry CAMELBEECK<sup>1</sup>

<sup>1</sup>Royal Observatory of Belgium, Seismology-Gravimetry, Brussels, Belgium  
<sup>2</sup>U.S. Geological Survey, Denver Federal Center, Denver, Colorado, U.S.A.



koen.vannoten@seismology.be  
http://www.seismology.be

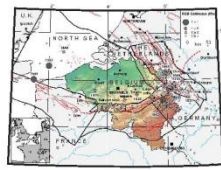
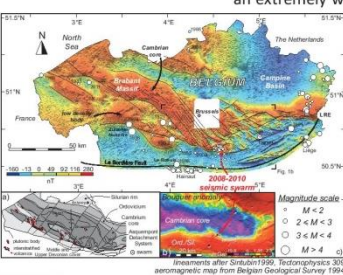
### 1. INTRODUCTION: STRUCTURAL GRAIN OF THE BRABANT MASSIF

Some moderate-magnitude earthquakes have occurred in the seismotectonic zone of the Lower-Palaeozoic Anglo-Brabant Massif, a zone which extends from central Belgium to the North Sea and SE U.K.

Between 2008 and 2010 a seismic swarm took place 20 km SE of Brussels. Thanks to the installation of a temporary seismic network, small magnitude events were recorded which allow, for the first time, to visualise and to study an extremely well documented seismic event in the Brabant Massif. We discuss the reactivation potential of an ancient geological structure in an intraplate setting.

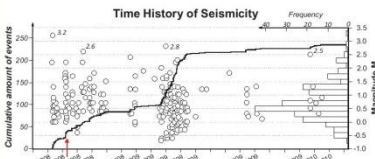
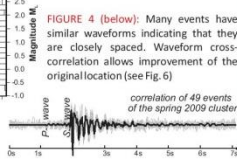
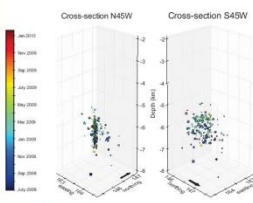
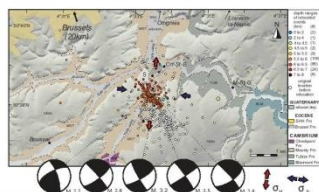
**The Brabant Massif**

- Symmetric disposition with a Cambrian core and an Ordovician/Silurian rim.
- Arcuate geometry due to compression of Cambrian core against a low density body.
- Pronounced NW-SE and WNE-ESE magnetic lineaments representative of dextral shear zones resulting from escape tectonics.

### 2. THE 2008-2010 WALLOON BRABANT SEISMIC SEQUENCE

In contrast to a classical foreshock-mainshock-aftershock sequence, seismic swarms are not characterised by one dominant event but usually show a large number of low-magnitude events clustered in time. The absence of an identifiable mainshock is a consequence of a weakened crust and indicates that a well-defined, single fault structure that would be capable to sustain and release higher strains is absent.

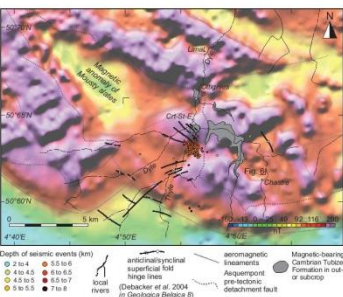





### 3. MAGNETIC ANOMALIES IN THE EPICENTRAL AREA

Several NW-SE magnetic ridges and magnetic lineaments represent the dominance of the high-magnetic bearing Tubize Formation in the subsurface.

The seismic swarm is situated between two magnetic ridges that have WSW-ESE and NW-SE orientations, respectively north and south of the swarm.

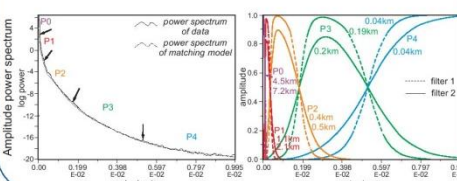
In order to deduce if these ridges correspond to shallow or deep sources, a strategic depth filtering needs to be applied.



### 4. MAGNETIC MATCHED BANDPASS FILTERING

Matched bandpass filtering of magnetic data is used to separate short-wavelength anomalies, that originate from shallow depths, from long-wavelength anomalies that generally originate at greater depths. The following methodology is followed:

- 1) Calculation of amplitude power spectra along line segments.
- 2) Each power spectrum has natural breaks that correspond to different depths.
- 3) Low- and bandpass filtering.
- 4) Inverse Fourier transformation to generate anomalies that highlight sources at the filtered depths.

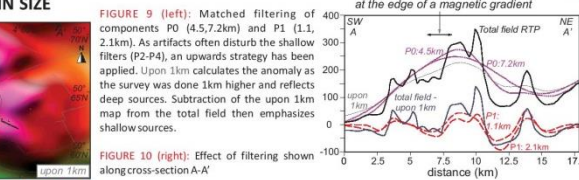
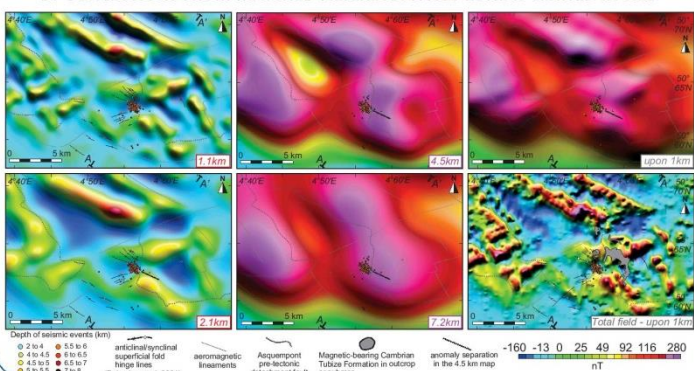


### 5. CONCLUSIONS FROM MATCHED FILTERING: FAULT ZONE IS LIMITED IN SIZE

Figure 9 (left): Matched filtering of components P0 (4.5,7.2km) and P1 (1.1, 2.1km). As artifacts often disturb the shallow filters (P2-P4), an upwards strategy has been applied. Upon 1km calculates the anomaly as the survey was done 1km higher and reflects deep sources. Subtraction of the upon 1km map from the total field then emphasizes shallow sources.

Figure 9 (right): Seismic swarm is located at the edge of a magnetic gradient. Total field RTP, P0: 4.5km, P1: 2.1km, P2: 1.1km, P3: 0.4km, P4: 0.2km.

Figure 10 (right): Effect of filtering shown along cross-section A-A'. Anomaly maps for deep sources show that the SE end of the structure responsible for the swarm is blocked by a positive magnetic anomaly that has a different orientation than the swarm. Shallow filters show that the NW end of the WNW-ESE anomaly. Matched filtering suggests that the structure is limited in size which potentially could result in a reduced seismic hazard for this region.

**ACKNOWLEDGEMENTS**  
Project Financed by BELSPO, contract MO33/028.  
Ideas and results on this poster are submitted to Tectonophysics.

